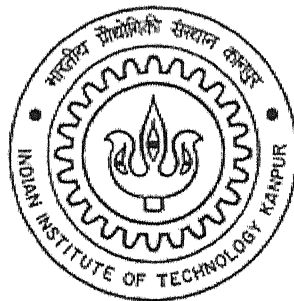# IN-PLANE LATERAL RESISTANCE OF MASONRY CONFINED BY GRID ELEMENTS

A Thesis submitted in partial fulfilment of the

requirements for the Degree of

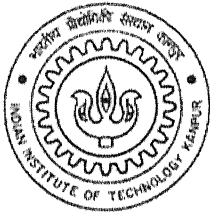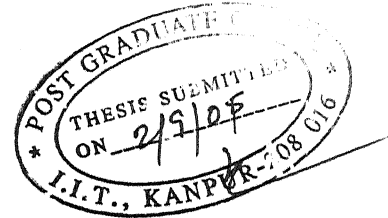Master of Technology

By

Samaresh Paikara

Department of Civil Engineering

Indian Institute of Technology Kanpur

September, 2005

CERTIFICATE

It is certified that the work contained in this thesis entitled "In-Plane Lateral Resistance of Masonry Confined by Grid Elements" by Mr. Samaresh Paikara (Y3103043), has been carried out under my supervision and this work has not been submitted elsewhere for a degree.

Durgesh C. Rai

Assistant Professor

Department of Civil Engineering

September, 2005

Indian Institute of Technology, Kanpur

ABSTRACT

The study is concerned with the evaluation of seismic behaviour of different confinement schemes on URM. Recent earthquakes, especially 2001 Bhuj earthquake and 2003 Bam earthquake have vividly demonstrated seismic vulnerability of masonry buildings and question the seismic performance of existing URM buildings. URM buildings designed only for gravity forces and not for lateral forces, present challenging engineering problems in hazard mitigation. Some conventional earthquake resistant designs of URM structures have shown acceptable performance during past earthquakes. Design of these structures depends on energy dissipation potential of well detailed portions and/or members of structures which undergo large but controlled inelastic deformations in the event of design earthquakes. These structures respond to the stress of the earthquake by working along the joints between the infill and the timber frame. Due to the presence of timber studs, which subdivide the infill, the loss of the portion or all of several masonry panels do not lead progressively to the destruction of the rest of the wall. The closely spaced studs prevent propagation of diagonal shear cracks within any single panel, and reduce the probability of the masonry falling out of the frame.

For investigation of the behaviour of confinement schemes both analytical and experimental works have been carried out. URM walls with various patterns of grid elements have been analysed. For analytical model timber and RC was chosen as grid material, whereas for experimental purpose only RC has been chosen as grid material. The experimental work was solely based on slow cyclic test on wall specimens. These slow cyclic tests provide the information needed to understand the behaviour of the structure in nonlinear range. The analytical work was carried out by Finite Element Model using the FEA tool ABAQUS. The analytical work involved a parametric study of various design variables controlling energy dissipation potential of confined wall systems. In this study in-plane deformation of URM wall panels and grid elements was monitored and their overall shear resistance was measured.

ACKNOWEDGEMENT

I express my deepest and sincere gratitude to my teacher and thesis supervisor, Professor Durgesh C. Rai, for his encouraging guidance and motivating association all through my M.Tech. program. I am indebted to all my teachers at IIT Kanpur for the knowledge I have gained during my stay at IIT Kanpur.

I am extremely thankful to Dr. K.K. Bajpai, Senior Scientific Officer, Structural Engineering Laboratory for his invaluable guidance in instrumentation and help during experiments. Help of Mr. N. Satyanarayana in experimental program and purchasing materials is deeply acknowledged. I am thankful to Mr. Digambar Urkude for doing the fabrication of test setup and specimens. I am also thankful to Mr. Radheyshyam and Mr. Vinay Dwivedi and all other laboratory staff for their cooperation and help in my laboratory work. Without them it would have been extremely difficult to successfully complete my experiments.

The unbound love and affection of my parents and younger sister Mou, can never be expressed in words. I have no words to express my gratitude to their caring support and encouragement throughout my life.

My stay at IIT Kanpur has been most memorable, thanks to Arindam, Kousikda, Paritosh, Pushpen, Saikat, Subhatosh. I am really thankful to them for the quality time I have spent with them. I am indebted to Hemant, Kaustubh, Goutam and Dipti Ranjan Sahoo for the discussions and unconditional help provided to me at various stages of my M.Tech. program.

Finally a note of appreciation is extended to all those who helped in one way or the other during this research.

<div align="right">Samaresh Paikara</div>

TABLE OF CONTENTS

Chapter 5   47

FINITE ELEMENT RESULTS AND COMPARISON WITH EXPERIMENTAL VALUES   47

Chapter 6   51

SUMMMARY, CONCLUSIONS AND FUTURE RESEARCH NEEDS   51

References   56

Tables   59

Figures   70

LIST OF TABLES

LIST OF FIGURES

LIST OF SYMBOLS

E_m	Modulus of elasticity of masonry
f_{bc}	Mean compressive strength of the masonry blocks
f_m	Compressive strength of masonry
f_{mor}	Mean compressive strength of the mortar
G_m	Shear modulus of masonry
H_u	Ultimate strength of wall
H_1^+	Lateral forces corresponding to first cycle displacement excursion level in positive direction
H_1^-	Lateral forces corresponding to first cycle displacement excursion level in negative direction
K	A factor which depends on the selected type of masonry block
K_i	Cycle stiffness
K_y	Initial stiffness of the wall
V_u	Shear resistance of wall specimens or peak ultimate shear load during a test
Δ_1	Average first cycle displacement
Δ_1^+	First cycle displacement excursion level in positive direction
Δ_1^-	First cycle displacement excursion level in negative direction
Δ_u	Ultimate displacement
δ_u	Ultimate ductility indicator wall specimen
δ_u	Working ductility indicator wall specimen

Chapter 1

INTRODUCTION

1.1 Motivation

The focus of many research and development activities in earthquake engineering has been on reducing seismic vulnerability of structure through development of newer materials of higher strength and using them economically in large structures, which can safely resist environmental loads and fulfil their functional requirements. However, this trend of research ignored low and medium rise buildings in which the common man dwells. People have moved from their age old traditional methods and materials for building construction to modern materials like steel and reinforced concrete to get strong and cost effective buildings which can resist earthquakes; but several issues of concern still remain. The recent earthquakes of Bam (Dec. 2003), Bhuj (Jan 2001) and Turkey (1999) have brought into focus some of the issues and necessitates that, we look back at our traditional ways of construction. At the same time we should bear in mind that it is not so much of the problem associated with the new age construction materials, but it is the problem associated with the building delivery process and construction practice followed.

Many traditional building construction practices exist in different parts of the world incorporating the concept of earthquake resistant design. However, no refinements on these age-old technologies or scientific studies on these vernacular, simple construction methodologies have been performed which have proven to perform better in deadly earthquakes. We can get some knowledge or clue from our traditional method of construction which can enrich our construction practices with modern materials.

For example, Timber-laced masonry construction has been in practice over years in different parts of the world by different communities. Depending on geographical location and availability of different raw materials some of the features have changed

1

but the basic features have remained unaltered. The construction practice is known as *half-timbered* in Britain, *fachwerk* in Germany, *colombage* in France, *dhajji-dewari* in Kashmir (India), *hımış* in Turkey, *pombalino* and *gaiola* construction in Portugal. In this type of construction the timber frame remains an important element by serving as the armature for the masonry infill. The main advantage of this type of construction is its large ductility and energy absorbing capacity during horizontal shaking. The basic principle in this weak, flexible frame with masonry infill construction is that there is no strong and stiff element to attract the full lateral force of the earthquake. The effectiveness behind this kind of design lies in the fact that the structure need not be designed for large lateral forces as they do have sufficient lateral deformation capacity to achieve a ductile response. When this type of structures are subjected to earthquake, they sustain incremental low level cracking which is distributed throughout the wall by the interaction of the timber structural elements with the confined masonry infill.

It is clear that the confinement of masonry into smaller panels and sliding motion of masonry infill along the panel faces and the cracks are the key to high energy dissipation capacity of this type of structures and it is possible to make a ductile structure using brittle material like masonry. The emphasis of the present work will be towards the investigation of energy dissipation capacity and ductility of this kind of confined small panel infill masonry and obtain results in parametric forms.

1.2   Summary of Justification for the Research

Recent Indian earthquakes, especially the 2001 Bhuj earthquake, have vividly demonstrated seismic vulnerability of a large number of masonry buildings, particularly the existing Unreinforced Masonry (URM) buildings. Such URM buildings, designed only for gravity forces and not for lateral forces, represent challenging engineering problems in hazard mitigation. Despite the fact that URMs constitute the majority of the building stock in the country, little has been done in the way of developing new techniques to enhance their earthquake resistance. There is an urgent need to develop a system of masonry elements which can make the buildings to meet acceptable performance limits during earthquakes.

The panels of URM walls can be confined by a grid of horizontal, vertical and/or diagonal elements which break a large wall into smaller wall areas confined

adequately by surrounding grid elements at the boundaries. The confinement of URM walls inside a reinforced concrete frame (i.e., infilled walls) has been shown to be more effective than unconfined masonry in resisting lateral loads due to earthquakes. However, the confining effect is significantly reduced in large walls and in the presence of openings. This technique in various forms is present in traditional masonry construction of many seismic active regions of the world.

Conventional earthquake resistant design of structures relies on energy dissipation potential of well detailed portions and/or members of structures which undergo large but controlled inelastic deformations during earthquakes. Cracking in masonry is not antithetical to the conventional earthquake resistant design philosophy, but it must be controlled in such a way that the cracked masonry does not seriously undermine the vertical load carrying capacity of the URM wall. Confining masonry in small patches by grid elements not only distributes cracking (inelastic activities) through out the URM wall but also help greatly improve their dynamic stability in the out of plane direction.

1.3 Objectives and Scope of the Study

The focus of the present study is to investigate the effect of different confinement schemes for enhancing the lateral load resistance of brittle and weak URM walls. The primary objective is to experimentally evaluate the lateral in-plane load resistance behaviour of different confinement schemes by grid elements. URM walls with various patterns of grid elements have been fabricated with due consideration of the ease of construction. For investigation of the behaviour of such confinement schemes both analytical and experimental works have been carried out. The material chosen for the grid elements in experimental studies is RC and analytical studies have been done on both RC and timber grid elements. The analytical work has been carried out by Finite Element Model using the FEA tool ABAQUS. To simulate the actual behaviour of the confined masonry in the analytical model extensive material tests for masonry have been done. In the present study in-plane deformations of URM wall panels and grid elements have been monitored and their overall shear resistance been measured.

The experimental work involves slow cyclic test on wall specimens. These slow cyclic tests give the information to understand the behaviour of the structure in nonlinear

3

range. The series of tests help to evaluate the load resistance mechanism, failure/damage pattern and the hysteretic behaviour of the proposed confinement schemes. These tests will provide the data for developing suitable design procedures for proportioning various elements of the confinement system. Tests show the mechanism and effectiveness of the measures in improving the seismic response of masonry structures. Supplemental tests on masonry materials and grid elements are performed.

The analytical work involved a parametric study for sensitivity analysis of various design variables controlling energy dissipation potential of confined wall systems. These analyses can help in finding out a design methodology for this kind of construction.

1.4   Organization of the Dissertation

This dissertation is organized in six chapters. Chapter 2 reviews briefly past researches in in-plane shear resistance of URM, URM with RC frame, and traditional confined masonry construction. Chapter 3 describes the analytical studies using finite element approach. In this chapter the modelling approach used is explained in detail, lateral load resistance behaviour of the confined masonry system is described and some parametric study is done based on the proposed model. In Chapter 4 the details of experimental study involving design and fabrication of test specimen, experimental setup and test procedure is recorded. Chapter 5 deals with the load-deformation relation predicted from the analytical model and compared with the experimental results. Finally, in Chapter 6, the summary, conclusions of this study and recommendations for future study are presented.

Chapter 2

LITERATURE REVIEW

2.1 Introduction

A review of existing literatures on masonry research shows that most of the effort has been directed towards the masonry as infill material or reinforced masonry walls. Not much scientific investigation has been carried out on confined masonry walls. Some researchers have reported a few unique properties of this type of construction from the experiences they had from the post-earthquake reconnaissance. Their reconnaissance revealed better overall response of traditional confined masonry construction than non-engineered RC and URM buildings made with modern day materials like high strength mortar, reinforced concrete and steel. A summary of research works particularly related to the in-plane behaviour of unreinforced masonry walls and modelling of masonry will be presented in this chapter.

2.2 Lessons learnt from the Traditional Construction Techniques

In the recent earthquakes of Bam (2003) and Turkey (1999), which observed high death toll, damages and collapse occurred to contemporary non-engineered buildings rather than traditional ones. The problem lies in the amalgamation of old traditional technology practiced in non-engineered construction earlier and today's non-engineered construction practice with high strength materials. Partial introduction of modern materials and systems in the construction process have rendered adverse results in the lateral load resistance capacity of those non-engineered modern buildings.

Post-earthquake reconnaissances have pointed out the seismic deficiencies in the non-engineered reinforced concrete structural system consisting of moment frames with masonry infill walls. The moment frames relied on the strength of the beam-

column connections to resist deformation and collapse in case of earthquakes. Inadequate strength and ductility in the frame joints led to the collapse during earthquakes. For the infill walls the weaker masonry elements were bonded together by stronger mortars without any intervening studs. Diagonal shear cracking through the weaker masonry units was predominant mode of failure and there was less or no chance of sliding at the interface of the masonry units or panel walls (Langenbach 2002).

Whereas, traditional confined masonry construction practiced from the historical time had some basic provision for lateral load resistance. The key to the high energy dissipation capacity of traditional timber laced confined masonry is the working of the infill along the joints between the infill and the timber frame; the straining and sliding of the masonry and timbers dissipates a significant amount of energy during earthquakes. Sliding along the bed joints is encouraged by the use of weak masonry and it delays the chances of cracking through the masonry units when masonry panels are deformed. This helps in better dissipation of energy and also reduces the incompatibility between rigid masonry panels and the flexible timber frame.

Turkish-Ottoman style of construction practice is such a traditional method of construction having earthquake-resistance features with timber lacing in the masonry walls. The basic features of this timber laced masonry construction are (a) the use of horizontal timbers embedded into bearing wall masonry, and (b) the insertion of masonry in between columns, beams and studs of a complete timber frame. This kind of construction where, masonry infill is primarily brick or rubble stone is referred as hımış in Turkish. Presence of timber studs, which subdivides the infill, arrests the loss of the portion or all of several masonry panels and resisted progressive destruction of the rest of the wall. The closely spaced studs prevent propagation of diagonal shear cracks within any single panel, and reduce the possibility of the out-of-plane failure of masonry (Gülkan and Langenbach 2004).

Similar study has been conducted on Portuguese traditional masonry building known as *pombalino*. These buildings were built in Lisbon downtown after the 1755 Lisbon earthquake to mitigate the loss of human life in case of earthquakes. While analysing structural details of those buildings it showed that aseismic provisions in the *pombalino* building were imparted mainly by inclusion of interior three

6

dimensional braced timber structure named *gaiola*. *Gaiola* was enclosed in masonry walls above the first floor for providing resistance to horizontal forces. Numerical model of two buildings, one with *gaiola* structure embedded within masonry and another without it showed that the *gaiola* structure increased the stiffness. Frequencies of the buildings with *gaiola* structure were higher than those obtained from the buildings without *gaiola* structure. According to the modal configurations observed for both buildings, the presence of *gaiola* prevented local vibration modes of the masonry structure. Local vibration modes were prevented because the out of plane displacements of each of the masonry walls (facades and masonry walls between adjoining buildings) no longer occurred independently from the rest of the structure. Out of plane displacements were equal for parallel masonry walls connected by the same *gaiola* wall. Local displacements were reduced by almost 70% due to the presence of *gaiola* walls. It was inferred that *gaiola* has a balancing function and building resistance to horizontal forces increases when compared to a same kind of construction except the presence of *gaiola*. The hysteretic energy dissipation capacity of *gaiola* enclosed masonry was improved due to the gaps between the timber elements and the crack opening in masonry. The presence of steel connectors at the connection between timber elements increased the ductility. Fundamental collapse mechanisms of the masonry buildings were also recognised, which were the out of plane failure movement or in-plane shear failure at ground floor level which can lead to a global failure mechanism. Low tensile strength and low shear strength of the masonry were the cause of these problems (Cardoso, Lopes and Bento 2004).

It was found that walls confined with horizontal and vertical reinforced concrete elements, bond beams and tie columns around the perimeter were included in the reconstruction of some cities that were destroyed in earthquakes such as Messina, Italy (1908). The initial objectives of the confining elements were to tie the walls, floors and roof together and to provide out of plane strength as well. The usage of confining elements in walls increased over the years in non-engineered construction due to its satisfactory performance under successive moderate and intense earthquakes. Usage of this kind of construction can be found in plenty in southern Europe and Latin America. The system was adopted in Mexico City in 1940 to control the wall cracking caused by large differential settlement in the soft soil area

7

but later it became popular in the other parts also due to its excellent seismic performance (Meli and Alcocer 2004).

2.3 Research on Unreinforced Masonry

Research has been performed based on different lines of thought to analyse masonry structures. The modelling of masonry has been performed based on no-tension constitutive laws, time independent incremental elasto-plastic models and use of limit analysis concepts. Following that way of research the modelling of masonry has been done based on damage mechanics model in association with plasticity laws. Prototype and model masonry specimens have also been tested to investigate the different behaviours of the URM and accordingly analysis schemes have been modified.

Magenes and Calvi (2002) pointed out the principal failure mechanisms of masonry piers subjected to seismic actions as following: (a) Rocking failure, in which with increasing horizontal load or displacement demand, bed joints crack in tension and shear is carried by the compressed masonry. The final failure is obtained by overturning of the wall and simultaneous cracking of the compressed corner which can give large deformation capacity. The energy dissipation potential by this method is related to drift and drift should be regulated to prevent non-structural damage. (b) Shear cracking, in which peak resistance is governed by the formation of inclined diagonal cracks. Inclined diagonal cracks may follow the path of bed and head joints or may go through the bricks, depending on the relative strength of mortar joints, brick mortar interface and bricks. Ultimate deformation capacity in this type of failure mechanism is very stable. However, the quantification of ductility is very much scattered even in same type of models using same materials. (c) Sliding is a failure mechanism in which potential sliding planes can form along the cracked bed joints due to the formation of tensile horizontal cracks in the bed joints when it is subjected to reverse seismic action. This failure mode is observed in case of low level of vertical loads and/or low friction coefficients. Though this mechanism can provide large energy dissipation by means of large deformation capacity but it is not suitable due to associated non-structural damages. It is also not found as a sole mechanism as it is often associated with other failure mechanisms. Figure 2.2 shows the schematic diagram of all these failure mechanisms.

2.3.1   Analytical Modelling of Unreinforced Masonry

The modelling of masonry is somewhat different than other materials due to its heterogeneous nature, orthotropic mechanical characteristics and much dependency on the interaction between its constitutive materials, e.g., brick and mortar. The masonry modelling can be done either as a heterogeneous model having discrete presence of brick and mortar or a homogeneous model based on a fictitious equivalent homogeneous material. Within each category damage and failure models can be done in two ways namely discrete crack approach and smeared crack approach. The smeared crack approach has the advantage over the discrete crack approach as it is computationally less expensive than the other as it considers the crack material as a whole equivalent continuum, over which the cracks are not localised but continuously distributed. Whereas, the discrete crack approach describes a new geometry for opening and closing of cracks thus making it cumbersome to model real masonry structures (Bull, 2001).

Masonry can be considered as a composite material that consists of units and mortar joints. The way in which the properties of the unit, mortar, and the unit mortar interface are represented in the model depending on those different modelling strategies can be followed (Lourenço 1996). The possible modelling strategies can be as followed:

1. Ideal modelling: each physical unit of masonry is represented by the mechanical properties of the unit material and mortar also has its mechanical property (Figure 2.1 a).

2. Detailed micro-modelling: units and mortar in the joints are represented by continuum elements whereas the unit-mortar interface is represented by discontinuous elements (Figure 2.1 b);

3. Simplified micro-modelling: expanded units are represented by continuum elements whereas the behaviour of the mortar joints and unit-mortar interface is lumped in discontinuous elements (Figure 2.1 c);

4. Macro-modelling: unit, mortar and unit-mortar interface are smeared out in the continuum (Figure 2.1 d).

For modelling unreinforced masonry, several researchers have used macro modelling. In this kind of modelling masonry is modelled as a composite material consisting of brick and mortar joints. Masonry was assumed to be a homogeneous material which had a relation between average stresses and strains (Chuang et al. 2004).

Giordano *et al.* (2002) conducted analytical studies on URMs with different analytical techniques and provided a brief description of merits and demerits of different techniques. The role of interface elements was investigated by applying "Finite Element Method (FEM)" with and without interface elements. While doing FE analysis masonry was considered as a homogeneous material and both micro modelling and macro modelling were considered. Micro modelling considered sliding at joints, crack propagation at the cost of a large number of elements whereas in case of macro modelling, a single element reproduced an average behaviour depending on homogeneous continuum model where topology of the structure controls the meshing. Analysis by "FEM Discontinuous Elements (FEMDE)" technique was introduced to consider the effects of the interface elements where blocks were modelled with linear or non-linear conventional continuum elements and the mortar joints were simulated by interface elements. It was concluded that block mesh and joint mesh must be connected together, so that they can be compatible and for meeting this interface joints are to be identically located. The joint elements have the limitations in their behaviour due to applicability in small displacement fields only due to problem of re-meshing and updating of contacts in case of large displacement fields.

The work done by Gambarotta and Lagomarsino (1997) regarding modelling of shear failure of solid brick masonry, described masonry as a layered material, whose properties were derived from brick and joint properties via homogenisation procedure. Scalar damage variables were used to reproduce the mechanisms like opening of bed joints, sliding of bed joints, shear failure of bricks and crushing of masonry in compression. The model simulated behaviour of brick masonry with weak mortar joints, typically found in old masonry constructions, in a reasonable way. The model was later verified by analysing the lateral response of brick masonry shear walls loaded in-plane either by cyclic horizontal actions superimposed on vertical loads or dynamic loads, which was representative of

10

seismic actions. In the finite element modelling of large scale structures by this model four noded finite isoparametric models were used giving due consideration to the complexity of the constitutive equations and position of mortar joints in horizontal plane. It had been also noted that smaller brick size in comparison to the wall or pier size increased the reliability of the homogenisation model. The work also included sensitivity analysis of model parameters which were related to elastic response, inelastic response of mortar joints and inelastic response of the bricks. The influence of the elastic moduli was found important in the phase preceding the limit strength of the wall until the inelastic strain are negligible. It was pointed out that parameters modelling mortar joint have a significant role on the response of the walls, as more significant damage and failure mechanism of brick masonry walls under seismic action take place in the mortar joints. Such parameters are: the friction coefficient, the tensile and shear strengths, the tangential inelastic compliance and the softening parameter. The tensile strength of the joints has little influence on the global influence and is applicable mainly to slender piers.

2.3.2   Modelling Unreinforced Masonry by FEM

The numerical modelling of masonry through the FEM is a computationally demanding because of extensive non-linear behaviour of constituent materials. Along with that, lack of experimental data has increased the uncertainty involved in using different numerical modelling schemes. Here some of the previous research work is being presented where masonry has been modelled by FEM and the results have been compared with either experimental data or the results from some other modified techniques.

Mandara and Scognamiglio (2003) used FEM techniques for modelling collapse behaviour of confined masonry. ABAQUS was used for modelling and material option *CONCRETE for representing masonry. The reasons behind using *CONCRETE was accurate reproduction of progressive development of cracking, the consequent tension stiffening effect and the actual shape of the interaction domain at failure. Though masonry had more non-homogeneity than concrete due to block to mortar interface it was used in case of small sized blocks with good quality mortars and assumed isotropic nature as much as possible.

11

Rai (1996) used FE approach to model unreinforced masonry and ABAQUS was used as the FE program. A two dimensional continuum in the state of plane stress was considered for all the masonry. Discretization of the masonry was done by square sized, 4-noded isoparametric CPS4 type element of the ABAQUS element library. The material behaviour of the masonry was modelled with the material option *CONCRETE. Material option *CONCRETE covers most of the characteristics of a brittle material in terms of its non-linear stress-strain relationship, cracking and failure.

Giordano *et al.* (2002) used ABAQUS *CONCRETE model to investigate the behaviour of part of the coloisters facade of the "Sao Vicente de fora" monastery in Lisbon. The results were supplemented by analysis results using "FEM Discontinuous Elements" and "Discrete Element Methods" and also experimental results. A fixed multi-crack model based on a simple yield surface with isotropic hardening and associated flow was considered, when the state of stress is predominantly compressive. Damaged elasticity model was used to account for cracking. It was concluded that proper material definition can ensure good model of masonry using *CONCRETE elements under monotonic loading. Experimental data was used in FEM model to define material characteristics as far as stress-strain curve is concerned. Meshing had been done using S8R thick shell elements with increased number of integration points through them.

2.3.3 Material Characteristics for Numerical Modelling

For a successful numerical model, material characteristics are the data of high importance. The most important of them are modulus of elasticity, Poisson's ratio, Shear modulus, compressive strength and tensile strength. There are no standard data for these characteristics due to variability and non-standard nature of the material. Normally these parameters are estimated by combination of analytical, semi-empirical and experimental results.

1. Modulus of Elasticity and Poisson's Ratio:

Various researchers have suggested different expressions for the modulus of elasticity (E_m) and all of them are related to compressive strength of the masonry (f_m). Eurocode-6 (1988) suggested $E_m = 1000 f_m$ for limit state analysis and

$E_m = 600f_m$ for limit state of serviceability. Hendry (1998) suggested $E_m = (400 \sim 600)f_m$ for secant modulus of elasticity and $E_m = (570 \sim 800)f_m$ for tangential modulus of elasticity. In a recent work (Kaushik, 2004) the modulus of elasticity has been found as $E_m = (250 \sim 1100)f_m$ and the proposed value of elasticity modulus is $E_m = 550f_m$. The typical range of Poisson's Ratio (ν) taken by many researchers is 0.10 to 0.20 (Bull, 2001).

2. Shear Modulus

The shear modulus can be estimated by the formula $G_m = E_m/2(1+\nu)$. Eurocode-6 (1988) has suggested $G_m = 0.4E_m$ for shear modulus.

3. Compressive and Tensile Strengths

Though the compressive strength of masonry can be evaluated by the prism test, several empirical relations exist which depend on type and strength of mortar and masonry units. The relation given in Eurocode-6 (1988) is $f_m = K \cdot f_{bc}^{0.65} \cdot f_{mor}^{0.25}$ where, f_{bc} is the mean compressive strength of the masonry blocks and f_{mor} is the mean compressive strength of the mortar and K depends on the selected type of block. Same type of relation was found from work of Kaushik (2004) based on experimental data with four different brick types and three different mortar types. The relation was $f_m = 0.63 \cdot f_{bc}^{0.49} \cdot f_{mor}^{0.32}$ where, the meaning of the variables are same as above. Bull (2001) suggested the compressive strength of masonry as the minimum of $\sqrt{f_{bc}}$, $\sqrt[3]{f_{bc}}$ and $\sqrt[4]{f_{mor}}$. In all the cases above, values of f_{bc}, f_{mor} are to be experimentally evaluated.

2.4 Experimental Modelling of Unreinforced Masonry

In general structural model has two main objectives. Firstly, they may be constructed and the experimental information gathered by testing may be used to confirm theoretical analysis. Secondly, this investigation could be utilised to analyse and provide calculations for the design of a prototype structure. In certain situations, where within the current provision and resources to conduct theoretical analysis,

analysis proves impossible then model analysis can be directly used to design the original prototype (Noor and Boswell, 1992).

Direct models of masonry structures require the use of materials to simulate the compressive and tensile strengths of the mortar along with the size effect of the stressed volume. Along with that these models being miniature of prototypes, require construction techniques that should be as close as possible to that of original prototypes. The success of direct model of this kind depends upon the degree of accuracy with which the relevant prototype properties and loading and boundary conditions are simulated (Harris and Sabnis, 1999). The scale of a model should be as large as possible but practical laboratory constraints dictate the model size. The behaviour of building elements or sub-assemblages under seismic conditions is governed by the effects of large amplitude, post yield reverse deformations on some critical regions. Seismic actions are normally dependant on the decreasing stiffness and the available ductility of building elements. The integrity of the structure is governed by the available strength after degradation due to cyclic loading. However, till date these fundamental structural characteristics are not easy to introduce in analytical treatments which are supplemented by laboratory experiments on small or large scale models tested under consecutive low rate cyclic deformations. Actuators are normally used in order to impose cyclic displacements at selected points of the model (Noor and Boswell, 1992).

Researchers have tried to derive a relation between the compressive strength of masonry and the compressive strengths of its individual components, units and mortar. However, regarding advanced numerical modelling, these procedures are not very interesting since they do not provide any other information besides the initial stiffness and compressive strength of masonry. Therefore, masonry prisms have to be tested under displacement-controlled experiments (Hendry, 1998).

2.5 Summary

Various analytical and experimental studies are summarized in this chapter, which show the behaviour of unreinforced masonry under static as well as dynamic lateral loading. Most of the research work is directed towards the engineered structures like infilled frame or reinforced masonry or unreinforced masonry. Not much amount of scientific information is available on the non-engineered construction practice as

14

discussed already which have performed fairly good in the past earthquakes. It is time to investigate, if it is possible to improve the non-engineered structures to life safety standard by adopting some simple techniques. The technology is drawn from history; the concept is not new, only research is needed to find out how to achieve ductility and energy dissipation out of it. Research is needed to find some optimized proportion or material to be used to achieve our goal towards making the structure perform better in case of horizontal shaking.

Chapter 3

ANALYTICAL INVESTIGATION OF THE CONFINED MASONRY WALLS

3.1 Introduction

Analytical studies of in-plane shear behaviour of confined masonry wall panels were undertaken. Finite Element (FE) approach was adopted to provide information at the microscopic level and to ascertain the key parameters which govern the load-deformation behaviour of the confined masonry wall as a whole system. Inhibitory computational cost and complexities involved with FE analysis for cyclic excitation restricted the study to only monotonic loading. However, this curtailed scheme of analysis is capable of providing essential load deformation behaviour of the confined masonry walls. Limitation of this FE modelling is that, it is incapable of handling the strength and stiffness degradation associated with reverse cyclic loading, which is associated with typical earthquake type motion.

A general purpose finite element program, ABAQUS was used for FE analyses. The program is capable to handle the nonlinearities expected in a complex system of masonry and its confinement. In the modelling approach masonry was in macroscopic level. However, the interaction between the different constituents of the confinement system and the interaction between the masonry and its confinement was done in microscopic level. Thus, the model provides the insight of the interaction between the various component of the whole system and stress-strain condition in them.

The model may not follow the behaviour of a real structure exactly; the reason behind this can be that many of the analysis input parameters describing material properties of the constituent elements of the FE model are not same all over the structure. For brittle materials such as brick masonry, most of these parameters exhibit a high degree of variability. Along with that, many assumptions regarding

the description of geometry, boundary condition, interaction between elements and load application involved gross simplification for the sake of modelling. A high degree of refinement in the FE model relative to these factors is not warranted. In fact walking on that path can lead to a false sense of confidence in the analysis results.

3.2 Finite Element Idealization and ABAQUS Modelling

The test specimens were differentiated into a mixture of different finite elements. A two dimensional continuum in the state of plane stress was considered for the masonry portion. Two dimensional linear elements were used to model the grid elements of the confinement schemes. The discretization of masonry was done by 0.05 m square sized, 4-noded iso-parametric CPS4R type elements of ABAQUS element library. Standard beam element of type B21 was used to model the confining grid elements.

The appropriate boundary conditions were achieved by either deleting or constraining relevant nodal degrees of freedom of various elements. All the degrees of freedom of the nodes in bottom most elements were deleted in order to simulate a fixed boundary condition. Connections between confining elements were modelled as hinge joint with rotational springs to specify their moment-rotation behaviour. However, the translational movement between the different confining grid elements was restricted. This simplification will have little effect on the load deformation relation. The main concept behind the new confinement scheme is presence of high energy dissipating capacity due to friction at the interface of the masonry and confining grid elements. Appropriate description of the interface between the confining grid elements and masonry modelled the frictional behaviour at the interface. However, due to complicacy in the interface modelling between the each masonry unit and mortar each masonry panel was modelled as a single unit. This simplification will not act upon the behaviour of the system as a whole, as the modelling of a masonry panel as a single part is capable of taking care of the cracks and deformation in the masonry.

Regarding the loading, the models were subjected to a fixed vertical loading to take care of the roof and the upper storeys if present and subsequently applied lateral

displacements. The FE models were subjected to monotonically increasing rather than cyclic lateral displacement at the top horizontal confining element.

3.3   Material modelling in ABAQUS

ABAQUS supports a large element library which can handle wide variety of materials. Out of many options which are available in ABAQUS library, options *ELASTIC and *CONCRETE were used for modelling brittle materials, like masonry and concrete. Options *ELASTIC and *PLASTIC were used for modelling materials, like steel and timber. Under these main options there were various sub-options and parameters associated with them to take care of the different properties of materials. The options, sub-options and parameters used in this study are described below:

3.3.1   Option *ELASTIC

In the elastic regime, all the materials (masonry, steel, concrete, timber) were modelled to behave as an isotropic elastic material. The two required constants were Young's modulus and Poisson's ratio. For the preliminary investigation two different types of masonry were used: (a) Masonry-1 was a weak masonry made of 100-year old reclaimed bricks with PCL (portland-cement, hydrated lime and sand) mortar of proportion portland-cement: hydrated lime: sand of 1:1:6 and (b) Masonry-2 was a strong new brick masonry with bricks available in Kanpur (India) and its vicinity with mortar of proportion portland-cement: sand of 1:3. The properties of above masonry were taken from two previous research works on masonry structures (Rai 1996, Kaushik 2004). Young's modulus for Masonry-1 and Masonry-2 were 950 MPa and 4510 MPa, respectively obtained from several compressive tests on brick prisms. The value of Poisson's ratio taken for all the masonry was 0.2. For timber Young's modulus and Poisson's ratio were 20 GPa and 0.25, respectively.

3.3.2   Option *PLASTIC

Beyond the elastic regime, the material behaviour of steel and timber was modelled with the material option *PLASTIC. This option is generally used to specify the plastic part of the material modelling for elasto-plastic materials. The parameters of the option *PLASTIC define the tensile stress strain relationship. The curve used for timber used in confining grid element of the model is shown in Figure 3.1.

3.3.3   Option *CONCRETE

Beyond the elastic regime, the material behaviour of the masonry and concrete was modelled with the material option *CONCRETE which is used to define the properties of plain concrete outside elastic range. Researchers have used this option to model masonry material with satisfaction (Rai 1996, Ghosh and Amde 2002, Mandara and Scognamiglio 2003). The option *CONCRETE is capable of handling most of the characteristics of a brittle material pertaining to its nonlinear stress-strain relationship, cracking and failure. The cracking behaviour of this kind of material is incorporated in the model in form of smeared crack propagation. The FE model calculates the constitutive relations at each integration point instead of tracking each individual macro cracks (Rai 1996). The effect of presence of crack is incorporated by means of modification of stress and material stiffness for the cracking at the integration points. The onset of cracking is defined by a "crack detection surface," which is a simple coulomb line expressed in terms of the first and second stress invariants. When the stress state reaches this surface, cracking is initiated. Damaged elasticity is then used to describe the post-failure behaviour with open cracks.

The parameters of option *CONCRETE define the compressive stress-strain relationship, even beyond the ultimate stress, by specifying the pairs of compressive stress and the corresponding plastic strain. The curves used for Masonry-1 and Masonry-2 are shown in Figure 3.2 and Figure 3.3, respectively. These curves are the simplified curves consisting of several straight line segments obtained from the observed behaviour of the prisms under compression. The three sub options associated with *CONCRETE are:

A. *FAILURE RATIOS

The *FAILURE RATIOS suboption describe the shape of the failure surface by specifying the ratios of ultimate strengths and strains in various stress states. The inputs are: a) Ratio of the ultimate biaxial compressive stress to the uniaxial compressive ultimate stress. b) Absolute value of the ratio of uniaxial tensile stress at failure to the uniaxial compressive stress at failure. c) Ratio of the magnitude of a principal component of plastic strain at ultimate stress in biaxial compression to the plastic strain at ultimate stress in uniaxial compression. d) Ratio of the tensile principal stress value at cracking in plane

19

stress, when the other nonzero principal stress component is at the ultimate compressive stress value, to the tensile cracking stress under uniaxial tension (Hibbit *et al.* 2003). The ultimate biaxial compressive stress and plastic strain were taken as 1.12 and 1.33 times the uniaxial compressive ultimate stress and plastic strain, respectively. These are the values used by the previous researchers in this field (Giordano *et al.* 2002). The ratio of the uniaxial tensile stress to ultimate compressive stress was taken as 0.08 in Masonry-1 and Masonry-2. This was assumed to be 0.1 for the concrete used in the confining grid elements of experimental specimens and 0.08 for masonry in all cases. This tensile strength corresponds to the bond strength at the brick unit-mortar interface, when the failure is due to the debonding under a tension normal to the bed joint. The last parameter, the tensile principal stress at cracking, when the other principal stress component is at the ultimate compressive stress was assumed to be 0.28 times the tensile cracking stress under uniaxial tension.

B. *TENSION STIFFENING

The postfailure behaviour for direct straining across cracks is modeled with the *TENSION STIFFENING option, which allows the user to define the strain-softening behaviour for cracked masonry or concrete. This option is used to define the retained tensile stress normal to a crack as a function of the deformation in the direction of the normal to the crack. Unfortunately, not much information is available on this parameter for unreinforced masonry. This sub-option was originally intended to simulate the interaction effects of reinforcing bars with concrete, to smear the cracking over the finite volume represented by an integration point, and to reduce the mesh size effect on the prediction of the cracking. The choice of tension stiffening parameters is important in ABAQUS/Standard since, generally, more tension stiffening makes it easier to obtain numerical solutions. Too little tension stiffening will cause the local cracking failure in the concrete to introduce temporarily unstable behavior in the overall response of the model. In this study, all simulations were performed with tension stiffening, which is described by the long and slow descending part of the tensile stress-strain curve of the

masonry. A total strain of 0.2 was chosen to represent the tensile stress ranging from failure to zero.

C. *REBAR

Reinforcement in concrete confining elements are defined with the *REBAR option. Rebars are one-dimensional strain theory elements (rods) that can be defined singly or embedded in oriented surfaces. Behaviour of the rebar material is defined with metal plasticity models and these rebars are superposed on a mesh of standard element types used to model the concrete. With this modeling approach, the concrete behavior is considered independently of the rebar. Effects associated with the rebar-concrete interface, such as bond slip and dowel action, are modeled approximately by introducing some "tension stiffening" into the concrete modelling to simulate load transfer across cracks through the rebar which has been mentioned earlier. Defining the rebar can be tedious in complex problems, but it is important that this is done accurately since it may cause an analysis to fail due to lack of reinforcement in key regions of a model.

3.4 Steps of the Analysis in ABAQUS

The loading was applied in two steps. The first step applies a static vertical loading to simulate the effect of the weight of the slab and the loads coming from the upper stories if present. The second step the monotonically increased lateral displacement. Applied load and boundary conditions used for analysis are shown in the Figure 3.4.

3.4.1   Step I: Initial

This step was meant for the simulating initial condition when no load was applied and boundary conditions and contact behaviour are specified in this step. A fixed boundary condition was specified by means of assigning all degrees of freedom of the nodes situated at the base to zero.

3.4.2   Step II: Vertical Static General load

In this static load step vertical loading was applied and inertia effects were ignored. Vertical concentrated loads were applied at some closely spaced nodes situated at the top most layer of the FE model. The material non-linearity as well as geometric

nonlinearity was taken into account. In all the models a constant vertical loading is maintained in such a fashion that a constant vertical pressure of 0.1 MPa is applied.

3.4.3   Step III: Lateral Static Riks load

The main objective of this step was to determine the lateral load displacement response of the specimen even beyond the elastic limit of the constituent materials. This step is a push-over analysis step in which lateral loads or displacements were incremented as structural members deform beyond their elastic limit. The lateral loads or displacements can be applied in a predetermined pattern. The intended result of the analysis is a push-over curve, which is a plot of base shear vs. top-level displacement. The curve represents the lateral load carrying capacity of the structural system. The analysis was performed by means of static "RIKS" method. In a non-linear analysis, the solution can not be calculated by solving a single system of linear equations, as done in case of a linear problem. Instead of that approach, the solution is found by specifying the loading as a function of time and incrementing time to obtain a nonlinear response. Therefore, ABAQUS breaks the simulation into a number of time increments and finds the approximate equilibrium configuration at the end of each time increment. The "RIKS" method uses the load magnitude as an additional unknown; it solves simultaneously for load and displacements. Therefore, another quantity must be used to measure the progress of the simulation; ABAQUS uses the arc length along the static equilibrium path in load deformation space. The approach provides solutions regardless of whether the solution is stable or unstable. The solution is usually obtained as series of increments, with iterations to obtain equilibrium within each increment. The choice of increment size is a matter of computational efficiency; large increments require more iteration within each increment. In this analysis step option *NLGEOM was activated to take care of the second order effects.

3.5   Contact between Masonry and Confining Grid Elements

The interaction between the confining grid elements and the infill masonry due to applied load plays the most important role in the behaviour of this kind of confined masonry system. The infill is connected to the confining elements by mortar joint, which plays an important role in dissipating the energy during the seismic excitation.

The interface should be modelled such as it is capable of transferring normal and shear forces in the elastic and inelastic ranges of the loading. The contact problems between the confining elements and the masonry have been properly taken into account in order to take care of the possible slip phenomena. To serve this purpose the *SURFACE INTERACTION option have been used, assuming *SURFACE BEHAVIOR, NO SEPARATION, PRESSURE OVERCLOSURE = HARD. To model the frictional behaviour during the relative movement between the confining grid elements and the masonry, friction is used to model that behaviour. For that *FRICTION, SLIP TOLERANCE = 0.005 is used and the value of friction coefficient is used is 0.6. This value is chosen on the basis of experimental results available in various technical literatures (Rai 1996, Buonopane et al. 1999, Magenes and Calvi 2002).

3.6 Connections between the Confining Grid Elements

The connection between the different elements of the confinement scheme is modelled as hinge joints with attached rotational spring kind of connector elements. The connectors were modelled using option *CONNECTOR ELASTICITY, NONLINEAR, COMPONENT=6. The moment rotation relationship was used for D.O.F. 6 which is the rotation about the axis perpendicular to the plane of the structure. Again the option *CONNECTOR FAILURE, COMPONENT=6 was used to mark the ultimate moment or rotation value after which the restraint of the connection fails in any particular D.O.F. and for the present model it was again D.O.F. 6. The connectors have the same kind of moment rotation relation that of the joints between the elements of the confinement scheme. In both of analytical and experimental model steel sections are used to tie the different elements of the confinement scheme. Moment rotation relationship of that section is used in the analysis. The moment rotation relationship used to model the joints is shown in Figure 3.5.

3.7 Choice of Elements

For modelling unreinforced masonry Chuang et al. (2004) used four-noded bi-linear two dimensional plane stress element, CPS4R. In this analysis also the same elements were used. The justification for choosing this element instead of higher-order elements (such as 8 noded elements) is that the nonlinearity in masonry is not due to

non-linear stress-stain behaviour of masonry, rather due to progressive cracking, which can be sufficiently taken care of by relatively fine meshing.

3.8 Geometry and Details of the Specimens

For the analysis of usefulness of different confinement schemes over the URM several confinement schemes were tested. The dimension of all the walls was considered as 3 m × 3m (Length × Height). The cross section of the confining grid elements were 200 mm × 100 mm (Width × Thickness) and the thickness of the masonry was 200 mm. The wall was fixed at the base. For connections between different confining grids in all the models hinge type joints with attached rotational spring having moment rotation relationship as shown in Figure 3.5 was used.

3.9 Confinement Schemes in Different Specimens

Six different configurations of confinement schemes with two different masonry properties were analysed and wall thickness was 200 mm.

3.9.1 Confinement Scheme 1 (only boundary confining grid elements)

Confinement scheme 1 (only boundary confining grid elements) was the simplest among the all confinement scheme tested under this study. A regular grid pattern was used in this confinement scheme where the confinement density was least. The confinement scheme consisted of only boundary confining elements which confine the whole wall and h/t ratio of the panel was 14.0. The confinement scheme used is shown in Figure 3.6.

3.9.2 Confinement Scheme 2 (boundary and horizontal at mid height confining grid elements)

Confinement scheme 2 had some (boundary and horizontal at mid height confining grid elements) modifications over the confinement scheme 1, where h/t ratio of the panels were reduced to 6.75 by introducing a additional horizontal confining elements which further divided the panel and this specimen finally had two panels each of 2800 mm × 1350 mm. The confinement scheme used is shown in Figure 3.7. The idea behind using the horizontal confining elements was that it would help in delaying the diagonal cracking through the joints while loading the specimens.

3.9.3 Confinement Scheme 3 (boundary and cross confining grid elements)

In confinement scheme 3 (boundary and cross confining grid elements) h/t ratio of the panels were maintained 6.75 as previous but by introducing two additional vertical confining elements which further divided the panels and this specimen finally had four panels each of 1350 mm × 1350 mm. A regular grid pattern, where confining elements crossed each other in right angle was followed for this specimen. The confinement scheme used is shown in Figure 3.8. The idea behind using the horizontal and vertical confining elements was that it would help in delaying the diagonal cracking through the joints as well as the panel size will be reduced. Reduced panel size will increase the out-of-plane stability of the panels and due to its square shape each panel will be better stressed.

3.9.4 Confinement Scheme 4 (boundary and single diagonal confining grid elements)

Confinement scheme 4 had a non-regular grid pattern. This kind scheme can be used in exterior walls where opening for doors and windows are required. The confinement scheme used is shown in Figure 3.9. The h/t ratio was different in different portion of the panel due to the presence of the diagonal elements and whole wall was divided into 2 triangular pieces. The diagonal element was used to introduce a predefined slip surface to the masonry panels.

3.9.5 Confinement Scheme 5 (boundary and cross diagonal confining grid elements)

Non regular grid pattern was also used for the confinement scheme 5 (boundary and cross diagonal confining grid elements) where two diagonal elements crossed each other and this scheme had a symmetric behaviour in case of horizontal displacement in both the direction. The confinement scheme used is shown in Figure 3.10.

3.9.6 Confinement Scheme 6 (boundary and star confining grid elements)

In confinement scheme 6 (boundary and star confining grid elements) beside the peripheral confining elements one horizontal and four diagonal elements were used.

The confining elements divided the wall in to six triangular panels which is shown in Figure 3.11.

3.10 Results of FE Analysis

The finite element mesh for confinement Scheme 1 is shown in the Figure 3.12. Same kind of meshing was done for all other confinement schemes also. The models were initially loaded by a constant vertical load and then horizontal load was applied incrementally in several stages as said already. This incremental load was applied using a "Riks" algorithm of numerical solution for non-linear systems. All the models except the confinement scheme 4, being symmetric, load response and other parameters were checked for loading in one direction. For confinement scheme 4 the model was separately analysed for loading in the reverse direction also. The solution could not be carried out upto an ultimate load or until a failure is reached. Slow convergence in a particular loading increment prematurely terminated the analyses due to a severe cracking and non-linear activities in the model. Though the convergence tolerance was set to a lower value, it could not be met in successive iterations. The results are discussed on following parameters: load deformation behaviour, deformation capacity, stress-strain behaviour, stiffness, ductility etc.

3.10.1   Load Deformation Behaviour

Figure 3.13 and Figure 3.14 show the overall shear force-displacement behaviour of the different confinement schemes. The plots are nonlinear form the beginning with a nature of decreasing stiffness with increasing drift. The load deformation plot obtained did not have much drift under constant load or decreasing load portion which marks that the analyses could predict only upto the beginning of severe cracking. The load deformation relation during the action of dry friction between the morter bonds in opening and closing of the cracks was not part of the plots.

3.10.2   Deformation Capacity

The deformed shape of the different confined masonry models and unconfined masonry wall model of the same dimensions at the end of the analyses are shown in Figure 3.15 to Figure 3.30. Figure 3.15 to Figure 3.22 shows the deformed shape for models made with Masonry 1 (weak masonry) and Figure 3.23 to Figure 3.30 show the deformed shape for models made with Masonry 2 (stiff masonry). Figure 3.15

26

and Figure 3.23 show the deformed configuration of the unconfined masonry model where it is prominent that the most of the displacement is concentrated at the bottom layer of the masonry. The reason may be the failure was subjected to a huge tensile cracking in the tensile portion and compression crushing in the opposite direction. The behaviour is similar to a rigid body like overturning failure, which was being balanced by the self weight of the wall and the vertical load applied to it. Deformed configuration of the different confined masonry schemes are showing a better response in terms of the displacement even in case of higher story drifts. While comparing the similar models made with weak and stiff masonry it is found that drifts attained before accumulating severe cracking in the weak masonry walls are considerably higher than those of stiffer masonry. The reason can be though both the masonry had similar kind of tensile and compressive strength, the elastic modulus of stiffer masonry was around five times of weak masonry. Due to that stiffer masonry attained its tensile or compressive limits in smaller drifts.

3.10.3 Stress-Strain Behaviour

Figure 3.30 to Figure 3.76 show the stress distribution (shear stress and Von-Mises stress) and vector plot of the major principal stress in the masonry portion of the models. The plots show a prominent formation of diagonal struts in all the models. The struts had a variable width at different portion of the panels and were narrowest at the corners, where load was applied and the corner diagonally opposite to those. Figure 3.45 and Figure 3.61 show the shear stress contour plot of unconfined masonry wall where the failure mechanism is tensile failure in the bottom portion of load application side and formation of diagonal strut is very limited. From Figure 3.46 to Figure 3.48 and Figure 3.62 to Figure 3.64 the continuous increment of the participation of wall portion in diagonal strut is observed which indicates the incremental better behaviour of the confinement scheme form 1 to 3. Figure 3.49 and Figure 3.50 for Masonry 1 (weak masonry) and Figure 3.65 and Figure 3.66 for Masonry 2 (stiff masonry) shows the shear stress contour plot of confinement scheme 4 which was only unsymmetrical model analysed. When loaded rightward the diagonal confining grid element was taking part in transferring most of the load and premature failure is observed. Figure 3.51 and Figure 3.52 for masonry 1 (weak masonry) and Figure 3.67 and Figure 3.68 for masonry 2 (stiff masonry) represents

27

the stress plot of confinement scheme 5 and 6. Observation of those plots indicates better behaviour of confinement scheme 6 over scheme 5.

3.10.4   Stiffness

From Figure 3.13 and Figure 3.14 it is found that confinement scheme 1 and 3 have almost same initial stiffness with unconfined masonry walls but the loading upto which those confinement schemes behave elastically is much higher than that of unconfined masonry wall. From the stress plot and vector plots it was also found that the failure mechanism in these confinement schemes were much stable and distributed over the whole wall compared to unconfined masonry. This observation indicates better energy dissipation potential of these schemes over unconfined masonry walls while maintaining same kind of stiffness which ensures same kind of dynamic property in shaking. Confinement scheme 2 has lower stiffness than unconfined masonry wall which can be attributed to change of the aspect ratio of the panels and inclusion of preferred plane of sliding along the horizontal at mid height. Confinement scheme 4 to 6 indicates not only higher stiffness but also higher ultimate load.

3.10.5   Ductility

From the comparison of Figure 3.13 and Figure 3.14 it is found that weaker masonry scores over the stiffer masonry in these confinement schemes in terms of ductility. The walls using weaker masonry could attain higher story drift without severe cracking which can be attributed to higher ratio of modulus of elasticity between confining element and masonry in case weak masonry than that of stiff masonry.

3.11 Limitations of the Model

The finite element model used in this analysis has some disadvantages which are encountered in this kind of homogeneous modelling of non-homogeneous material like masonry. The approach taken here for modelling masonry was smeared crack approach which can accurately model failure mechanisms, such as rocking and shear failure through bricks. However, this approach is incapable of handling excessive cracking in case of shear failure through bed and head joints and sliding failures, which are already discussed in chapter 2. The smeared cracking model is able to predict the behaviour of the structure upto crushing in compression with good

accuracy. However, it is capable of modelling tension only upto the development of cracks in the model. Therefore, the analysis can predict the maximum strength which can be attained by the model and the corresponding displacement; the behaviour beyond the point from which the load deformation behaviour is governed by the opening and closing of cracks can not be predicted. The structure can not be called structurally failed as it will take a considerable fraction of the maximum strength even after the displacement at which the analysis stops due to severe discontinuity in the finite element model. After the closing of the cracks the structure goes on resisting load and the confinement prevents its different portions from shearing off. To know the behaviour of the model beyond this point, either some other analysis scheme with "Finite Element Method with Discrete Elements" or experimental investigation may be useful.

3.12 Summary and Conclusions

Several confinement schemes were analysed with two different kind of masonry in this chapter. The results show that the some of these confinement schemes can improve the behaviour of unconfined masonry without increasing its stiffness. The confinement schemes improve the behaviour in terms of ductility and strength. Some of the confinement schemes had higher stiffness and much higher strength capability. However, they had limitation in terms of story drift before attaining heavy cracking. After a good amount of parametric studies in terms of confinement schemes and material properties it will be possible to design a wall with a balance between stiffness, strength and drift terms. The analyses terminated before severe cracking in the masonry portion. However, masonry being confined and subjected to lesser h/t ratio than the native unconfined masonry wall, the opening and closing of cracks can be a good energy dissipating mechanism without much worry about the out of plane stability also. The analyses also showed that the stiffer masonry can be detrimental to these confinement schemes and weak masonry with sufficient confinement will behave better. This preliminary analysis gives launching pad for the further investigation of this age-old construction technology and subsequently experimental investigation was carried out on different confinement schemes.

29

Chapter 4

EXPERIMENTAL INVESTIGATION ON THE CONFINED URM WALLS

4.1 Introduction

The chapter consist of the details of the experimental program and details of the tests conducted on materials used, construction of the test specimens. The loading history, responses measured and observations during the test are also included in this chapter. The details of damage to the test specimens during test and failure patterns are also presented.

4.2 Geometry and Details of the Specimens

The experimental work has been carried out on half scale model of three confined wall specimens. The overall dimensions of the considered prototype wall were 5 m × 3 m (Length × Height). Therefore, for 1:2 reduced scale modelling the dimensions of the constructed model walls were 2.5 m × 1.5 m. The cross-sections of the confining grid elements were 60 mm × 40 mm (Width × Thickness). Two reinforcing wires were provided in the middle of the cross section of the confining grid elements as shown in Figure 4.1. The specimens were constructed on ISMB 250 steel girder which acted as the bottom most confining grid element. Hence, the constructed height of the model walls from top of I section was 1460 mm. In the first model all confining grid elements were 40 mm thick. However, in the second and third specimens, the thickness of top horizontal confining grid elements were increased to 100 mm for better grip of load transferring mechanism from actuator. To accommodate these changes, the lengths of the vertical confining grid elements were accordingly reduced to maintain the same overall height.

30

4.2.1   Confinement Schemes in Different Specimens

Three reduced scale (1:2) specimens were tested with different configurations of confinement schemes. The wall panels were half-brick thick and made with lime cement mortar of 1:1:6 (cement: lime: sand) proportion by weight. The masonry walls were left un-plastered and moist cured for 15 days by regularly sprinkling water on the surface. The age of the masonry in each specimen on the day of test is given in Table 4.1. The various confinement schemes are discussed as follows:

A. *Confinement Scheme 1*

Confinement scheme 1 is the simplest among the all confinement schemes tested under this study. A regular grid pattern was used in this confinement scheme. This kind of scheme can be used in both cases of interior and exterior walls as confinement density is very low and openings for doors and windows can be easily made. The confinement scheme consisted of boundary and one vertical confining element, which divided the whole wall into two panels and h/t ratio in each panel was 23.7. The confinement scheme used is shown in Figure 4.2.

B. *Confinement Scheme 2*

Confinement scheme 2 had some modifications over the confinement scheme 1, where h/t ratio of the panels was reduced to 11.0 by introducing two additional horizontal confining grid elements which further divided the panels and this specimen finally had four panels each of 1190 mm × 660 mm. A regular grid pattern, where confining grid elements crossed each other at right angles, was also followed for this specimen. The confinement scheme used is shown in Figure 4.3. The idea, behind using the horizontal confining grid elements was that it would help in delaying the diagonal cracking through the joints.

C. *Confinement Scheme 3*

A non-regular grid pattern was used in this confinement scheme. This scheme can be used in exterior walls where confinement density is quite high as opening for doors and windows can be easily made between two diagonal members. The confinement scheme consisted of boundary, one vertical, two

31

horizontal and two diagonal confining elements, which divided the whole wall into eight panels. The confinement scheme used is shown in Figure 4.4.

4.3   Construction of the Test Specimens

The different confining grid elements of the specimens were cast in wooden mould separately. Along with that standard cubes and cylinders of the same concrete were cast. These members and standard cubes and cylinders were demoulded after 24 hours and moist cured for 28 days. After curing they were assembled and fabricated to make the confining cage for the confined masonry. The different confining grid elements were connected by 90° bend metal straps of 3 mm × 25 mm cross-section having two legs of 150 mm. For connecting those metal straps 6 mm dia bolts were used and holes in proper places were left in the concrete sections during casting. Then masonry was constructed inside the panels, and was cured in-situ for 15 days.

4.4   Material Properties

Necessary material properties of the various materials used in the preparation of the specimen were ascertained by standard test methods as described in the following sections.

4.4.1   Cement

The cement (Portland Pozzolona Cement 33 grade) used in concrete and masonry mortar, was tested as per IS: 4031-1988 and the results are shown in Table 4.2. The 3 day and 7 day and 28 day cube compressive strengths were 23.0 MPa, 25.5 MPa and 36.9 MPa, respectively.

4.4.2   Reinforcement bars

Two different types of reinforcing steel were used. In the first specimen Galvanised Iron (G.I.) wire were welded to make the reinforcing mesh and for the second and third specimen welded wire mesh was directly used after cutting them in proper dimensions. In both the cases the average diameter of the steel bars was 3.18 mm. Uniaxial tensile tests were conducted on these two kinds of wires and their behaviour is shown in Figure 4.5 and 4.6, respectively. The yield stresses for two types of steel were 357.0 MPa and 372.0 MPa, respectively. The ultimate stress was measured 466.5 MPa and 494.6 MPa, respectively.

32

4.4.3   Concrete

Concrete used for making confining grid elements was designed as per IS: 10262-1982 for target strength of 30 MPa. The design mix proportion was water: cement: sand: coarse aggregate = 0.5: 1: 1.572: 2.421. The sand used in the concrete conforms to grading zone II mentioned in IS: 383-1970. As the concrete was used for constructing very small cross-sectional elements the maximum aggregate size was restricted to 12.5 mm. The compressive strength of the concrete of each specimen was determined from three standard 150 mm cubes. The other properties were determined from 3 standard cylinders. The average modulus of elasticity was 55.0 GPa. The average strength of concrete for all three specimens at 28 days is 38.7 MPa. The results are given in Table 4.3

Fibre was used in the concrete to increase the bending capacity of concrete members. Commercially available Recron 3s polyester fibre of 12 mm length manufactured by Reliance Industries Limited was used as secondary reinforcement to improve flexural and compressive strengths of the concrete. Fibre was used at 0.1% volume fraction in the concrete.

4.4.4   Brick

Well burnt specially manufactured 1:2 scaled model bricks were used in the model specimens. The average dimensions of the bricks are given in Table 4.4. The compressive strength tests on bricks were performed as per IS: 3495 (Part 1)-1992. The results are described in Table 4.4. The average compressive strength of the bricks was measured 37.9 MPa. This conforms to the Class 35 bricks (IS: 1077-1992) which are of medium strength. Water absorption test of bricks were performed as per IS: 3495 (Part 2)-1992 and results are described in Table 4.4. The average percent of water absorption is found to be 13% by weight, which is within the permissible limit of 15% specified in, IS: 1077-1992 for well burnt first class bricks.

4.4.5   Cement Lime Mortar

A lime cement mortar of 1:1:6 (cement: lime: sand) proportion by weight was used in the brick masonry work. 50 mm cubes of this mortar were tested for their 28-day compressive strength as specified by IS: 2250-1981. The strength obtained is given in Table 4.5. The average 28-day mortar strength is 4.0 MPa. The mortar composition

used pertains to standard Indian masonry construction. The lime was slaked to make it hydrated lime according to platform slaking method as described in IS: 1635-1992. The mortar type is M1 and the minimum compressive strength required for this type of mortar is 3.0 MPa, as specified in IS: 1905-1987. As the experimental program was on a scaled model, the height of the mortar course was reduced to certain amount, as exact 1:2 scaling of the mortar layer thickness was not possible due to construction difficulties. Similar kind of problem was faced by earlier researchers also (Mosalam *et al*, 1997, Harris and Sabnis, 1999). The average height of the mortar courses were 7.5 mm. For constructing such scaled layer of mortar the sand of maximum grain size of 2.36 mm was used instead of normal practice of maximum grain size of 4.75 mm. The Grading curve of the sand is shown in Figure 4.7.

4.4.6   Masonry

Brick masonry prisms were constructed to obtain the compressive strength and load-deformation behaviour of the masonry. The test was conducted as per IS: 2212-1991. 1:2 reduced scale bricks were used to construct the brick prisms. The sizes of the prisms conform to IS: 1905-1987. The results of the compressive test of prisms are given in Table 4.6 to Table 4.8. The average compressive strength obtained was 8.9 MPa and strain level at that stress was 0.74%. The stress strain curve obtained from the tests is shown in Figure 4.8.

4.5   Test Set-up

A test set-up was designed as shown in Figure. 4.9. The maximum expected strength of all the specimens were well within ± 250 kN capacity of the available servo-hydraulic actuator. The experimental set-up was designed in such a way that it will restrict any out-of-plane movement of the specimen, and load the specimen in its own plane.

The actuator is capable of applying forces statically and dynamically upto a maximum displacement stroke of ± 75 mm. Both displacement and force controls are possible through a controller unit and a function generator enabled the servo-controlled actuator to produce pre-programmed load or displacement histories. However all load application was done under displacement control mode. Load and displacements in the specimens were measured with a load cell built into the MTS

actuator arm and a Linear Variable Displacement Transducer (LVDT) built into the actuator. Load and displacement were monitored and recorded using a Data Acquisition System in conjunction with a computer. In addition, an online X-Y plot displayed load-displacement curves on computer screen for immediate visual observation of results.

The vertical load on the specimens was applied by flexible wire rope arrangement as shown in Fig. 4.9. Tensile load was applied on the wire ropes by turn buckle arrangement at predefined four positions along the length of the specimen. The tensile load in the wires was transferred as compressive vertical load to the wall, distributed by plate and roller arrangement. Load cells were placed along the wires to measure the amount of vertical load applied on the specimen as shown in Figure 4.9. The horizontal load was transferred from the actuator to the specimen through roller assembly and appropriate connections to simulate uniform movement of the top beam throughout the loading history. The specimens were constructed in-situ on an ISMB 250 which was adequately fastened to the strong floor to ensure almost no slippage or overturning. The lateral out-of-plane movement of the whole specimen was restrained by providing side supports with rollers as shown in Figure 4.10 with unrestricted in-plane movement. This arrangement provided the stability to the system and prevented out-of-plane bending or twisting. Photographs of experimental set-up along with the specimen are shown in Figure. 4.11. to 4.13.

4.5.1   Servo-Hydraulic Actuator and Controller

Servo-hydraulic (SH) actuator namely Model 244.31A (manufacturer: MTS Systems Inc., Minnesota, USA) used in the present experiment. The actuator includes a servo-valve and requires a Hydraulic Power Supply (HPS), cooling system, and a servo-controller for its operation. Model 244.31A has a force rating of 250 kN in compression and 250 kN in tension and stroke rating of ± 75 mm. The operation of this actuator is controlled by MTS 458.10 Controller.

4.5.2   Instrumentation and Sensors

The adequate amount of instruments was mounted on the specimens to measure the quantities describing the load-deformation behaviour of the panels for the interpretation of cyclic load tests. The instrumentation process consists of installation

of proper sensors on the specimen, calibration of sensors before the tests, data acquisition from sensors after the tests, reduction and analysis of the acquired data for interpreting force-deformation relation (Rai, 2001). In the present experimental study, the instrumentation consists of transducers which are electronic devices that sense physical phenomenon and convert it into electrical signals of voltage or current to be picked by recording devices or computers after necessary processing. The instrumentation used to measure these included Load cells and Linear Variable Differential Transducers (LVDTs).

4.5.3   Displacement Transducers

Linear Variable Differential Transducers (LVDTs) were used at different locations of specimen to monitor displacements during cyclic tests. These transducers measure displacements based on electro-magnetic induction principle. Horizontal LVDTs were mounted on three positions on top beam to measure the movement of the actuator apart from LVDT built into the actuator. These LVDTs helped to determine whether there was any slippage between the different components of the test set-up. The tip of each transducer touched a smooth plexi glass plate fixed at convenient positions on the top beam. A pair of these transducers was also mounted on one face of the specimens along diagonals to measure the shear deformations in the panels of the specimens as shown in Figure 4.9. In the present study, for measurement of strains, displacement readings from LVDT (MTS displacement) built into the actuator has been used.

4.5.4   Load Cells

Load cells namely Model TH/1590-05 (manufacturer: SENSOTEC, Columbus, Ohio) were used to measure the compressive force in the four locations where vertical load was applied by means of the flexible wire ropes. The capacity of the load cells is 500 kN. As the load cells were connected to the online data acquisition system, information about the variation of the compressive load applied with the movement of the wall was also obtained.

The measurement of lateral forces in the specimens was accomplished directly via a load cell located in the actuator.

4.5.5 Data Acquisition and Control

The data acquisition by means of 12-bit data acquisition system was used in the present experimental study. The transducers were connected to Model 5100 Scanner. The Model 5100 Scanner provides data acquisition and digitization of 20 channels of various analog inputs. It is AC powered and accepts upto three input cards (twenty channels per scanner) and scans and digitizes 20 channels of input within 1 milisecond. Scanner 1 was assigned to channels 1 through 20, Scanner 2 was assigned to channels 21 through 40 and Scanner 3 was assigned to channel 41 through 60. The Scanner amplifies the analog electric inputs as generated by the transducers and gives an output to the computer as 10V DC signals. The digital data outputs were stored in the computer hard disk.

4.6 Loading History used in the Experimental Program

As stated earlier, the objective of this study is to understand the force-deformation behaviour of the model confined masonry specimens under slow-cyclic loading. "slow-cyclic" implies that load or deformation cycles are imposed on a test specimen in a slow, controlled and predetermined manner, and dynamic effects as well as rate of deformation effects are not considered. Therefore, the specimens were subjected to cyclic loading in displacement controlled regimes.

One of the most important points in slow-cyclic tests is the type of loading history to be used. In the present study, a simple multi-step loading history based on ATC-24 (1992) guidelines was applied. According to this, if the purpose of the test program is to assess the seismic performance of a component, then multi-step loading history which consists of symmetric cycles of increasing amplitude in predetermined steps is adequate. The selected load histories consisted of symmetric reversed cycles of increasing displacements in predetermined steps at frequency of 0.05 Hz in the ramp wave form. Three cycles were performed at each magnitude of displacement. Cycles were performed at displacement levels of ±1, 2, 3, 4, 6, 8, 12, 15, 20, 25, 30 (mm) etc. displacements until failure of the specimen. Failure of the specimen is defined as substantial loss of load resisting capacity or failure of confining grid elements. The push displacement applied by the actuator was taken as positive and the pull displacement as negative. A typical "displacement control" loading history used in this investigation is shown in Figure. 4.14.

4.7 Test Procedure

The specimens were connected to the bottom beam which was connected to the floor by proper fasteners. The load from the actuator was transferred to the top confining grid element which is almost analogous to the application of load at the floor level of prototype structure. An arrangement was made with four tie rods to pull the specimens in negative loading direction. The 250 kN actuator was set at its mid stroke length so that the piston can move in both directions. DC error in the controller was set to zero before the start of the displacement application to avoid the sudden jerk that may be experienced by the specimen. Except for the first specimen, each level in loading history was programmed in the MTS GPA software in the external PC attached to the controller. For the first specimen, each level of loading history was programmed manually in the controller directly. Each level was divided into seven segments starting from initial zero to peak, then positive peak to negative peak and vice versa and last segment ends at zero. The frequency was set to 0.05 Hz which specifies the rate of displacement application. The data acquisition for this entire study was controlled by WIN System 5000 software program to monitor electronically the response of the specimens. The general block diagram for the testing and data acquisition system used in this study is shown in Figure. 4.15.

Vertical load was not applied in specimens with confinement schemes 1 and 2. In case of specimen with confinement scheme 3, initially the vertical load was applied to maintain a vertical pressure of 0.1 MPa on the specimen. In doing that a total vertical load of 15 kN was applied. While applying horizontal load at first ±1 mm cyclic displacement was applied on the specimen. The displacements were recorded by means of LVDTs. After completion of ±1 mm cyclic displacement, ± 2mm cyclic displacement level was programmed in MTS GPA and applied. This process of cyclic loading was continued till the failure of specimen was observed.

4.8 Response Measured

Displacements at different locations of the topmost horizontal confining grid element and two main panels were measured using LVDTs. The locations of the LVDTs in the test conducted are shown in Figure. 4.9. LVDT MTS and LVDT 5, LVDT 7, LVDT 8 all of them measured the horizontal displacement in the topmost horizontal confining grid element. They can also be used to detect if any slip is developed in

between the different components of loading arrangement. Diagonal LVDTs LVDT 1, 2 and LVDT 3, 4 measured the diagonal displacement in the two main panels of the confined wall.

4.9   Observations from the Test of Specimens

Slow cyclic tests were performed on three confined masonry specimens with confinement schemes as described above. The displacement excursion levels in the description below indicate the first cycle of displacement during loading unless otherwise mentioned.

4.9.1   Confinement Scheme 1

The first crack formed at the interface of masonry and vertical grid element at a displacement excursion level of +2 mm. At the end of 2 mm cycle vertical separation cracks formed in both the end vertical interfaces. These vertical separation cracks intensified with increase in displacement excursion and slightly inclined cracks started to form at the corner regions of panels at displacement excursion level of +3 mm. Flexural cracks in the vertical grid elements were observed at a displacement excursion level of +4 mm. Diagonal stepped cracks started to form from the edge at +5 mm displacement and those cracks reached the centre at 12 mm displacement excursion level. The ultimate load of 22.5 kN was observed at a displacement of +6 mm. Some amount of corner crushing was observed at 8 mm displacement excursion level. During the 15 mm displacement cycle opening and closing of cracks were prominent and upto 10 mm opening of cracks was observed. Snapping of one vertical member was observed at displacement excursion level of 25 mm. However, the displacement cycle of 30 mm was continued and during this the specimen resisted around 75% of the ultimate load. The failed specimen is shown in Figure 4.16. The details of the progressive damage are summarized in Table 4.9.

4.9.2   Confinement Scheme 2

The first crack formed was a horizontal crack observed in between top most layer and layer next to that at displacement excursion level of +4 mm. The cracking of interface of masonry and vertical grid element was formed at the at a displacement excursion level of +5 mm. In the subsequent cycles the horizontal shear crack and the crack at grid element interface propagated. Flexural cracks in the vertical grid

elements were observed at a displacement excursion level of +6 mm. At a displacement excursion level of 8 mm the middle vertical grid element was damaged in flexure. The ultimate load of 29.21 kN was observed at a displacement of +12 mm. Except for a very limited places along the boundary no diagonal cracks in the masonry panels were visible; the masonry started moving along the cracks at the interface of masonry and grid elements. During the loading the panels started to rock inside the grid elements at 15 mm displacement cycle. Finally, at 20 mm displacement excursion level left most outer vertical grid element snapped due to tensile force in the vertical grid elements and the strength was reduced to less than 50% of the ultimate strength. However, while loading in other half of the cycle it resisted load nearly to its ultimate strength. The masonry portion was almost undamaged. The experiment was stopped at this 20 mm displacement excursion level. The failed specimen is shown in Figure 4.17. The details of the progressive damage are given in Table 4.10.

4.9.3   Confinement Scheme 3

The first crack formed at the Interface of diagonal grid elements and end masonry panels at a displacement excursion level of +3 mm. At the end of 3 mm cycle vertical separation cracks formed in both the end vertical interfaces in the upper half of the wall. The next prominent cracking was visible at a displacement excursion level of 5 mm at top trapezoidal panel in the loading side which were diagonal cracks through the mortar joints. These diagonal cracks intensified with increase in displacement excursion and slightly inclined cracks started to form at the corner regions of panels at displacement excursion level of +6 mm. Horizontal cracks started to form from the edge at +8 mm displacement and those cracks reached the diagonal grid at 12 mm displacement excursion level. In 15 mm displacement excursion level, horizontal cracks began to form at the lower trapezoidal panels also. The ultimate load of 53.4 kN was observed at a displacement of +20 mm. During the 20 mm displacement cycle almost all the interfaces of the grid elements and masonry separated and opening and closing of cracks were observed. At 30 mm displacement excursion level horizontal cracks were observed at bottom trapezoidal panel opposite to the loading side. Bending of one vertical member was observed at displacement excursion level of 35 mm. Flexural cracks in the vertical grid elements were observed at a displacement excursion level of +35 mm. However, the displacement cycle of 40 mm

was continued and during this the specimen resisted around 50% of the ultimate load. There was no sign of corner crushing and horizontal and diagonal cracks through the mortar at different places of the panels, which signifies the mode of failure was shear.

The level of applied prestress with story-drift is shown in Figure 4.18. Applied vertical prestress of 0.1 MPa was maintained upto 0.75% story-drift and average vertical prestress of 0.08 MPa was maintained upto 1.6% story drift. After that the prestress reduced significantly and cyclic loadings after that story drift were performed under lesser prestress and range of variation of prestress is shown in Figure 4.19. The failed specimen is shown in Figure 4.20. The details of the progressive damage are given in Table 4.11.

4.10 Analysis and Discussion of the Results

The analysis of the test results and related discussion are presented in this section. Various behavioural quantities which are noted from the envelope backbone load displacement curve are shown in Figure. 4.21. The calculation procedure for some quantities used in the discussion of the results is also stated in this section.

4.10.1 Load Displacement Response

The lateral load displacement hysteretic response for specimens 1, 2 and 3 are shown in Figures 4.22 to 4.24. The envelope backbone curves of the specimens are shown in Figure 4.25. Specimen 1 reached its ultimate load at a displacement level of 6.0 mm whereas for specimen 2 and 3 it was 12.0 mm and 20.0 mm, respectively. The reason of above behaviour can be contributed to lesser damage to masonry in case of specimen 2 compared to specimen 1 at the same displacement excursion level. For specimen 3 the higher load carrying capacity and higher displacement level to reach the ultimate load can be contributed to better confinement and introduction of preferred plane of slippage and the sliding mode of failure.

4.10.2 Initial Stiffness

The initial stiffness of the wall is taken as the average of lateral forces H_1^+ and H_1^- corresponding to the first cycle displacements Δ_1^+ and Δ_1^-, respectively divided by the average first cycle displacement Δ_1.

41

$$K_y = \frac{H_1^+ + H_1^-}{\Delta_1^+ + \Delta_1^-}$$

<div align="right">(4.1)</div>

The initial stiffness of specimens 1, 2 and 3 were found to be 11.36 kN/mm, 9.1 kN/mm and 12.4 kN/mm, respectively.

4.10.3 Ductility Indicator

Computation of the conventional ductility parameters is difficult due to absence of well defined yield points and, therefore, separate definitions of ductility indicators are attempted. These indicators are based on average peak ultimate load V_u and safe and reliable working ultimate load V_w. Average peak ultimate load V_u is defined as the mean of peak ultimate loads attained during a test and maintained for more than one cycle of loading. It should be noted that V_u is not the maximum shear load resisted by the specimen during the test. The other strength indicator V_w reflects the safe and reliable working ultimate load for these relatively brittle systems and V_w is taken as the 70% of V_u.

The first set of ductility indicator δ_u is defined as the ratio of displacement range over which average ultimate peak loads V_u's were maintained. δ_u is defined as the ratio of the displacement at which the pier can no longer sustain the average peak ultimate load V_u to displacement at which V_u is first attained. Similarly another set of ductility indicators δ_w is associated with reliable working ultimate load V_w. This indicator reflects the average working ductility for the confined masonry walls. Schematic diagram of various quantities related to ductility indicators is given in Figure 4.26. In Figures 4.22 to 4.24, strength and ductility indictors as defined above are computed for three specimens. The average ultimate loads were found to be approximately 90% of peak ultimate loads. Ductility indicators δ_u corresponding to average ultimate peak loads were 1.4, 2.1 and 1.7 for specimen 1, 2 and 3, respectively. Working ductility indicators δ_w were 15.4, 9.1 and 9.9, respectively.

4.10.4 Energy Dissipated

The energy dissipated in each cycle is the area enclosed by the hysteresis loop corresponding to that cycle. A schematic representation of that is made in Figure

4.27. Plots of cumulative energy dissipated per unit volume vs. cumulative strain, cumulative energy dissipated per unit volume vs. story drift and total cumulative energy dissipated vs. story drift for different specimens and their two main panels are shown in Figure 4.28 to Figure 4.36. The results show that for specimen 1 and specimen 3 the energy dissipation per unit volume is the almost same for panels and whole wall. However it is different in case of specimen 2, where the energy dissipated per unit volume in masonry panels was less than that of whole wall. The energy dissipated by whole wall is calculated from the horizontal displacement of top of the wall measured by LVDT built in the actuator and which is verified by other three horizontal LVDTs; this calculation is more or less accurate. However the energy dissipated by panels is calculated from the displacement measurement by the diagonal LVDTs on the panels; sometimes due to extensive cracking those diagonal LVDTs (LVDT 1 to LVDT 4) could not measure the displacements correctly and this may be the cause of the observed discrepancy. It was further justified by the plots shown in Figure 4.30, Figure 4.33 and Figure 4.36 where it is found that sum of energy dissipated by the panels matched with the energy dissipated by the whole wall in case of specimen 1 and specimen 3 whereas, for specimen 2, sum of energy dissipated by the two main panels were lesser than the energy dissipated by the whole wall. Comparative plots of cumulative energy dissipated per unit volume vs. cumulative strain and cumulative energy dissipated per unit volume vs. story drift of different specimens are shown in Figure 4.37 and 4.38.

4.10.5   Ultimate Strength

The ultimate strength H_u is taken as the maximum load reached along the positive part of the envelope backbone load-displacement curve. Ultimate strength increased with introduction of grid elements. Ultimate strengths of specimens 1, 2 and 3 were found to be 22.5 kN, 29.2 kN and 53.4 kN, respectively.

4.10.6   Cycle Stiffness

As observed in the hysteretic response of all the specimens, the lateral stiffness of the specimens and panels was on continuous decline with each cycle of loading. In order to illustrate this stiffness degradation occurring between different loading sequences, an indicator, Cycle Stiffness (K_i) is introduced. Cycle Stiffness is the slope of the line

joining the maximum excursion point in the positive cycle and the maximum excursion point in the negative cycle.

$$K_i = \frac{H_i^+ + H_i^-}{\Delta_i^+ + \Delta_i^-}$$ (4.2)

Variation of the cycle stiffness of the specimens with story drift is shown in Figure 4.39. The results show that at the same story drift level, the stiffness of the walls improved with introduction of more grid elements.

4.10.7   Strength Deterioration

A loss in the strength occurs in the repeat cycle with respect to the strength in the first cycle for a given displacement excursion. The loss of the strength expressed as a percentage of strength in the first cycle, is known as strength deterioration. In general the trend of strength deterioration in first and second repeat cycle was same. However, it was found to be higher in second repeat cycle than the first repeat cycle. Similar trends were observed for positive and negative portion of the cycle and the average of the strength degradation in positive and negative portions of the cycle in first repeat cycle is plotted for different specimens in Figure 4.40. Strength deterioration of specimen 1 started after 15 mm displacement excursion level and it continuously deteriorated till the failure. For specimen 2, more than 25% strength deterioration took place in the first repeat cycle of 15 mm displacement excursion level and it failed at 20 mm displacement excursion level. The strength deterioration of specimen 3 was never more than 17% in a particular excursion level.

4.10.8   Stiffness Degradation

A reduction in the stiffness occurs in the repeat cycles with respect to the stiffness in the first cycle for a given displacement excursion. The reduction, expressed as a percentage of stiffness in the first cycle, is known as stiffness degradation. Similar to the trend of strength deterioration the trend of stiffness deterioration in first and second repeat cycles were the same but it was found to be higher in second repeat cycle than the first repeat cycle. Similar trends were observed for positive and negative portions of the cycle and the average of the strength degradation in positive and negative portions of the cycle in first repeat cycle is plotted for different specimens in Figure 4.41. For specimens 1 and 2, the highest levels of stiffness

deterioration were observed at 15 mm displacement excursion level. Therefore, it can be concluded that in the repeat cycles of 15 mm displacement excursion level the specimen 1 an 2 had major damage. For specimen 3 this displacement level was 20 mm. Specimen 3 reached its ultimate load at the same displacement level.

4.10.9   Failure modes

In this study, failure is regarded as a state of significant loss of strength, stiffness or stability of the specimens. The cracking of the masonry is not considered as failure as long as it does not impair the load carrying capacity of the system and does not threaten the stability of the cracked masonry elements. The loading on specimen 1 was stopped when one of the confining grid elements snapped. Till that stage the masonry was in diagonal compression when, opening and closing of cracks took place under reverse cyclic load. The failure was predominantly due to diagonal compression of the masonry panels which is indicated by tension and compression cracks in the masonry panels and corner crushing. For specimen 2, horizontal sliding started in the upper two layers and few diagonal cracks were formed at the corners showing a tendency of diagonal strut formation at later stages. For specimen 2, the final failure took place when the whole wall began to rock after severe damage to the outside vertical element. However, in specimen 3, from the beginning horizontal and diagonal cracks were observed. There were no sign of rocking or flexural cracking on the masonry portion. The damage seen was mostly horizontal and diagonal cracks through bed and head joints. The failure mode was sliding along those cracks and interface of masonry and confining grid elements.

4.11 Summary and Conclusions

The following general conclusions can be made on the observations of the hysteretic behaviour of confined masonry walls:

(a) The hysteretic behaviour of confined masonry was predominantly flexure in the first two specimens where vertical load was not applied. Panels had a rocking tendency which was being resisted by the confining grid elements.

(b) For the first specimen diagonal strut formation took place which signifies the rocking of the panels. For the second specimen at lower load level some amount

of horizontal sliding was observed but finally diagonal strut formation took place and the specimen failed in flexure.

(c) For the first specimen stable energy dissipation by opening and closing of cracks was observed through inelastic activities and load resistance was nearly 80% of the maximum strength at a story-drift level of 2%.

(d) For the third specimen the failure mode was sliding along the bed and head joints of the masonry and along the interface of the masonry and confining grid elements.

(e) For specimen 1 and specimen 2 the degradation of hysteretic response was observed in the range of 0.33% to 2% of story drift. This was primarily caused by diagonal cracking of masonry and toe crushing and damage to the confining grid elements.

(f) In general, confinement scheme 3 resisted increased amount of load with more ductility. Specimen 3 reached its ultimate load at 1.33% story drift, and maintained 50% of ultimate strength upto story drift of 2.7%. There was no sign of masonry falling off the panel.

(g) Steel wire ropes used in the third experiment carried large axial forces and in-turn applied pre-compression to the wall. There were no signs of rocking of wall as a whole. The behaviour can be certified by the not significant increment of tensile force in the steel wire ropes with the displacement level. If it was rocking, the tensile force in exterior steel wires was observed to be linearly related to the lateral displacement of the rocking pier.

Chapter 5

FINITE ELEMENT RESULTS AND COMPARISON WITH EXPERIMENTAL VALUES

5.1 Introduction

Three specimens which were experimentally tested were also analysed in ABAQUS. The analytical model is complementary to the experiments done as some important force and deformation quantities could not be monitored in the experiments. The analytical models for the specimens were developed in the same fashion as the specimen with timber confinement as described in Chapter 3. The FE mesh and appropriate boundary conditions are shown in Figure 5.1 to 5.3. Definitions of material parameters used are identical to the parameters used for the specimens discussed in Chapter 3. The properties used are obtained mostly from the experimentally observed results as explained in Chapter 4. Young's modulus for the masonry used in the experimental models was found to be 1388 MPa. Young's modulus and other reference material properties for masonry are mentioned in the Table 5.1. The value of Poisson's ratio taken for all the masonry was 0.2. For steel reinforcement used in concrete confining grid members Young's modulus and Poisson's ratio were taken as 220 GPa and 0.3, respectively. For fibre reinforced concrete Young's modulus was measured 55 GPa and Poisson's ratio was taken as 0.15, respectively. For those properties which could not be experimentally obtained, results reported in the literature were used (Rai 1996, Buonopane et al. 1999, Magenes and Calvi 2002).

Regarding the loading, the models were subjected to a constant vertical loading to represent the loads from the upper floors and subsequently applied lateral displacements. The only difference in analyses from experiments is that lateral displacements were applied monotonically rather than the cyclic loading.

5.2 Results of FE Analysis

The loading condition in the experiments is already described in chapter 4 and simulation of the condition in analysis is done by the procedure described in chapter 3. The confinement scheme 3 of experimental study was loaded by a constant vertical load at first and then horizontal load was given incrementally in several stages as said already. This incremental load was applied using Riks algorithm of numerical solution for non-linear systems. However, for confinement scheme 1 and 2 no vertical load was applied; they were checked for their stability and in-plane load resistance without application of vertical load, which will improve its behaviour. All the models being symmetric load response and other parameters were checked for loading in one direction. The solution could not be carried out upto an ultimate load or until the failure. Slow convergence in a particular loading increment prematurely terminated the analyses due to a severe cracking and non-linear activities in the model. Though the convergence tolerance was set to a lower value, it could not be met in successive iterations.

Figure 5.4 to 5.6 shows the deformed shape for the three specimens, which were analysed. Figure 5.7 to Figure 5.15 show the stress distribution (shear stress and Von-Mises stress) and vector plot of the major principal stress in the masonry portion of the models. The plots show a prominent formation of diagonal strut in all the models. The struts had a variable width at different portion of the panels and were narrowest at the corners where load was applied and the corner diagonally opposite to those corners.

5.3 Comparison of FE Results with Experimental Envelope Values

The ABAQUS results for the monotonically increasing loading, as presented in this chapter, are compared with the corresponding envelope values measured in the cyclic testing of these specimens. The parameters discussed here are: total horizontal shear and story drift. Figure 5.16 to 5.18 shows the plot of total horizontal shear with applied displacement, as measured in the experiments and predicted by FE analysis. A close match is seen throughout the entire loading history before the major cracking appeared in the specimen and the load deformation behaviour was governed by the opening and closing of cracks.

For specimen 1 the analytical result upto which it could be obtained matched exactly with the experimental results and for specimen 2 and 3 analytical results were little stiffer than the experimental results. The analytical results predicted more strength and stiffness at every displacement level.

The correlations described above between the analysis and experiments are generally in good agreement. However, these comparisons should be considered taking into consideration following points which can identify some of the basic differences inherent in these approaches:

1. The differences in the test results between monotonic and cyclic loading are expected. The cyclic loading tends to soften and damage the masonry with successive non-linear excursion whereas in analytical model monotonic loading is applied onto the un-softened specimen.

2. Experimental results were not symmetrical for positive and negative cyclic excursions. This discrepancy is most likely due to variations in the masonry material. This variation in the material in different position of the masonry is ignored in the analytical model and an average property is used in the whole model.

3. The formation of the large cracks also adds to the non-linearity of the original model whereas in the analytical model it is considered as homogeneous smeared cracking.

4. The smeared crack approach is most suitable for predicting the behaviour of masonry when its failure mode is shear-cracking through bricks. In present study the failure modes observed are either shear cracking through bed and head joints due to weak mortar and subsequent sliding or rocking. Due to that the analysis could predict upto the point, when the cracks were not severe. The smeared crack approach is mostly governed by the compressive stress-strain properties of the masonry. After the development of large cracking, the behaviour of the masonry is not characterised by its compressive stress-strain properties. Due to that the analytical results matched exactly for the specimen 1 where the failure occurred due to diagonal compression of masonry and subsequent cracking. Though the analytical model approach of smeared cracking

49

had taken into account the sliding in-between masonry and confining grid elements, could not follow the sliding of bricks through brick joints. For that reason the analytical results for specimen 2 and 3 were stiffer than the experimental results and had poor match with experimental results.

5.4   Summary and Conclusions

Finite element studies affirmed the experimentally observed various aspect of the behaviour of confined masonry specimens. The conclusions that can be drawn from the above analytical study are as summarized below:

1. Simple finite element analysis using ABAQUS successfully predicted the envelope response of test specimens. The strength and stiffness of the confined masonry wall specimens were predicted more or less accurately.

2. The experimental and analytical analysis confirmed that the shear resistance and stiffness of confined masonry is drastically affected by confinement density and arrangement of grid elements.

3. The analytical model is best suitable for predicting the behaviour when there is limited sliding and failure is mainly due to diagonal compression and shear-cracking through bricks.

Chapter 6
SUMMMARY, CONCLUSIONS AND FUTURE RESEARCH NEEDS

2.1 Summary

This study is mainly concerned with improved in-plane lateral resistance of URM walls by the use of confining grid elements. The technology is not a new invention. It is a scientific study on an already known but gradually less used construction practice. It was observed in the past earthquakes, buildings with such confined masonry performed satisfactorily, the displacement ductility and energy dissipation capacity improve considerably by use of these confining grid elements. The confining grid elements and their placement and spacing greatly influence the behaviour of the system as a whole. RC confining grid elements have been used in both of analytical and experimental studies and timber confining grid elements has been used only for analytical studies.

2.1.1 Analytical Work

The analytical work has been carried out through finite element (FE) modelling of confined masonry walls by the finite element program ABAQUS. FE approach was adopted to provide information at the microscopic level and to ascertain the key parameters which govern the load-deformation behaviour of the confined masonry wall as a whole system. In the modelling approach masonry was modelled in macroscopic level and the interaction between the different constituents of the confinement system and the interaction between the masonry and its confinement was done in microscopic level. The masonry portion was modelled by smeared crack approach. The interface between the confining grid elements and masonry was modelled as frictional behaviour at the interface. The connections between different confining grid elements were modelled as rotational springs of very small stiffness. A two dimensional continuum in the state of plane stress was considered for the

masonry portion. Two dimensional linear elements were used to model the grid elements. In the analytical investigation several confinement schemes were analysed with two different kind of masonry.

The results showed that the some of these confinement schemes can improve the behaviour of unconfined masonry without increasing its stiffness. The confinement schemes improve the behaviour in terms of ductility and strength. Some of the confinement schemes had higher stiffness and much higher strength capability. The analyses terminated at onset of severe cracking in the masonry portion. The analyses also showed that the stiffer masonry can be detrimental to these confinement schemes and weak masonry with sufficient confinement behaves better. This preliminary analysis gives basis for the further investigation of this age-old construction technology and subsequently experimental investigation was carried out on different confinement schemes.

2.1.2   Experimental Work

The experimental work involved slow cyclic test on three wall specimens. These slow cyclic tests give the information to understand the behaviour of these structures in nonlinear range. In the first specimen the whole wall had boundary confinement and an additional vertical element to divide the wall into two panels. The change in second specimen from the specimen 1 was inclusion of two horizontal elements at the mid height to further divide the masonry portion to a total of four panels. The first two specimens initially showed diagonal compression in panels and their failure modes were mainly flexure. In the third specimen two additional diagonal members were introduced to create a preferred sliding plane along those diagonal confining grid elements and vertical precompression was applied. Sliding action along the interface of diagonal confining elements and masonry was observed as expected and strength and deformation capacity of the specimen increased considerably without significant increase in stiffness.

The series of tests help to evaluate the load resistance mechanism, failure/damage pattern and the hysteretic behaviour of these confinement schemes. Tests show the mechanism and effectiveness of the measures in improving the seismic response of masonry structures. Tests also show the limitation of the finite element modelling by smeared crack approach. The analysis by FE approach could not be carried out

beyond the point when severe cracking in masonry takes place. The experimental results supplied data beyond that point. The experiments showed that the confined masonry walls can resist 70-80% of their ultimate strength at story drift level of as high as 2%. Confinement to the URM is found to have a beneficial effect not only in terms of stiffness of the structure but also in terms of the displacement, thereby in terms of ductility. Supplemental tests on masonry materials and grid elements were also performed to give the input data in analytical models.

2.2   Conclusions

The following conclusions are drawn from the present study:

Stress Strain property of the masonry plays an important role in lateral load resistance behaviour of the confined masonry structures and it is found that weak masonry in terms of deformability performs better than the stiff masonry.

The walls with squat type of wall-panels perform better than with slender type of panels in dissipating energy in confined masonry. The slender panels had tendency to rock whereas, confined masonry is more effective in shear failure mode.

The role of denser grid elements is not in terms of increased stiffness; they improve the performance in providing the plane of separation and providing guided shearing plane, there by increasing the energy dissipation potential of the confinement scheme.

Introduction of diagonal plane of sliding improves the lateral behaviour of confined masonry by sliding along that plane without significant increase of stiffness. It also changes the failure mode from rocking to sliding along bed joints and at interfaces with grid elements as observed in case of experimental specimen 3.

In no experiment masonry was seen to fall off the wall. This indicates the improvement in out of plane stability of the wall panels due to sub-panelling by introduction of confining grid elements.

A close match is seen between the observed experimental results and estimated analytical results before the major cracking appeared in the specimen and the load deformation behaviour was governed by the opening and closing of cracks. The

reason can be formation of the large cracks also adds to the non-linearity of the original model whereas in the analytical model it is considered as homogeneous smeared cracking.

The smeared crack approach is most suitable for predicting the behaviour of masonry when its failure mode is diagonal shear-cracking. Due to that the analytical results follow closely for the specimen 1 where the failure occurred due to diagonal compression of masonry and subsequent cracking. However, for specimen 2 and 3, the analytical model predicted some stiffer load-deformation curve. This softer behaviour of specimen 2 and 3 can be contributed to sliding of masonry along the joints which could not be predicted by smeared crack approach of modelling.

2.3   Suggestions for Future Research

The areas for possible further research which were identified during the course of this study are summarized here:

I.   A more detailed study with different spacing of the confining grid elements is needed.

II. Experimental results are also needed to quantify the influence of the masonry stress strain property in the hysteretic behaviour of the confined masonry structure.

III. Studies with inclined layers of masonry are needed.

IV. Similar experimental studies are needed on wall specimens with openings.

V.   Role of confining grid elements in improving the out of plane lateral behaviour can be studied.

VI. Similar studies can be made with confining grid elements of other materials such as steel, timber, aluminium and ferro-cement.

VII. Study can be conducted on the behaviour of the confined masonry when used as infill material to the RC framed structures.

REFERENCES

ATC (1992). "Guidelines for Cyclic Seismic Testing of Components of Steel Structures," Applied Technology Council, Publication ATC-24, Redwood, California.

Bull, J.W. (2001). "Computational Modelling of Masonry, Brickwork and Blockwork Structures," Saxe-Coburg Publications, Dun Eaglasis, Station Brae, Kippen, Stirling, FK8 3DY, UK.

Buonopane, S. G., White, R. N. (1999). "Pseudodynamic Testing of Masonry Infilled Reinforced Concrete Frame," J. Struct. Engrg., ASCE, 125(6), 578-589.

Cardoso, R., Lopes, M., Bento, R. (2004). "Earthquake Resistant Structures Of Portuguese Old 'Pombalino' Buildings," Proc., 13th World Conf. on Earthquake Engineering, Vancouver, B. C., Canada, Aug 1-6, 2004, Paper No. 918.

Chuang, S., Zhuge, Y., and McBean, P.C. (2004). "Seismic Retrofitting of Unreinforced Masonry Walls by Cable System," Proc., 13th World Conf. on Earthquake Engineering, Vancouver, B. C., Canada, Aug 1-6, 2004, Paper No. 3228.

Eurocode No 6 (1988). "Common Unified Rule for Masonry Structures," Commission of the European Communities, Report EUR 9888 EN.

Ewing, B. D., Kowalsky, M. J. (2004). "Compressive Behavior of Unconfined and Confined Clay Brick Masonry," J. Struct. Engrg., ASCE, 130(4), 650-661.

Gambarotta, L., Lagomarsino, S. (1997). "Damage models for the seismic response of brick masonry shear walls. Part II: The Continuum Model and its Applications," J. Earthquake Engineering and Structural Dynamics, John Wiley & Sons. Ltd., 26, 441-462.

Ghosh, A. K., Amde A. M. (2002). "Finite Element Analysis of Infilled Frames," J. Struct. Engrg., ASCE, 128(7), 881-889.

Giordano, A., Mele, E. (2002). "Modelling of historical masonry structures: comparison of different approaches through a case study," Engineering Structures, 24, 1057-1069

Gülkan, P., Langenbach, R. (2004) "The Earthquake Resistance of Traditional Timber and Masonry Dwellings in Turkey," Proc., 13th World Conf. on Earthquake Engineering, Vancouver, B. C., Canada, Aug 1-6, 2004, Paper No. 2297.

Harris, H. G., Sabnis G. M. (1999). "Structural modelling and experimental techniques," CRC Press LLC, 2000 Corporate Blvd., N.W., Boca Raton, Florida 33431.

Hendry, A. W. (1998). "Structural Masonry," Macmillan Press Ltd., Hounmills, Basingstoke, Hampshire RG21 6XS, London.

Hibbit, D., Karlson B., Sorensen P. (2003). "ABAQUS theory manual"

IS: 1077-1992, 1992 Indian Standard Common Burnt Clay Building Bricks - Specification, Bureau of Indian Standards, New Delhi.

IS: 10262-1982, 1982 Indian Standard Recommended guidelines for concrete mix design, Bureau of Indian Standards, New Delhi.

IS: 1635-1992, 1992 Indian Standard Code of practice for field slaking of building lime and preparation of putty, Bureau of Indian Standards, New Delhi.

IS: 1905-1987, 1987 Indian Standard Code of Practice for Structural use of Unreinforced Masonry, Bureau of Indian Standards, New Delhi.

IS: 2212-1991, 1991 Indian Standard Code of practice for brickwork, Bureau of Indian Standards, New Delhi.

IS: 2250-1981, 1981 Indian Standard Code of Practice for Preparation and Use of Masonry Mortars, Bureau of Indian Standards, New Delhi.

IS: 3495 (Part 1)-1992, 1992 Indian Standard Methods of Tests of Burnt Clay Building Bricks, Bureau of Indian Standards, New Delhi.

IS: 3495 (Part 2)-1992, 1992 Indian Standard Methods of Determination of Water Absorption, Bureau of Indian Standards, New Delhi.

IS: 383-1970, 1970 Indian Standard Specification for coarse and fine aggregates from natural sources for concrete, Bureau of Indian Standards, New Delhi.

IS: 4031-1988, 1988 Indian Standard Methods of physical tests for hydraulic cement, Bureau of Indian Standards, New Delhi.

Kaushik, H. (2004). "Personal Communication with the research scholar", Dept. of Civil Engg., Indian Institute of Technology, Kanpur.

Lourenço, P. B. (1996). "Computational Strategies for masonry structures", Delft University Press, Delft.

Madan, A., Reinhorn, A. M., Mander, J. B. and Valles, R.E. (1997)."Modeling of masonry infill panels for structural analysis," J. Struct. Engrg., ASCE, 123(10), 1295-1302.

Magenes, G., Calvi, G. M. (2002). "In-plane seismic response of brick masonry walls," J. Earthquake Engineering and Structural Dynamics, John Wiley & Sons. Ltd., 26, 1091-1112.

Mandara, A., Scognamiglio, D. (2003). "Behavior of Multi-Perforated Clay Brick Walls under Earthquake-Type Loading," 2003 ABAQUS Users' Conference.

Mehrabi, A. B., Shing, P. B. (1997). "Finite Element Modeling of masonry Infilled RC frames," J. Struct. Engrg., ASCE, 123(5), 604-613.

Meli, Roberto, Alcocer, S. M. (2004). "Implementation of Structural Earthquake-Disaster Mitigation Programs in Developing Countries," Natural Hazards Review, ASCE, 5(1), 29-39.

Molina J., Pape Y. Le., Pegon P. (2001). "Seismic assessment of masonry structures-Experimental program," Proceedings of Historical Constructions. Lourenço, Roca (Eds.), Guimarães.

Mosalam, K. M., White, R. N., and Gargely, P. (1997). "Static Response of Infilled Frames using Quasi-static Experimentation," J. Struct. Engrg., ASCE, 123(11), 1462-1469.

Mosalam, K. M., White, R. N., and Gargely, P. (1997). "Seismic Evaluation of Frames with Infill Walls using Quasi-static Experiments," Technical Report: NCEER-97-0019, National Center for Earthquake Engineering Research, State University of New York at Buffalo, Buffalo, New York, USA.

Mosalam, K. M., White, R. N., and Gargely, P. (1997). "Seismic Evaluation of Frames with Infill Walls using Pseudo-Dynamic Experiments," Technical Report: NCEER-97-0020, National Center for Earthquake Engineering Research, State University of New York at Buffalo, Buffalo, New York, USA.

Noor, F. A., Boswell, L. F. (1992). "Small scale modelling of concrete structures," Elsevier Science Publishers Ltd., Crown House, Linton Road, Barking, Essex IG11 8JU, England.

Rai, D. C. (1996). "Seismic strengthening of unreinforced masonry buildings with steel elements," Ph.D. Dissertation, Dept. Civ. Engg, Univ. of Michigan, Ann Arbor, Mich.

Rai, D. C. (2001). "Slow Cyclic Testing for Evaluation of Seismic Performance of Structural Componenets," ISET Journal of Earthquake Technology, paper No. 480, Vol. 1, 35-65.

Table 4.1   Age of masonry on the day of test

Specimen	Confinement Scheme	Age(days)
Specimen 1	Confinements divided wall into two rectangular panels of h/t ratio 23.67	29
Specimen 2	Confinements divided wall into four rectangular panels of h/t ratio 11	22
Specimen 3	Confinements divided wall into four rectangular panels of h/t ratio 11 which were further by two diagonal members into total 8 panels	21

Table 4.2   Reference properties of cement used in experiments

Cement Property		Results
Standard Consistency		34%
Specific Surface		381 m²/kg
Setting Time	(a) Initial	185 min.
	(b) Final	275 min.
Compressive Strength of 70 mm cubes		
	at 3 days	23 MPa
	at 7 days	25.5 MPa
	at 28 days	36.9 MPa

Table 4.3   Reference properties of concrete used in the confinement elements

Cylinder Compression Test			Cube Compression Test
Peak Stress f'_{conc} MPa	Modulus E_{conc} GPa	Strain at Peak Stress ε'_{conc}	Stress MPa
36.35	55	0.00075	37.11
29.71	57.1	0.0004953	36.94
23.94	53.1	0.000441	41.97
Avg. = 30.0 COV = 14.11%	Avg. = 55.06 COV = 2.46%	Avg. = 0.0005621 COV = 22.29%	Avg. = 38.67 COV = 5.68%

Table 4.4   Reference properties of bricks used in the masonry

Tests on Compressive Strength of Brick				
Sl. No.	L (mm)	B (mm)	Load (kg)	Stress (MPa)
1	120	59.57	29500	41.26
2	120	59.57	31500	44.06
3	120	59.57	20250	28.32
				Avg. = 37.88 COV = 16.82 %

Table 4.5   Reference properties of mortar used in the masonry

	Sl. No.	L (mm)	B (mm)	Load (kg)	Stress (MPa)
Specimen 1	1	50.0	50.5	1050	4.16
	2	49.6	49.1	800	3.28
	3	50.0	50.4	1150	4.56
					Avg. = 4.00 COV = 11.94 %
Specimen 2	1	49.5	50.7	1150	4.58
	2	50.5	50.1	800	3.16
	3	51.2	50.1	1150	4.48
					Avg. = 4.07 COV = 14.94 %
Specimen 3	1	49	49.3	850	3.52
	2	50	49.5	1150	4.64
	3	49.5	50.0	1050	4.24
					Avg. = 4.14 COV = 9.9 %

Table 4.6   Reference properties of masonry used in the specimen 1

1	5-Brick Standard Prism Compression Test [a]		
	Peak Stress f'_m MPa	Modulus E_m MPa	Strain at Peak Stress ε'_m
	8.29	986	0.00833
	9.63	1709	0.005925
	8.37	2217	0.00488
	Avg. = 8.76 COV = 6.59%	Avg. = 1637.33 COV = 26.52%	Avg. = 0.00638 COV = 20.39%
2	Compressive Strength of Mortar (1:1:6)[b] : Avg.= 4.00 MPa, COV = 11.9%		
3	Compressive Strength of Bricks [c] : Avg.= 37.88 MPa, COV = 16.82 %		

a. Avg. height of 5-brick prism = 204.33 mm

b. Tests on 50 mm (2 in.) cube specimens (ASTM C109-84).

c. Avg. size of brick, L:B:H= 120:59.6:34 mm

Table 4.7   Reference properties of masonry used in the specimen 2

1	5-Brick Standard Prism Compression Test[a]		
	Peak Stress f'_m MPa	Modulus E_m MPa	Strain at Peak Stress ε'_m
	10.44	1134	0.00918
	9.31	1196	0.00781
	7.41	1085	0.008275
	Avg. = 9.05 COV = 12.10%	Avg. = 1138.33 COV = 3.38%	Avg. = 0.00842 COV = 6.00%
2	Compressive Strength of Mortar (1:1:6)[b] : Avg.= 4.07 MPa, COV = 14.94%		
3	Compressive Strength of Bricks [c] : Avg.= 37.88 MPa, COV = 16.82 %		

a. Avg. height of 5-brick prism = 204.67 mm

b. Tests on 50 mm (2 in.) cube specimens (ASTM C109-84).

c. Avg. size of brick, L:B:H= 120:59.6:34 mm

Table 4.8   Reference properties of masonry used in the specimen 3

1	5-Brick Standard Prism Compression Test[a]		
	Peak Stress f'_m MPa	Modulus E_m MPa	Strain at Peak Stress ε'_m
	9.21	1521	0.00833
	8.47	1458	0.00721
	8.58	1462	0.00688
	Avg. = 8.75 COV = 3.48%	Avg. = 1480 COV = 1.83%	Avg. = 0.00744 COV = 7.64%
2	Compressive Strength of Mortar (1:1:6)[b] : Avg.= 4.07 MPa, COV = 14.94%		
3	Compressive Strength of Bricks [c] : Avg.= 37.88 MPa, COV = 16.82 %		

a. Avg. height of 5-brick prism = 204.00 mm

b. Tests on 50 mm (2 in.) cube specimens (ASTM C109-84).

c. Avg. size of brick, L:B:H= 120:59.6:34 mm

Table 4.9   Details of progressive damage in specimen 1
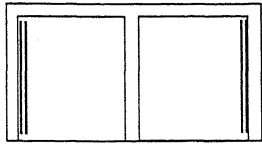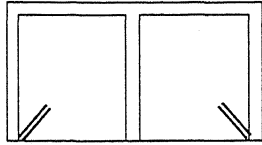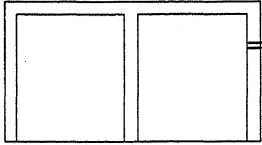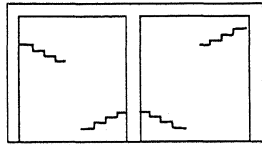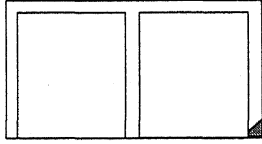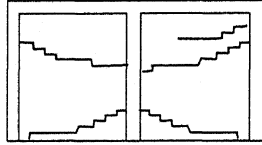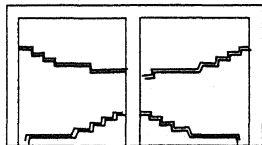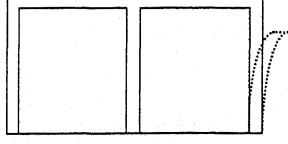
Damage description	Crack location	Displ. level (mm)	Schematic figure of damage
Separation at the interface of masonry and grid elements	Interface of end vertical grid elements and masonry	2	
Formation of inclined cracks	Bottom corners	3	
Formation of flexural cracks in the vertical grid elements	Mid height of vertical grid elements	4	
Diagonal stepped shear cracks	Corners and edges	5	
Cracking in infill due to corner crushing	Toe of the panels	8	
Diagonal stepped shear cracks	Centre of the masonry panels	12	
Opening and closing of cracks and shear sliding	Corners and edges	15	
Snapping of on of the vertical confining grid elements	Little above mid height of the confining grid element	25	

Table 4.10   Details of progressive damage in specimen 2
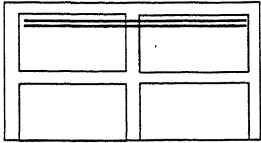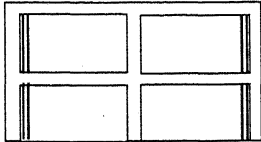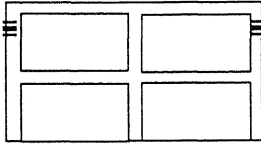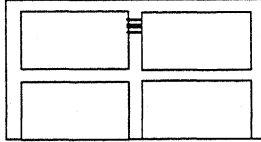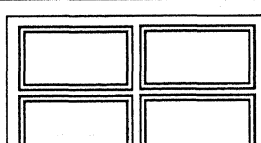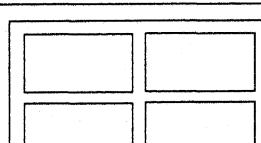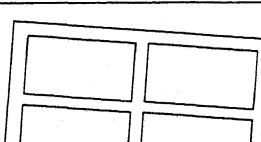
Damage description	Crack location	Displ. level (mm)	Schematic figure of damage
Horizontal crack	In between top most layer and layer next to that	4	
Separation at the interface of masonry and grid elements	Interface of end vertical grid elements and masonry	5	
Formation of flexural cracks in the vertical grid elements	Top portion of end vertical grid elements	6	
Formation of flexural cracks in the vertical grid elements	Top portion of middle vertical grid elements	8	
Sliding along crack	At the interfaces	15	
Snapping of one of the vertical confining grid elements	Bottom most portion of a vertical confining grid element	20	
Uplifting of whole wall due to application of lateral load	Little above mid height of the confining grid element	20	

Table 4.11   Details of progressive damage in specimen 3
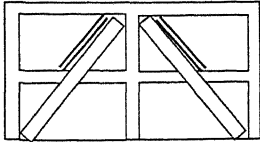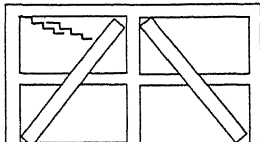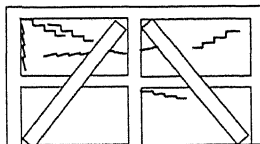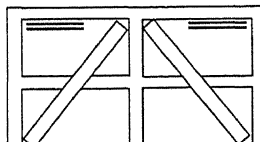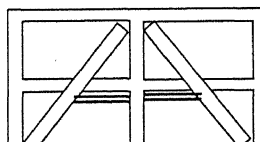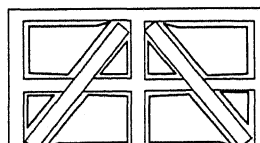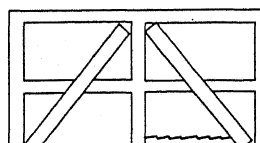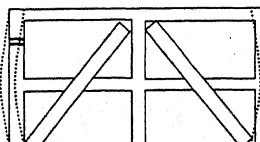
Damage description	Crack location	Displ. level (mm)	Schematic figure of damage
Separation at the interface of masonry and grid elements	Interface of diagonal grid elements and end masonry panels	3	
Formation of inclined cracks in masonry	Top trapezoidal panel in loading side	5	
Formation of inclined cracks in masonry	All top panels	6	
Horizontal cracks	Two top end panels	8	
Horizontal cracks	Internal lower panels	15	
Separation at the interface of masonry and grid elements	All the masonry panels	20	
Horizontal cracks	Bottom trapezoidal panel opposite to loading side	30	
Bending of the vertical boundary grid elements and flexural cracks	Vertical boundary grid elements	35	

Table 4.12   Comparison of Various Confined Masonry Schemes tested during this Study

Specimen	Description	Initial Stiffness (kN/mm)	Ultimate Displ. (mm)	Ultimate Load (kN)
1	Regular Grid Pattern with 2 Panels	11.36	29.36	22.47
2	Regular Grid Pattern with 4 Panels	9.06	20.05	29.21
3	Non-Regular Grid Pattern with 8 Panels	13.98	40.10	53.39

Table 4.13   Strength in the Specimens in different displacement excursion levels

Applied Displacement Level (mm)	Strength in First Cycle (kN)			Strength in Repeat Cycles (kN)					
				CM 1 Repeat Cycle		CM 2 Repeat Cycle		CM 3 Repeat Cycle	
	CM 1	CM 2	CM 3	1	2	1	2	1	2
1.00	8.22	9.88	11.55	8.03	7.83	7.44	7.37	10.91	10.39
-1.00	-14.44	-9.77	-16.97	-14.33	-14.23	-9.83	-9.86	-16.99	-17.00
2.00	15.69	17.62	26.93	12.82	12.66	16.81	16.32	25.58	24.90
-2.00	-20.55	-18.84	-29.37	-19.22	-19.04	-18.31	-17.94	-29.07	-28.91
3.00	20.62	21.98	36.24	18.74	18.96	19.42	18.38	34.72	33.83
-3.00	-23.34	-23.81	-38.50	-21.55	-20.46	-22.05	-21.08	-37.28	-36.44
4.00	21.89	21.58	40.98	20.30	19.53	17.59	16.20	38.99	37.50
-4.00	-23.11	-21.56	-40.87	-22.00	-21.23	-19.07	-17.70	-39.26	-38.37
5.00	22.11	21.58	42.91	20.12	19.58			40.34	38.82
-5.00	-17.72	-21.56	-43.66	-15.66	-15.26			-41.47	-40.11
6.00	22.47	21.58	44.47	17.38	13.92			41.37	39.69
-6.00	-17.68	-21.56	-44.43	-17.71	-17.26			-41.89	-40.44
8.00	17.22	21.70	47.68	15.12	14.55	20.19	19.30	43.30	40.66
-8.00	-18.49	-21.66	-46.14	-16.93	-13.99	-20.06	-19.11	-42.75	-41.02
12.00	18.37	29.21	52.99	16.97	15.52	25.31	24.00	46.14	43.04
-12.00	-14.78	-28.76	-52.10	-12.85	-11.82	-25.98	-24.44	-47.08	-44.55
15.00	18.14	28.17	51.56	16.62	16.62	15.20	14.30	45.63	42.99
-15.00	-14.61	-26.66	-49.94	-15.44	-15.44	-24.38	-21.96	-45.17	-42.18
20.00	15.72	11.95	53.39	13.18	11.82	8.55	8.48	45.82	40.75
-20.00	-15.44	-26.37	-49.25	-13.58	-12.50	-20.85	-18.45	-40.73	-34.20
25.00	16.62		44.30	13.94	13.23			37.99	32.93
-25.00	-14.49		-34.34	-11.85	-10.15			-28.14	-23.30
30.00	16.17		37.32	7.60	6.32			32.00	26.85
-30.00	-10.84		-27.94	-10.03	-9.38			-24.58	-22.89
35.00			31.67					25.56	22.58
-35.00			-28.78					-26.07	-24.95
40.00			26.19					22.78	18.44
-40.00			-27.84					-25.80	-24.51

Table 4.14   Strength deterioration in the Specimens studied as a percentage of Strength in first cycle

Applied Displacement Level (mm)	Strength in First Cycle (kN)			Strength Deterioration (%)					
				CM 1 Repeat Cycle		CM 2 Repeat Cycle		CM 3 Repeat Cycle	
	CM 1	CM 2	CM 3	1	2	1	2	1	2
1.00	8.22	9.88	11.55	2.41	4.82	24.71	25.41	5.55	9.99
-1.00	-14.44	-9.77	-16.97	0.79	1.48	-0.62	-0.94	-0.09	-0.14
2.00	15.69	17.62	26.93	18.33	19.30	4.59	7.36	5.02	7.54
-2.00	-20.55	-18.84	-29.37	6.46	7.35	2.80	4.78	1.01	1.56
3.00	20.62	21.98	36.24	9.10	8.03	11.66	16.38	4.19	6.66
-3.00	-23.34	-23.81	-38.50	7.65	12.32	7.40	11.47	3.17	5.35
4.00	21.89	21.58	40.98	7.28	10.80	18.52	24.92	4.88	8.49
-4.00	-23.11	-21.56	-40.87	4.82	8.15	11.54	17.90	3.94	6.11
5.00	22.11	21.58	42.91	9.01	11.42			5.99	9.53
-5.00	-17.72	-21.56	-43.66	11.62	13.86			5.00	8.11
6.00	22.47	21.58	44.47	22.65	38.03			6.97	10.76
-6.00	-17.68	-21.56	-44.43	-0.17	2.38			5.74	8.98
8.00	17.22	21.70	47.68	12.19	15.51	6.96	11.07	9.17	14.71
-8.00	-18.49	-21.66	-46.14	8.46	24.34	7.36	11.77	7.35	11.10
12.00	18.37	29.21	52.99	7.64	15.49	13.34	17.84	12.92	18.78
-12.00	-14.78	-28.76	-52.10	13.01	20.03	9.66	15.04	9.63	14.49
15.00	18.14	28.17	51.56	8.37	8.37	46.02	49.22	11.50	16.62
-15.00	-14.61	-26.66	-49.94	-5.70	-5.70	8.55	17.62	9.55	15.56
20.00	15.72	11.95	53.39	16.16	24.79	28.42	29.05	14.19	23.68
-20.00	-15.44	-26.37	-49.25	12.06	19.07	20.94	30.05	17.30	30.56
25.00	16.62		44.30	16.15	20.42			14.25	25.66
-25.00	-14.49		-34.34	18.21	29.95			18.05	32.14
30.00	16.17		37.32	53.02	60.90			14.25	28.06
-30.00	-10.84		-27.94	7.46	13.51			12.05	18.08
35.00			31.67					19.28	28.68
-35.00			-28.78					9.41	13.31
40.00			26.19					13.00	29.58
-40.00			-27.84					7.35	11.98

Table 4.16   Stiffness deterioration in the Specimens studied as a percentage of Stiffness in first cycle

Applied Displacement Level (mm)	Average Cycle Stiffness in First Cycle (kN/mm)			Stiffness in Repeat Cycles (kN)						Stiffness Deterioration (%)					
	CM 1	CM 2	CM 3	CM 1 Repeat Cycle		CM 2 Repeat Cycle		CM 3 Repeat Cycle		CM 1 Repeat Cycle		CM 2 Repeat Cycle		CM 3 Repeat Cycle	
				1	2	1	2	1	2	1	2	1	2	1	2
±1	11.39	9.78	14.15	11.31	11.24	8.59	8.51	13.83	13.55	0.70	1.33	12.12	12.90	2.30	4.29
±2	8.83	9.07	14.00	8.18	8.11	8.73	8.52	13.57	13.38	7.36	8.23	3.72	6.03	3.10	4.42
±3	7.37	7.60	12.40	6.79	6.50	6.88	6.55	11.94	11.66	7.83	11.80	9.44	13.83	3.70	5.98
±4	5.76	5.37	10.19	5.40	5.21	4.56	4.22	9.74	9.45	6.29	9.55	15.05	21.44	4.41	7.27
±5	4.07	5.37	8.63	3.65	3.56			8.15	7.86	10.13	12.51			5.58	8.96
±6	3.41	5.37	7.38	2.98	2.65			6.91	6.65	12.50	22.39			6.35	9.89
±8	2.28	2.70	5.84	2.04	1.82	2.51	2.39	5.36	5.09	10.31	20.11	7.15	11.38	8.27	12.94
±12	1.41	2.41	4.37	1.26	1.18	2.13	2.01	3.87	3.64	10.36	16.38	11.51	16.44	11.30	16.68
±15	1.13	1.82	3.37	0.55	0.55	1.32	1.21	3.02	2.83	51.65	51.65	27.80	33.84	10.54	16.15
±20	0.80	0.96	2.56	0.69	0.63	0.73	0.67	2.16	1.87	13.66	21.49	23.26	29.73	15.69	26.99
±25	0.64		1.57	0.53	0.48			1.32	1.12	16.99	24.73			15.91	28.49
±30	0.46		1.08	0.30	0.27			0.94	0.83	35.09	42.08			13.31	23.79
±35			0.86					0.74	0.68					14.58	21.36
±40			0.67					0.61	0.54					10.09	20.51

Table 5.1   Reference Properties of Masonry Materials Used in Analytical Studies

1	5-Brick Standard Prism Compression Test [a]		
	Peak Stress f'_m MPa	Modulus E_m MPa	Strain at Peak Stress ε'_m
	Avg. = 8.9, COV = 9.93%	Avg. = 1387.83, COV = 27.629%	Avg. = 0.0074, COV = 17.99%
2	Compressive Strength of Mortar (1:1:6) [b] : Avg.= 4.05 MPa, COV = 11.6%		
3	Compressive Strength of Bricks [c] : Avg.= 37.86 MPa, COV = 12.7 %		
a. Avg. height of 5-brick prism = 204.33 mm			
b. Tests on 50 mm (2 in.) cube specimens (ASTM C109-84).			
c. Avg. size of brick, L:B:H= 120:59.6:34 mm			
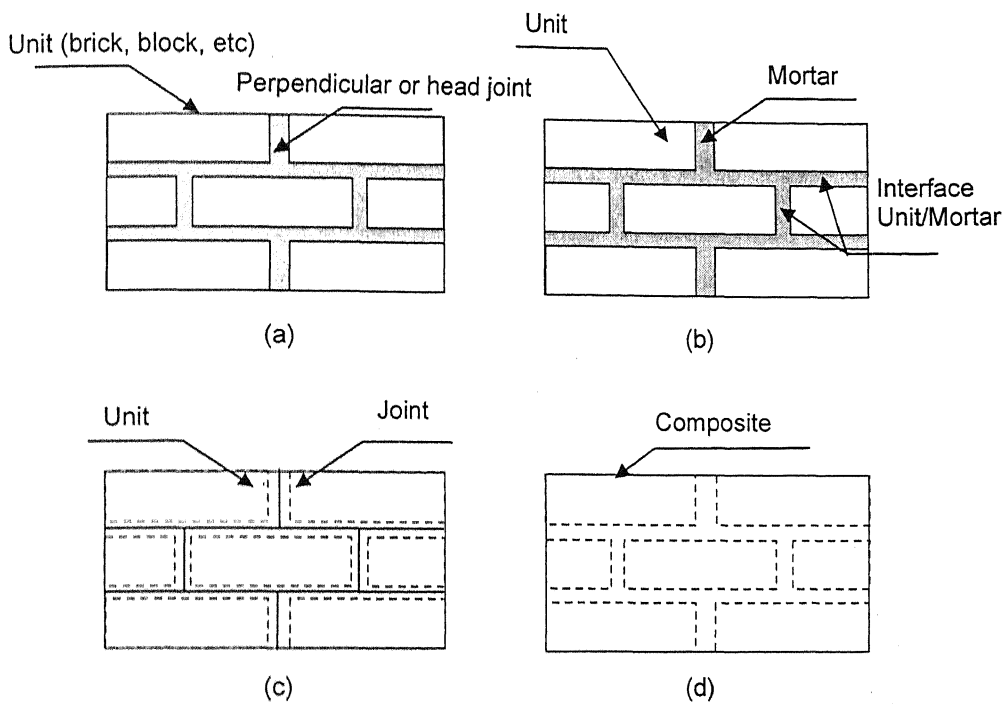
Figure 2.1   Modelling Strategies for masonry structures.
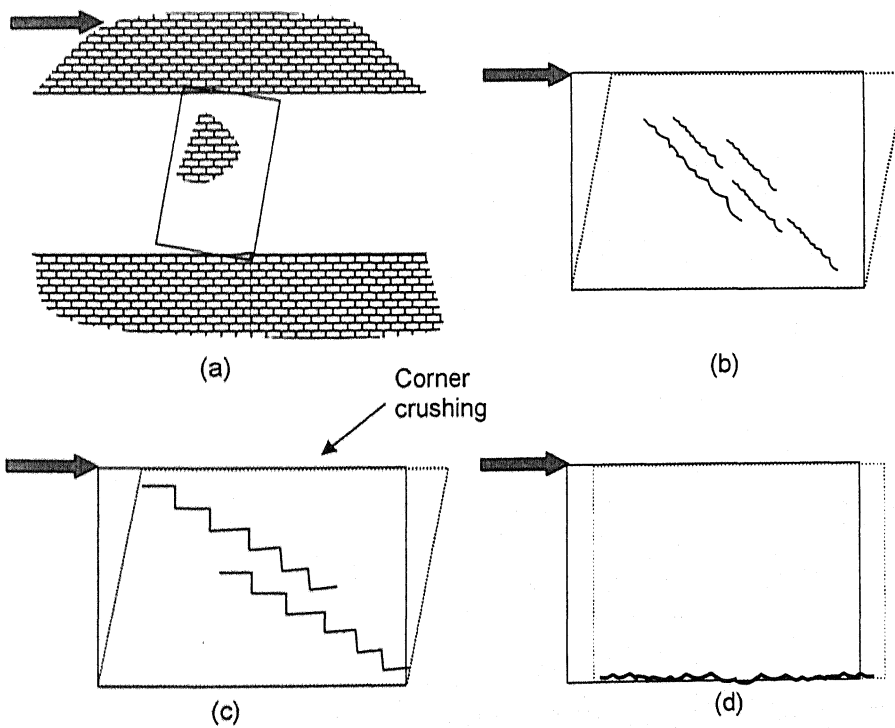
Figure 2.2   Failure mechanisms of masonry subjected to seismic actions: (a) Rocking failure, (b) Shear cracking through the bricks, (c) Shear cracking through bed and head joints, and (d) Sliding failure.
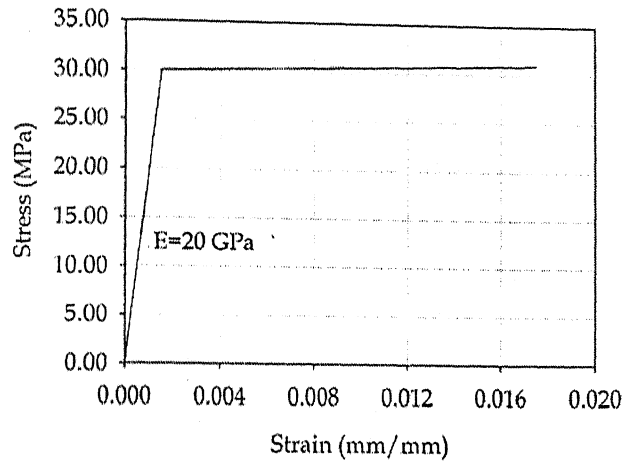
Figure 3.1   Tensile behaviour of timber used in FE analysis.
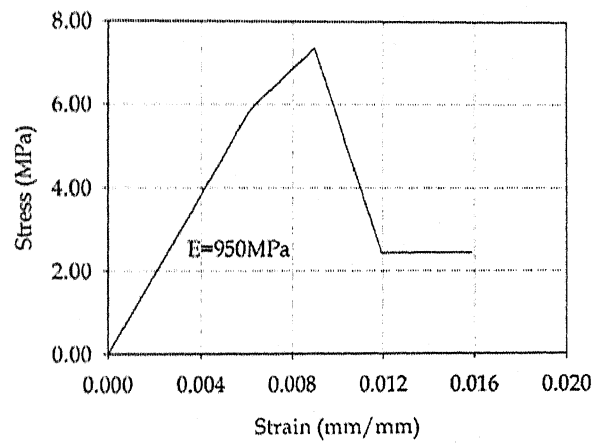
Figure 3.2   Piece-wise idealization of compressive behaviour of Masonry 1 (weak masonry) used in FE analysis.
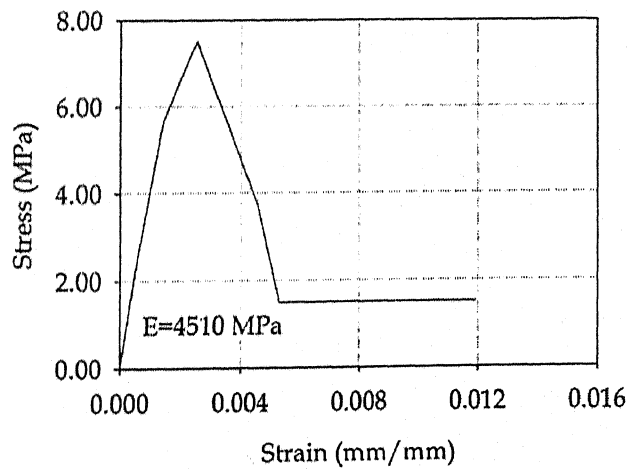
Figure 3.3   Piece-wise idealization of compressive behaviour of Masonry 2 (stiff masonry) used in FE analysis.

71
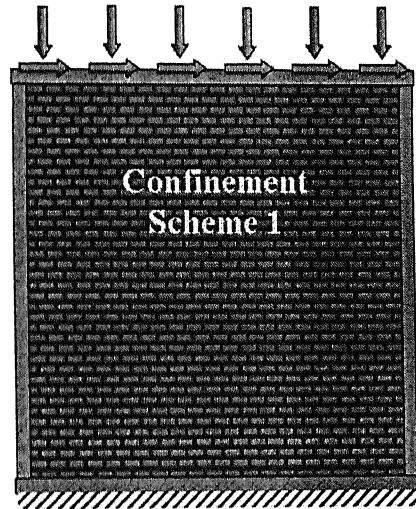
Figure 3.4   Load application and boundary conditions used for analysis
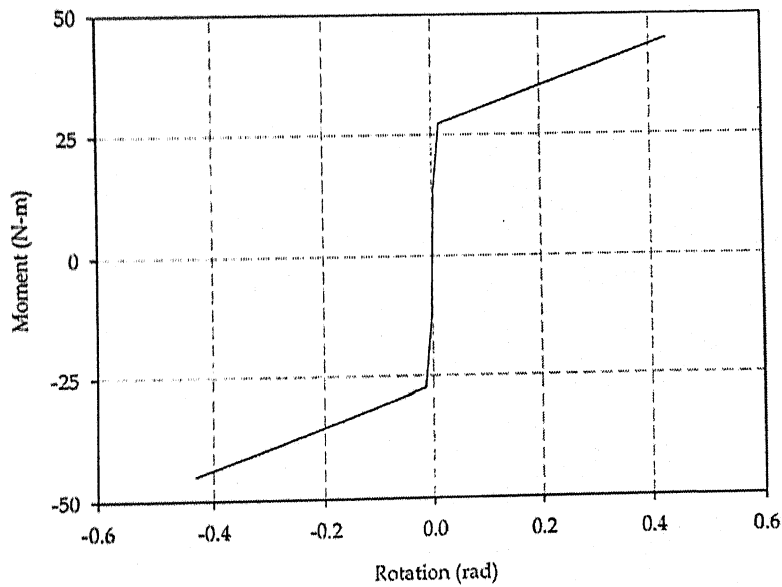
Figure 3.5   Moment-rotation relation of the joints used in the FE analysis.
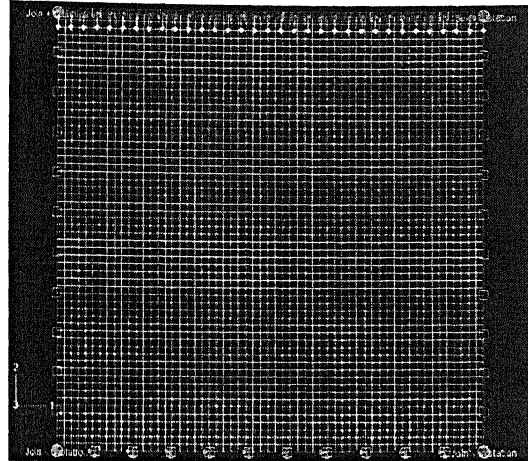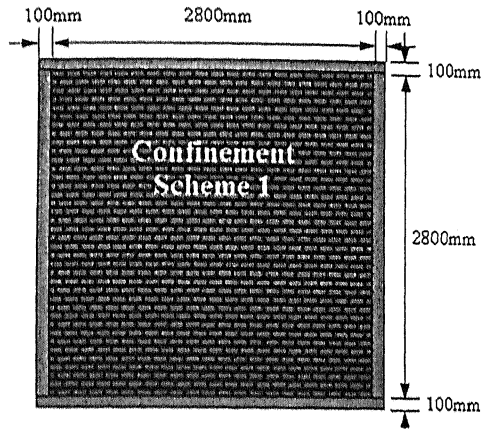
Figure 3.6 Confinement scheme used in confined masonry model 1 and its FE representation.
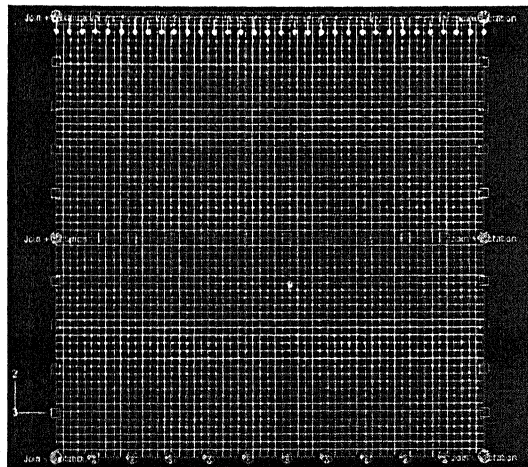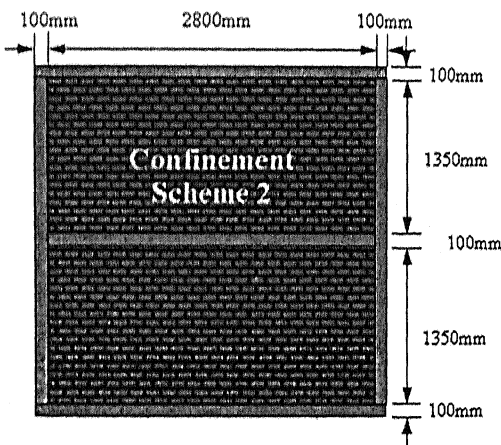
Figure 3.7 Confinement scheme used in confined masonry model 2 and its FE representation.
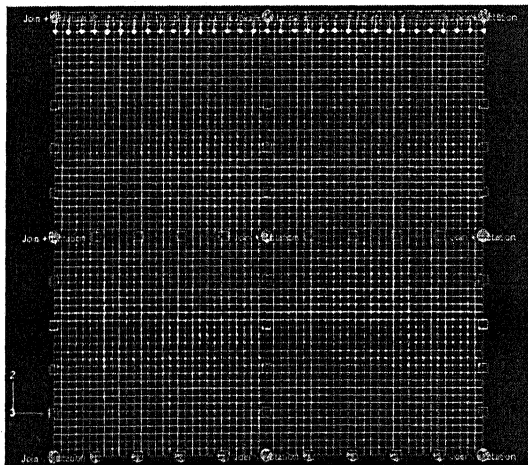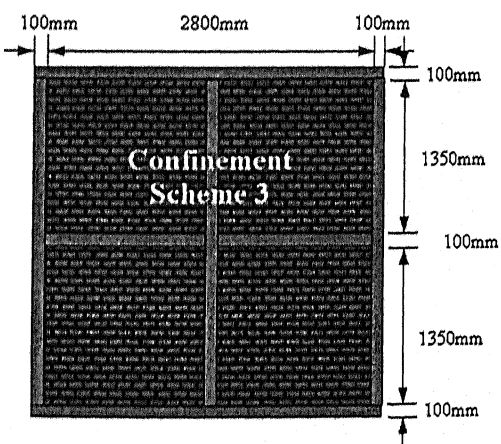
Figure 3.8 Confinement scheme used in confined masonry model 3 and its FE representation.

73
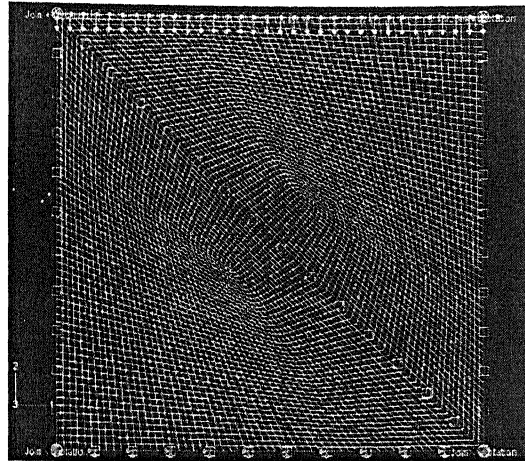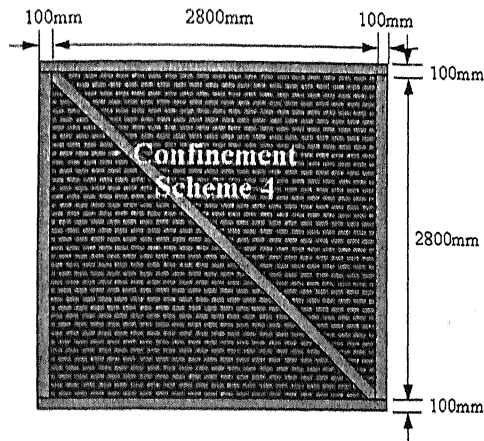
Figure 3.9   Confinement scheme used in confined masonry model 4 and its FE representation.
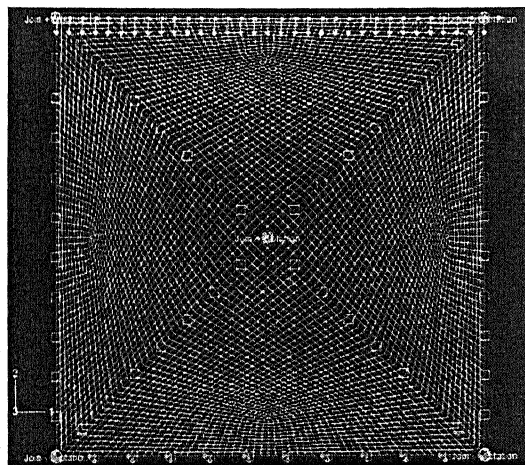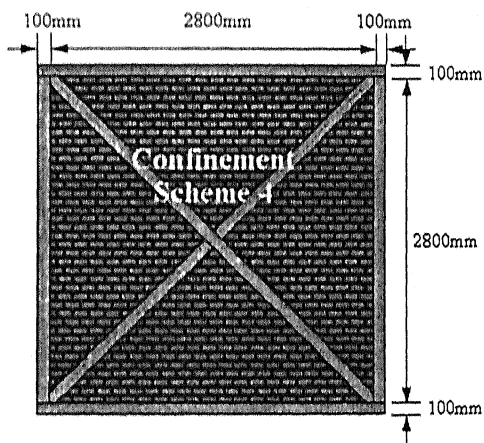
Figure 3.10   Confinement scheme used in confined masonry model 5 and its FE representation.
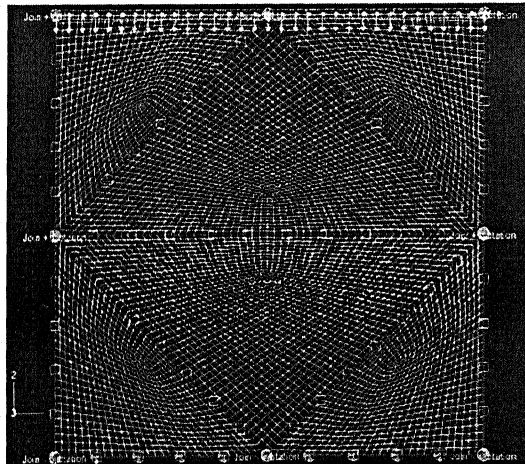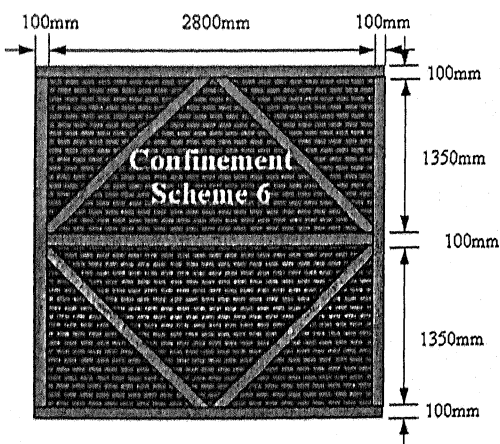
Figure 3.11   Confinement scheme used in confined masonry model 6 and its FE representation.
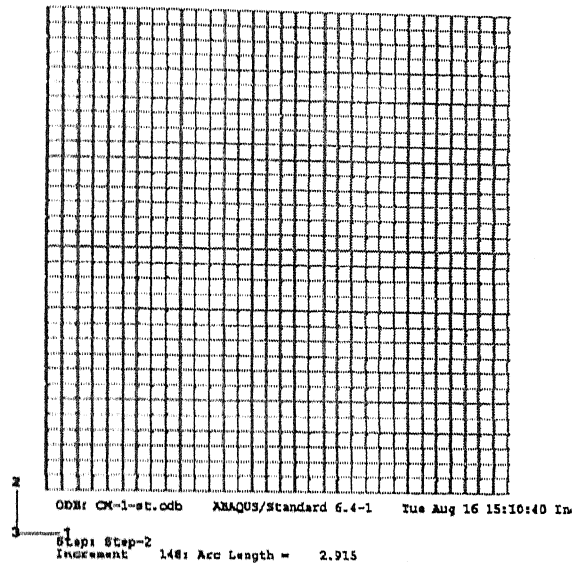
Figure 3.12 Finite element idealization of the wall with Confinement masonry scheme 1.
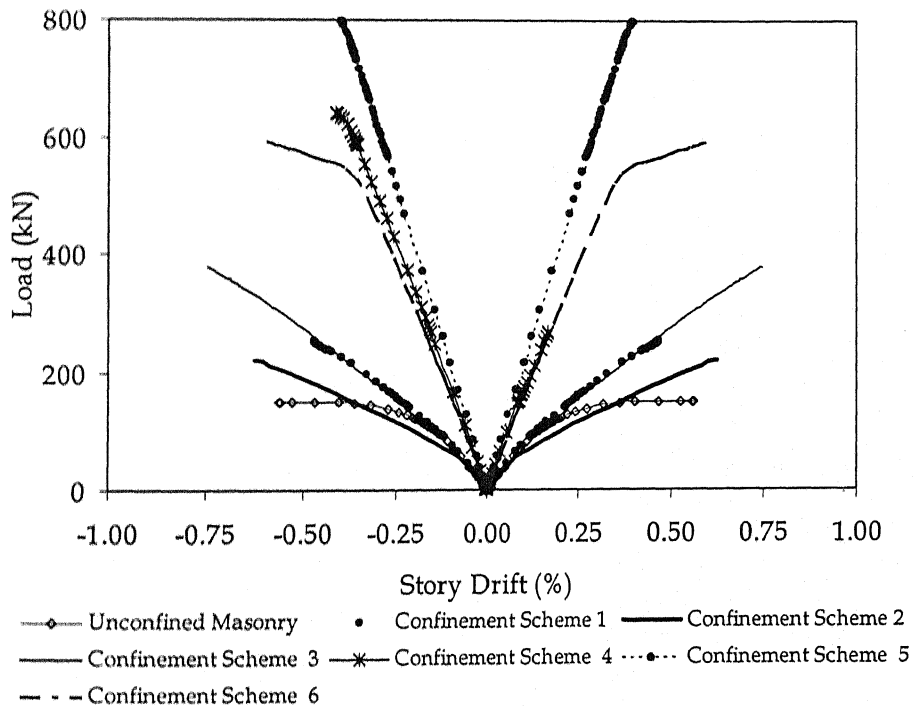
Figure 3.13 Shear force-deformation behaviour of different confinement schemes using Masonry 1 (weak masonry) as predicted by FE analysis.

75
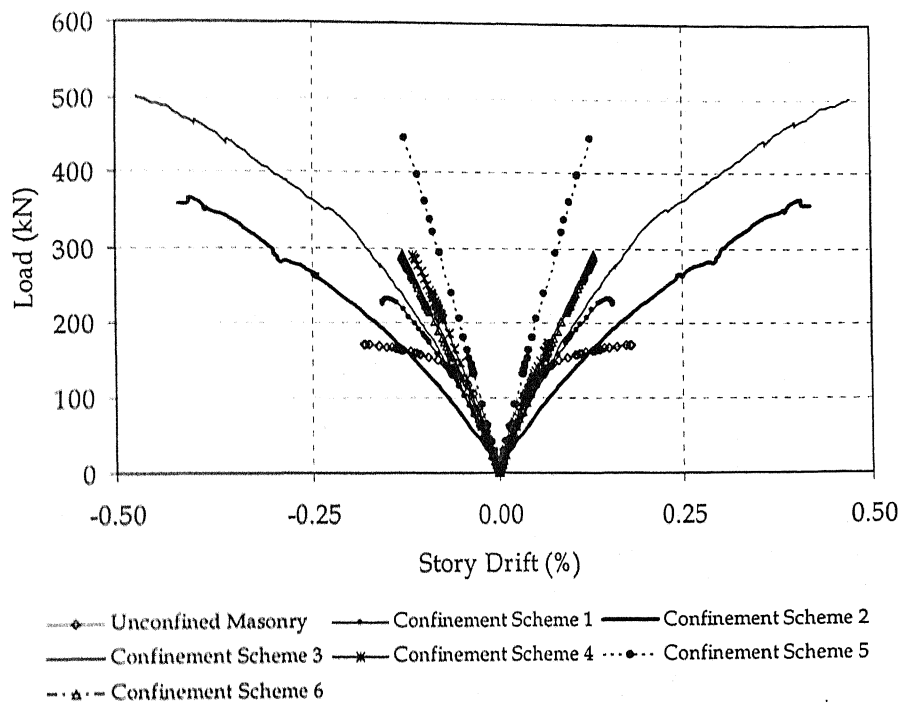
Figure 3.14 Shear force-deformation behaviour of different confinement schemes using Masonry 2 (stiff masonry) as predicted by FE analysis.
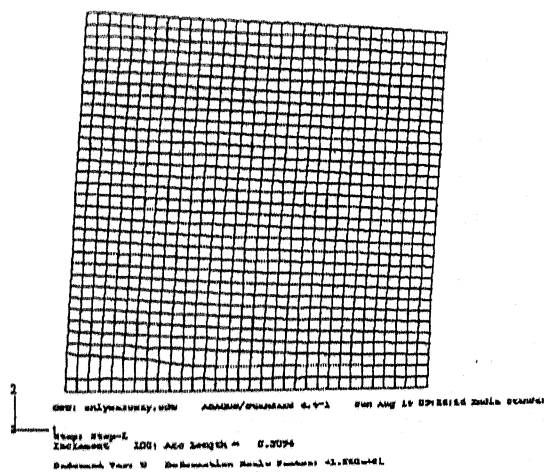
Figure 3.15 Deformed geometry of the Unconfined Masonry model using masonry 1 (weak masonry) at 0.56% story drift rightwards.
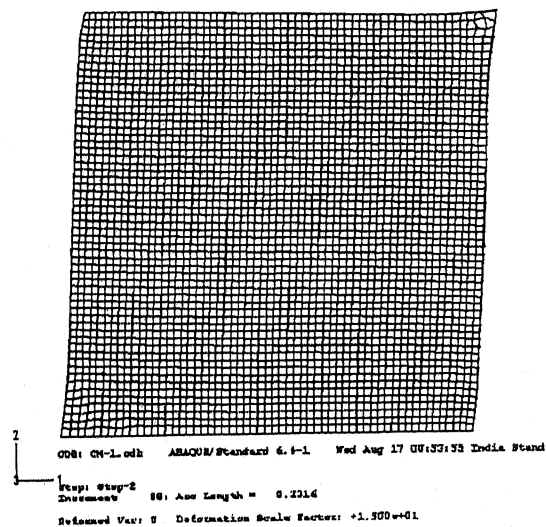
Figure 3.16 Deformed geometry of the Confinement Scheme 1 (only boundary confinement elements) using masonry 1 (weak masonry) at 0.47% story drift rightwards.
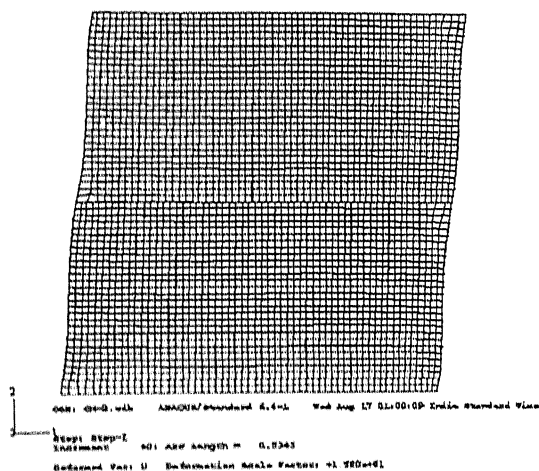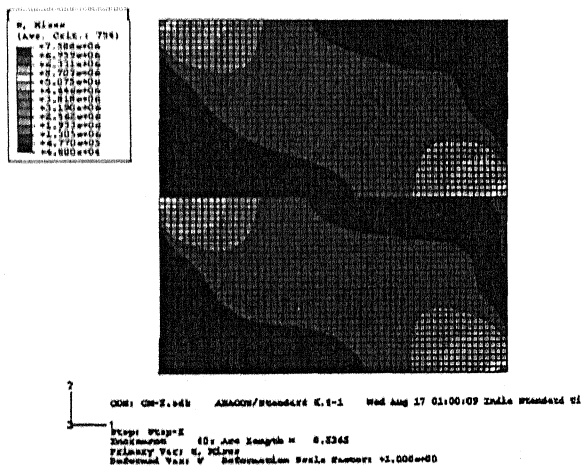
Figure 3.17 Deformed geometry of the Confinement Scheme 2 (boundary and horizontal at mid height confinement elements) using masonry 1 (weak masonry) at 0.62% story drift right-wards.
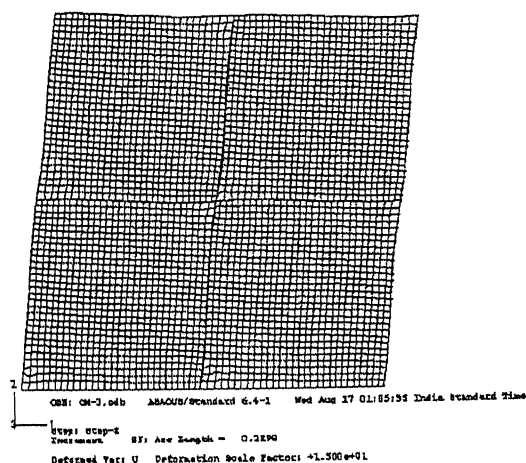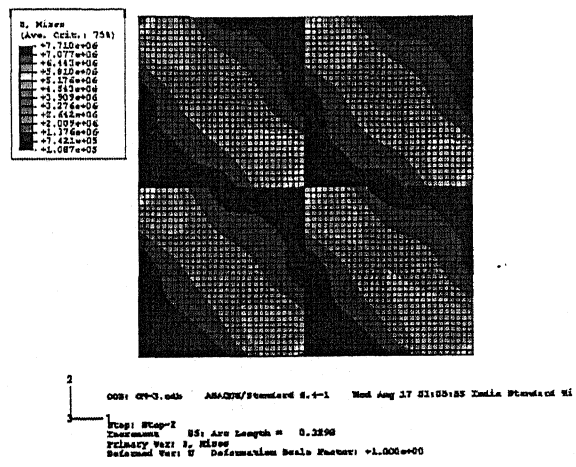

Figure 3.18 Deformed geometry of the Confinement Scheme 3 (boundary and cross confinement elements) using masonry 1 (weak masonry) at 0.74% story drift right-wards.
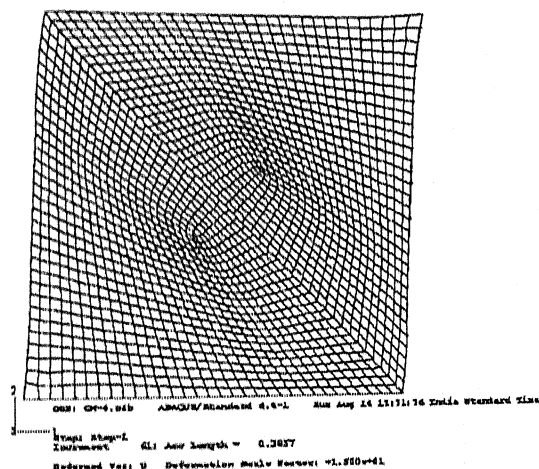
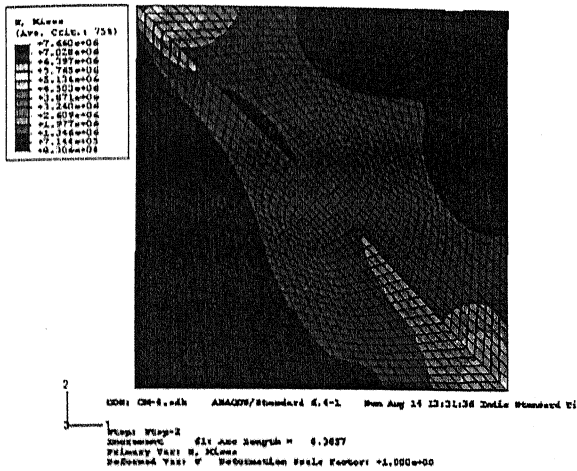**Figure 3.19** Deformed geometry of the Confinement Scheme 4 (boundary and cross diagonal confinement elements) using masonry 1 (weak masonry) at 0.16% story drift right-wards.
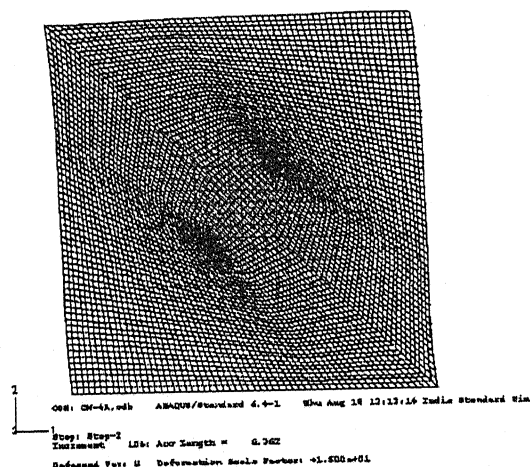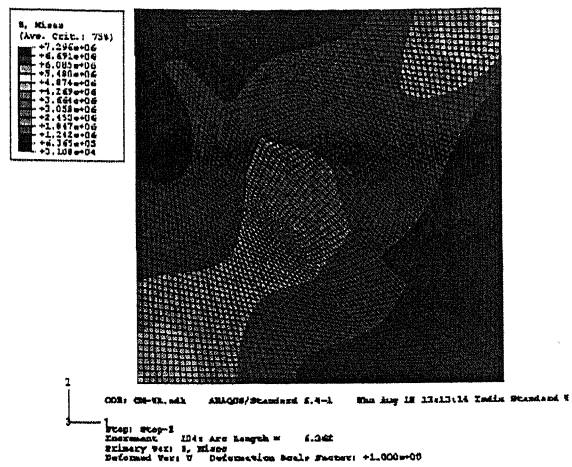

Figure 3.20 Deformed geometry of the Confinement Scheme 4 (boundary and cross diagonal confinement elements) using masonry 1 (weak masonry) at 0.41% story drift left-wards.
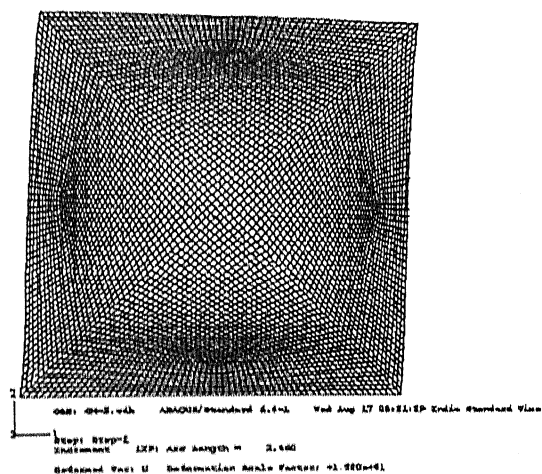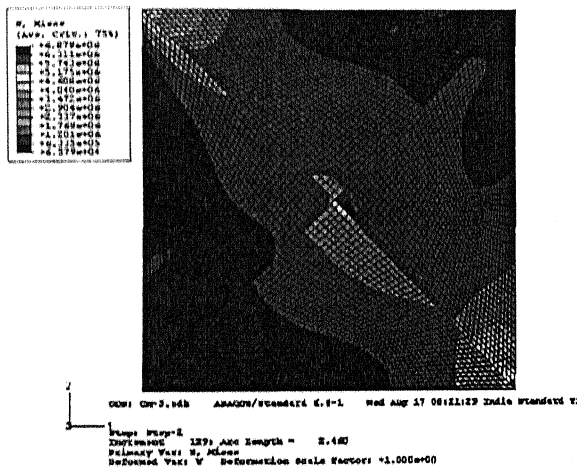
Figure 3.21 Deformed geometry of the Confinement Scheme 5 (boundary and cross diagonal confinement elements) using masonry 1 (weak masonry) at 0.4% story drift right-wards.
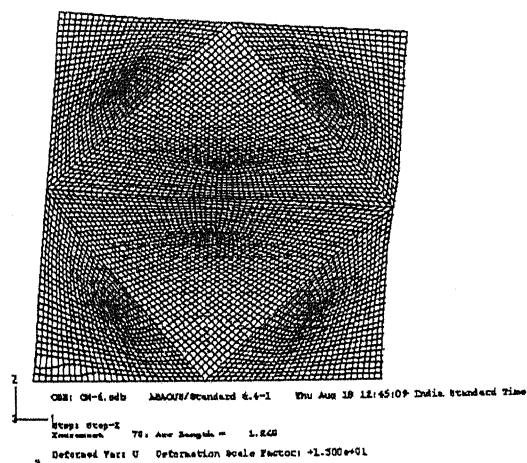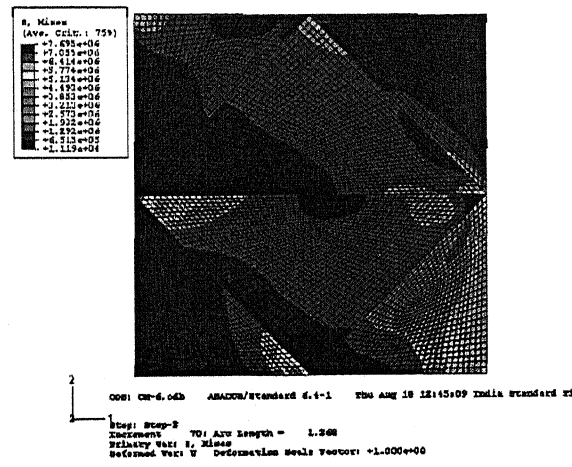

Figure 3.22 Deformed geometry of the Confinement Scheme 6 (boundary and star confinement elements) using masonry 1 (weak masonry) at 0.59% story drift right-wards.
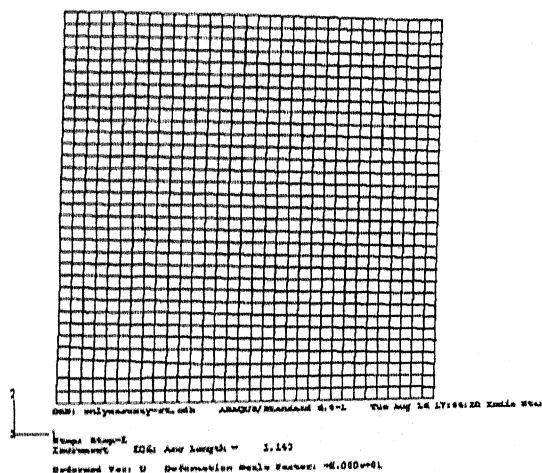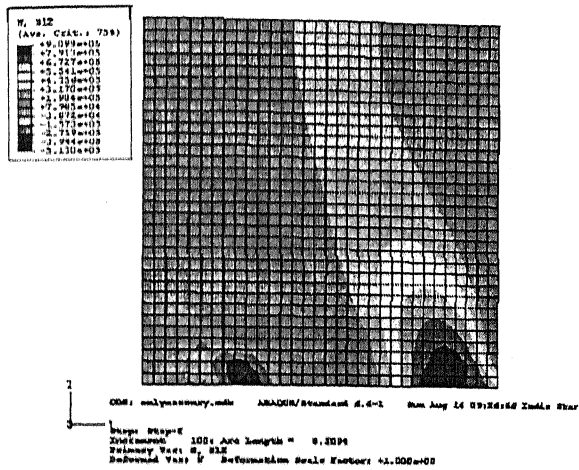

Figure 3.23 Deformed geometry of the Unconfined Masonry model using masonry 2 (stiff masonry) at 0.18% story drift right-wards.
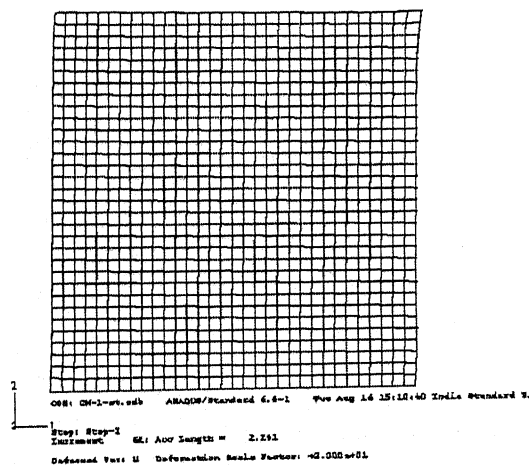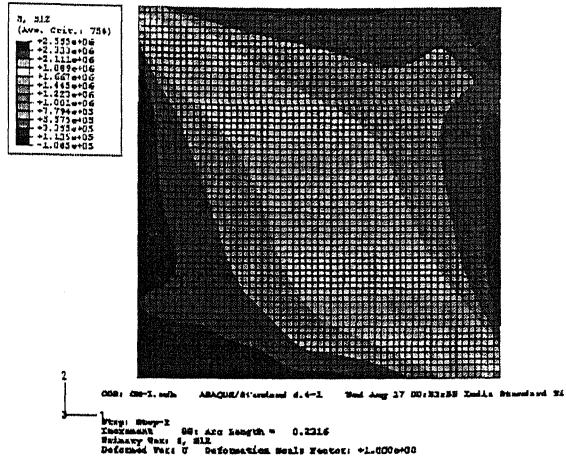

Figure 3.24 Deformed geometry of the Confinement Scheme 1 (only boundary confinement elements) using masonry 2 (stiff masonry) at 0.16% story drift right-wards.
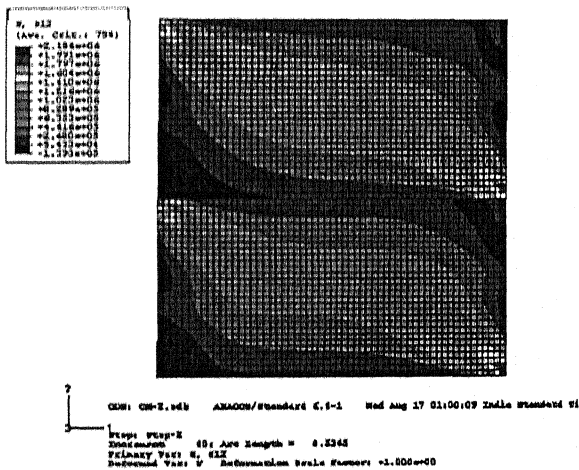
78
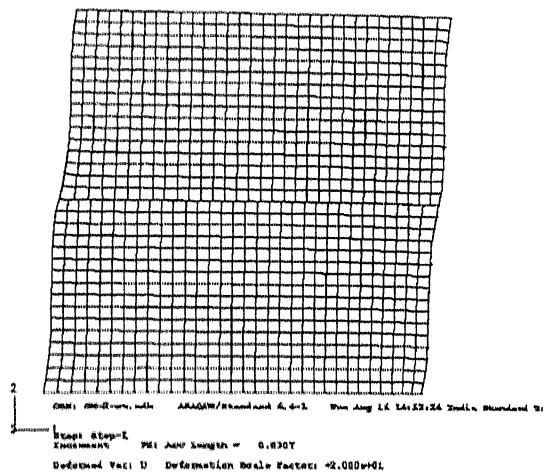
Figure 3.25 Deformed geometry of the Confinement Scheme 2 (boundary and horizontal at mid height confinement elements) using masonry 2 (stiff masonry) at 0.42% story drift right-wards.
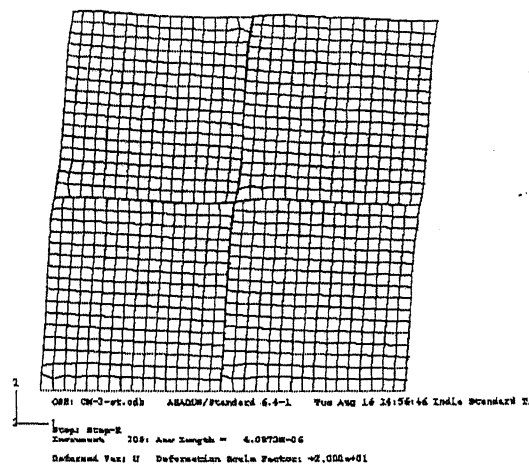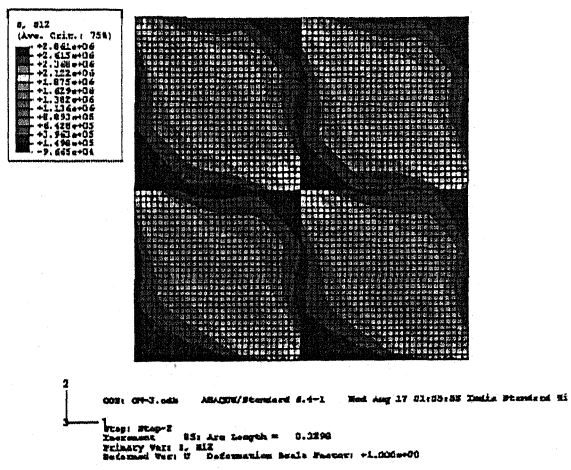

Figure 3.26 Deformed geometry of the Confinement Scheme 3 (boundary and cross confinement elements) using masonry 2 (stiff masonry) at 0.47% story drift right-wards.
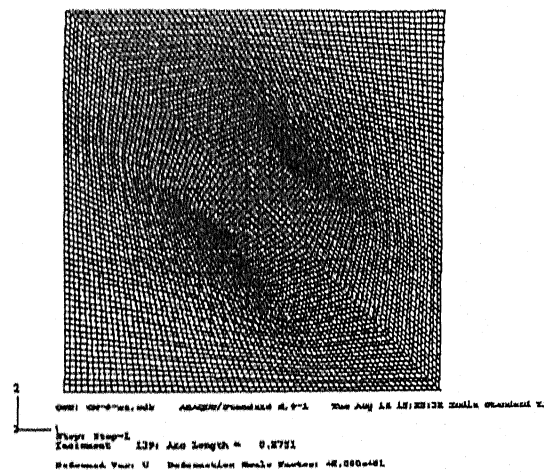
Figure 3.27 Deformed geometry of the only Confinement Scheme 4 (boundary and single diagonal confinement elements) using masonry 2 (stiff masonry) at 0.07% story drift right-wards.
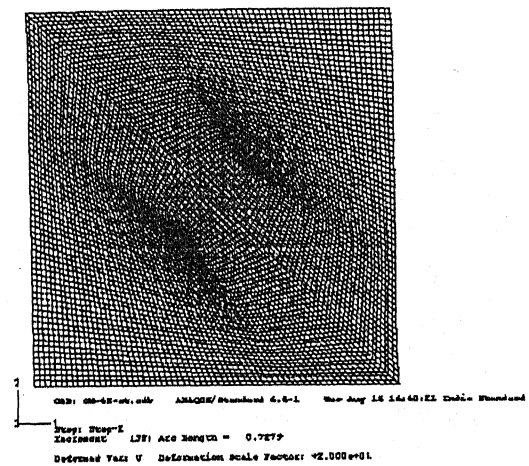
Figure 3.28 Deformed geometry of the Confinement Scheme 4 (boundary and single diagonal confinement elements) using masonry 2 (stiff masonry) at 0.12% story drift left-wards.

79
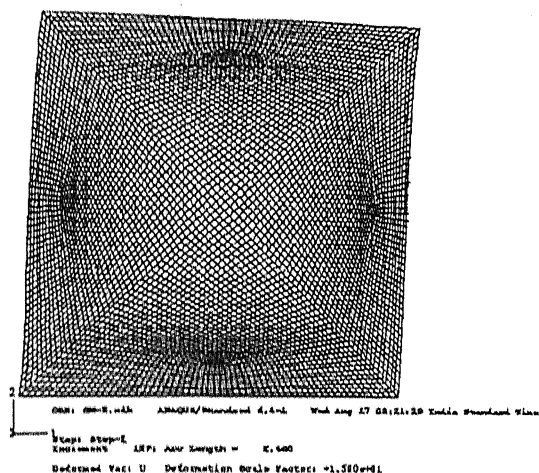
Figure 3.29   Deformed geometry of the Confinement Scheme 5 (boundary and cross diagonal confinement elements) using masonry 2 (stiff masonry) at 0.13% story drift right-wards.
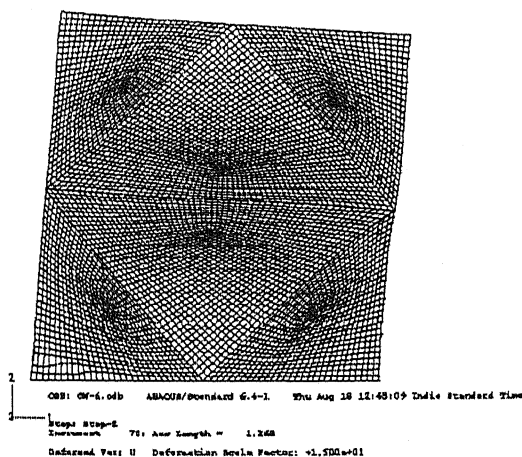
Figure 3.30   Deformed geometry of the Confinement Scheme 6 (boundary and star confinement elements) using masonry 2 (stiff masonry) at 0.18% story drift right-wards.
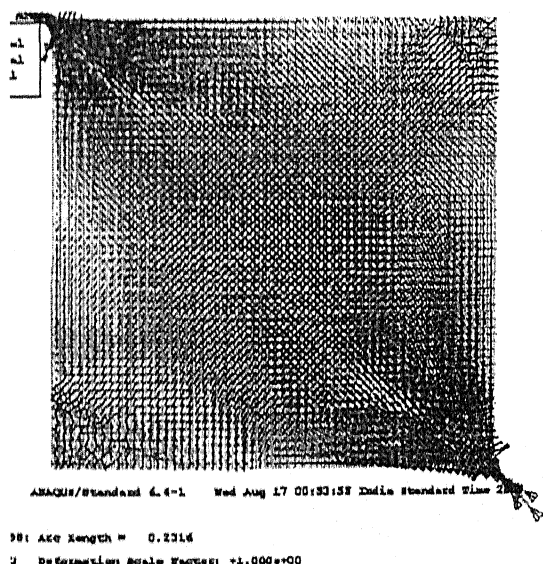

Figure 3.31   Vector plot of major principal stress in Confinement Scheme 1 (only boundary confinement elements) using masonry 1 (weak masonry) at 0.47% story drift right-wards.
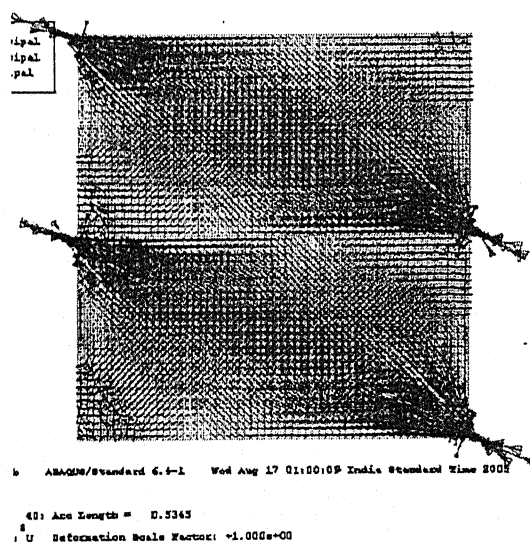
Figure 3.32   Vector plot of major principal stress in Confinement Scheme 2 (boundary and horizontal at mid height confinement elements) using masonry 2 (weak masonry) at 0.62% story drift right-wards.
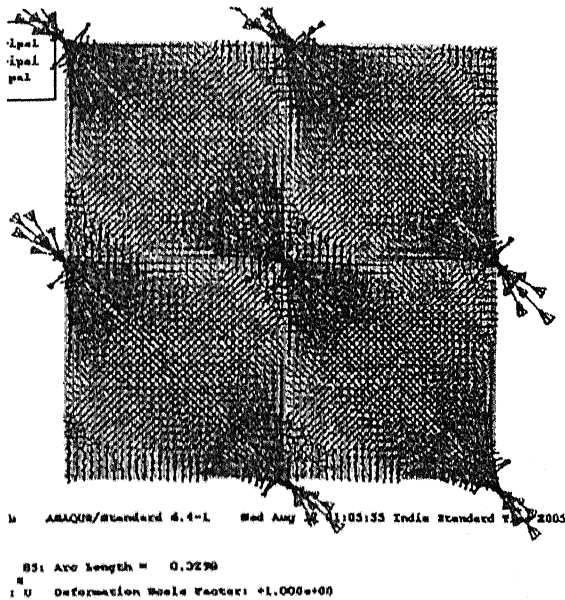
Figure 3.33 Vector plot of major principal stress in Confinement Scheme 3 (boundary and cross confinement elements) using masonry 1 (weak masonry) at 0.74% story drift right-wards.
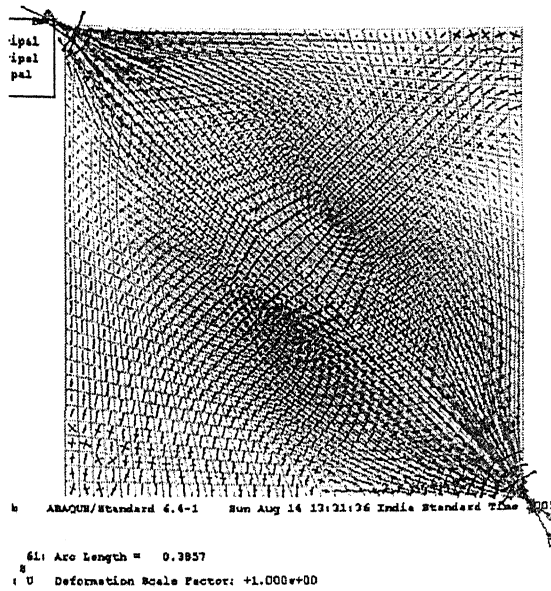
Figure 3.34 Vector plot of major principal stress in Confinement Scheme 4 (boundary and single diagonal confinement elements) using masonry 1 (weak masonry) at 0.17% story drift right-wards.
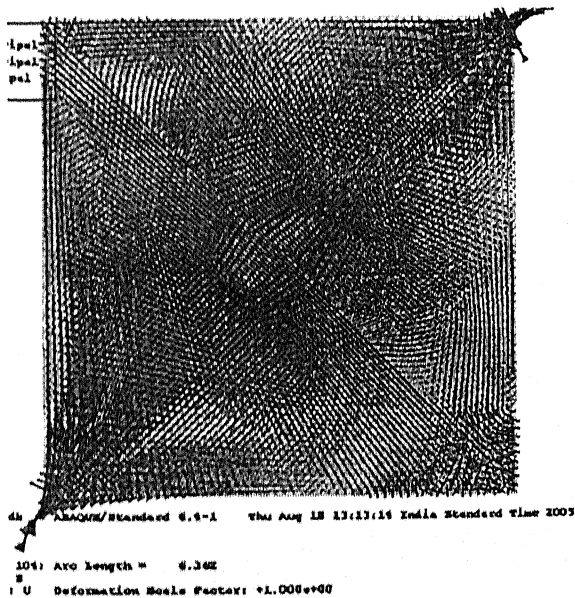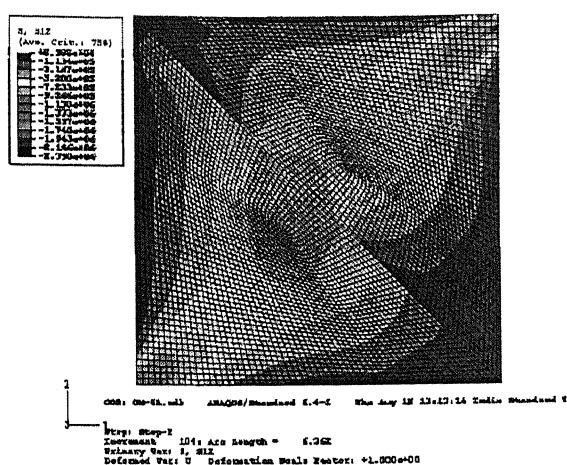

Figure 3.35 Vector plot of major principal stress in Confinement Scheme 4 (boundary and single diagonal confinement elements) using masonry 1 (weak masonry) at 0.41% story drift left-wards.
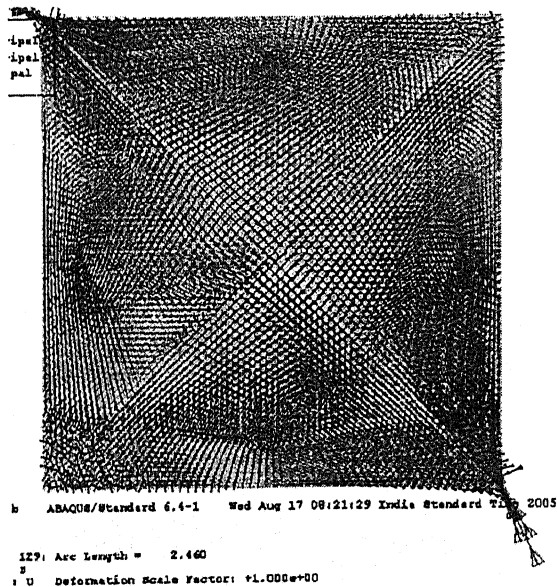
Figure 3.36 Vector plot of major principal stress in Confinement Scheme 5 (boundary and cross diagonal confinement elements) using masonry 1 (weak masonry) at 0.39% story drift right-wards.

81
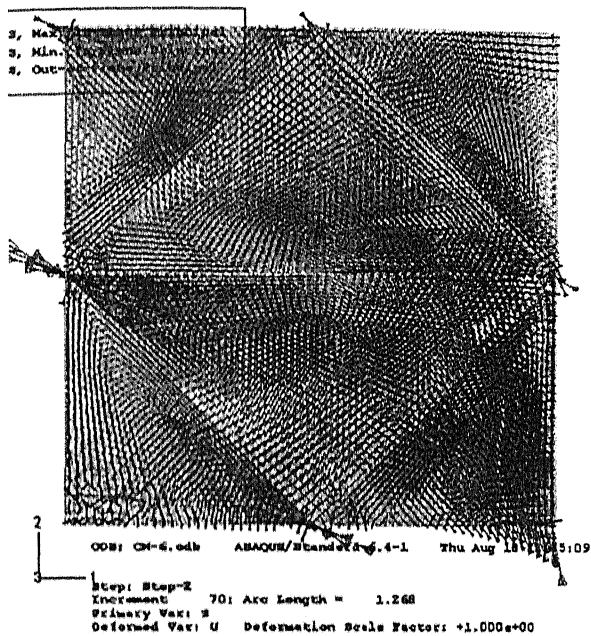
Figure 3.37 Vector plot of major principal stress in Confinement Scheme 6 (boundary and star confinement elements) using masonry 1 (weak masonry) at 0.59% story drift right-wards.
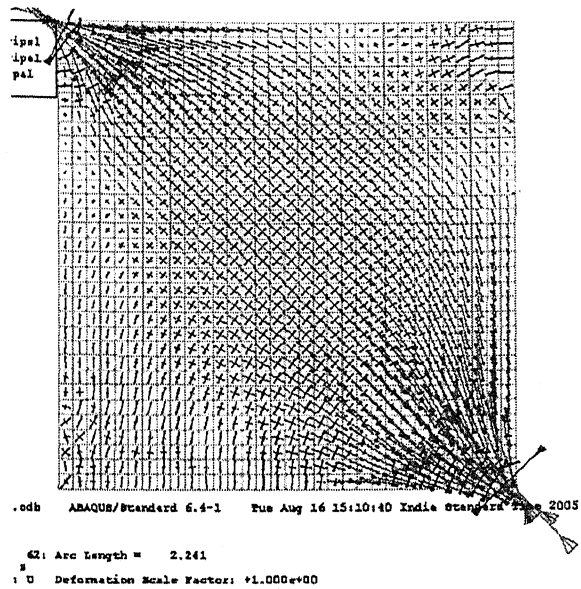
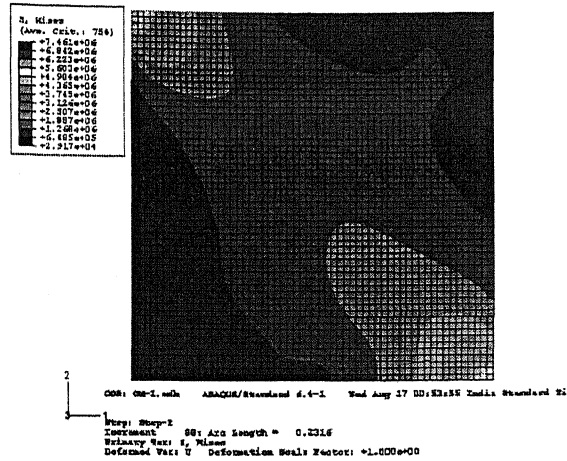**Figure 3.38** Vector plot of major principal stress in Confinement Scheme 1 (only boundary confinement elements) using masonry 2 (stiff masonry) at 0.16% story drift right-wards.
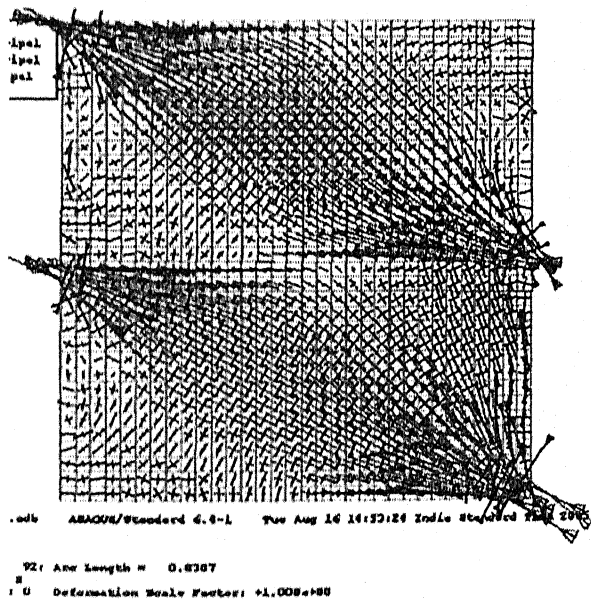
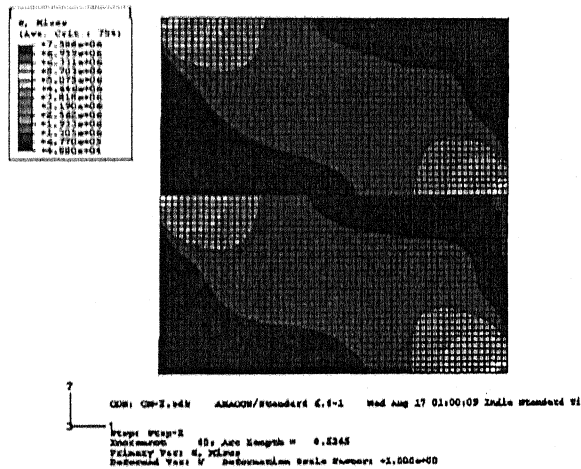**Figure 3.39** Vector plot of major principal stress in Confinement Scheme 2 (boundary and horizontal at mid height confinement elements) using masonry 2 (stiff masonry) at 0.42% story drift right-wards.
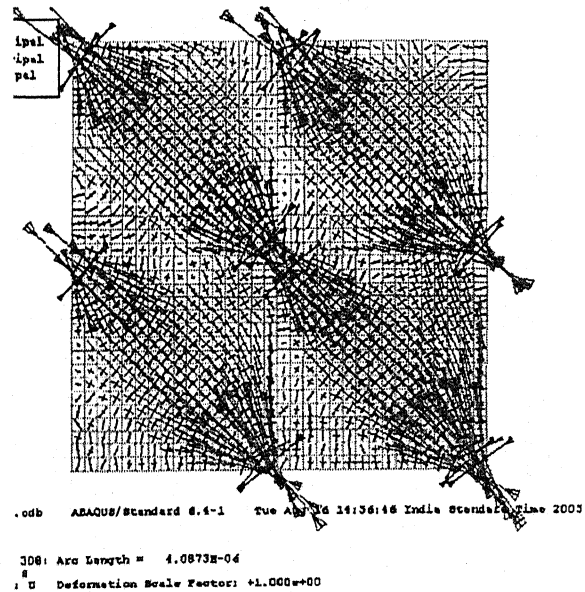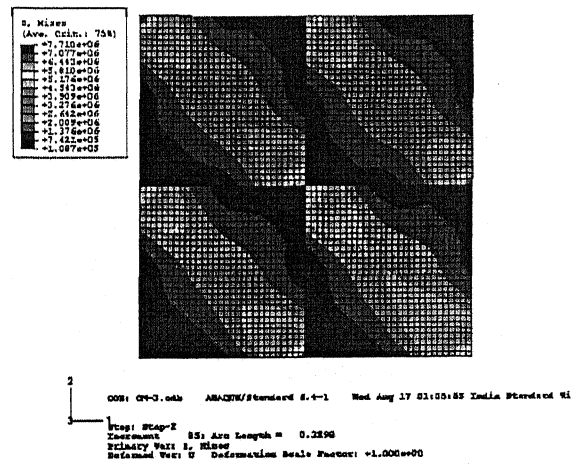

Figure 3.40 Vector plot of major principal stress in Confinement Scheme 3 (boundary and cross confinement elements) using masonry 2 (stiff masonry) at 0.47% story drift right-wards.
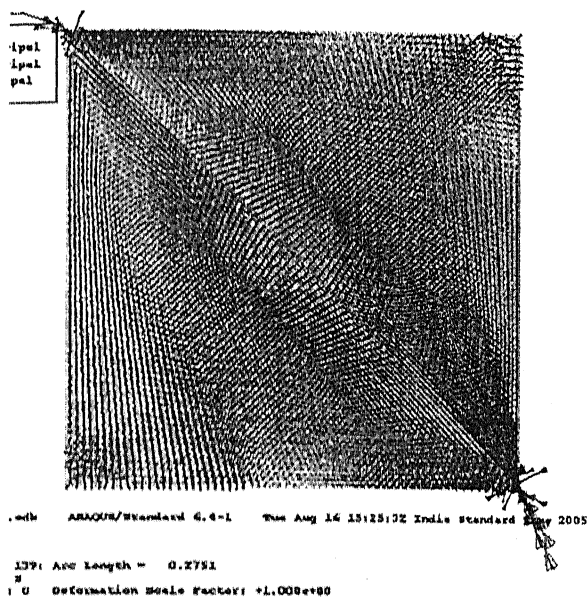
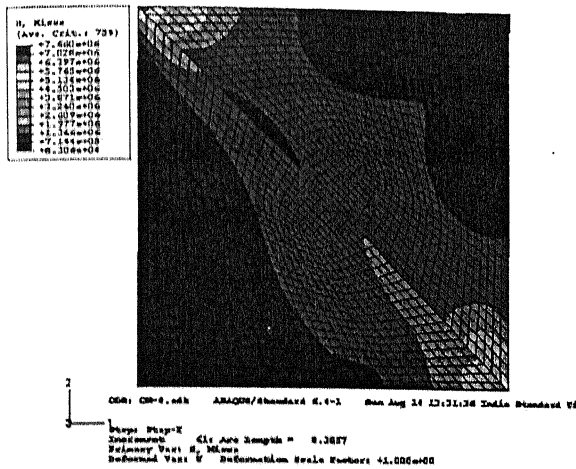**Figure 3.41** Vector plot of major principal stress in Confinement Scheme 4 (boundary and single diagonal confinement elements) using masonry 2 (stiff masonry) at 0.07% story drift right-wards.
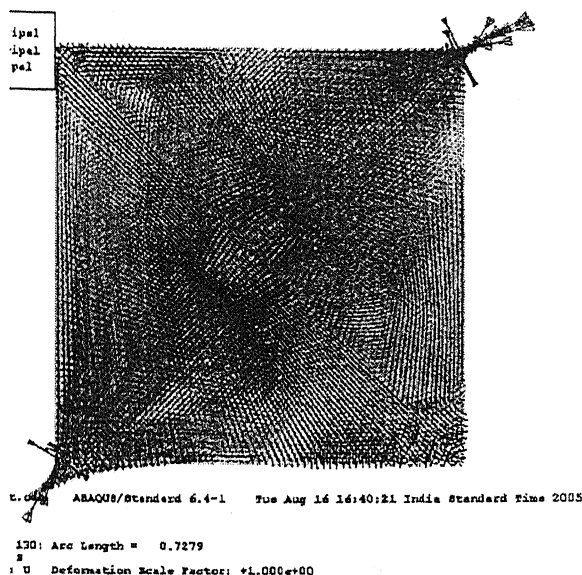
Figure 3.42 Vector plot of major principal stress in Confinement Scheme 4 (boundary and single diagonal confinement elements) using masonry 2 (stiff masonry) at 0.11% story drift left-wards.
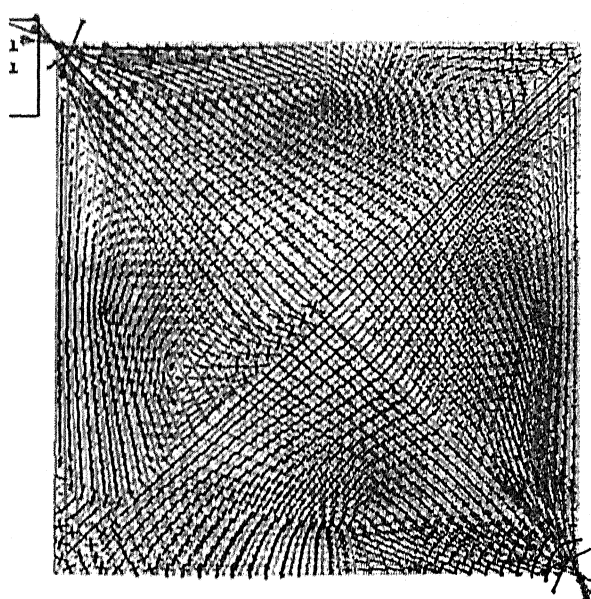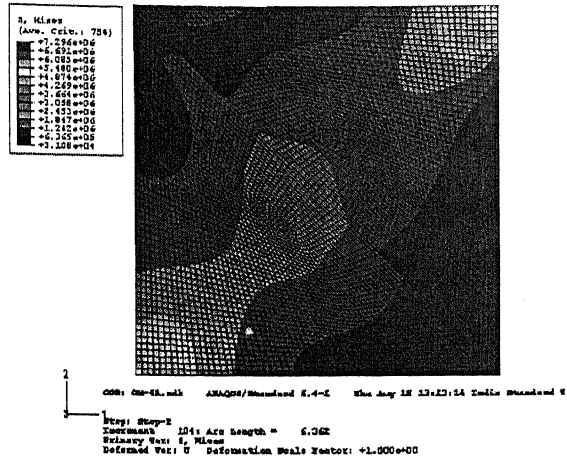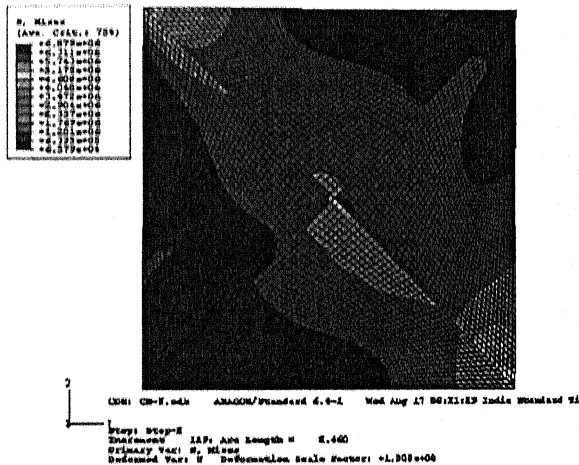
Figure 3.43 Vector plot of major principal stress in Confinement Scheme 5 (boundary and cross diagonal confinement elements) using masonry 2 (stiff masonry) at 0.12% story drift right-wards.
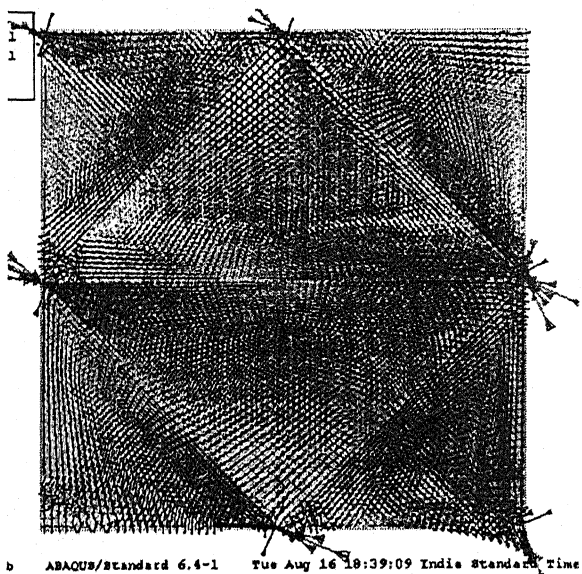
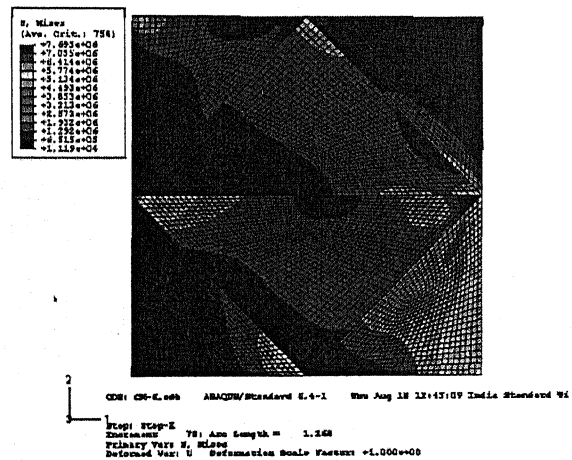**Figure 3.44** Vector plot of major principal stress in Confinement Scheme 6 (boundary and star confinement elements) using masonry 2 (stiff masonry) at 0.13% story drift right-wards.

83
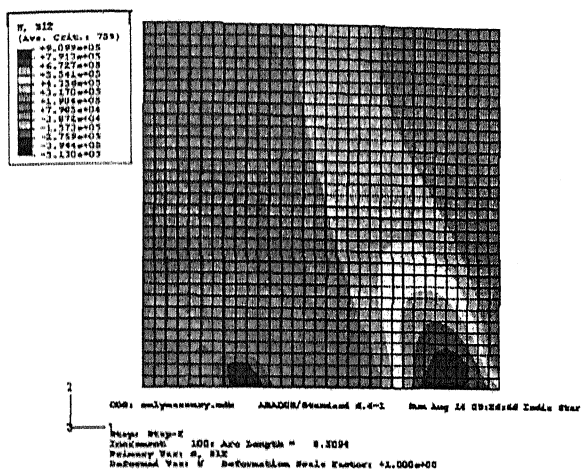
Figure 3.45 Contours of the shear stress in Unconfined Masonry model using masonry 1 (weak masonry) at 0.56% story drift right-wards.
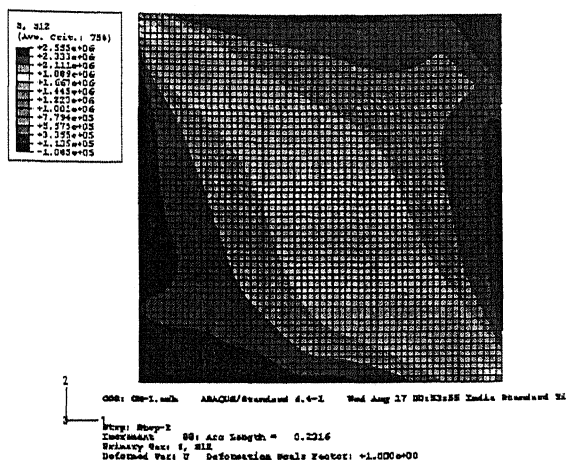
Figure 3.46 Contours of the shear stress in Confinement Scheme 1 (only boundary confinement elements) using masonry 1 (weak masonry) at 0.46% story drift right-wards.
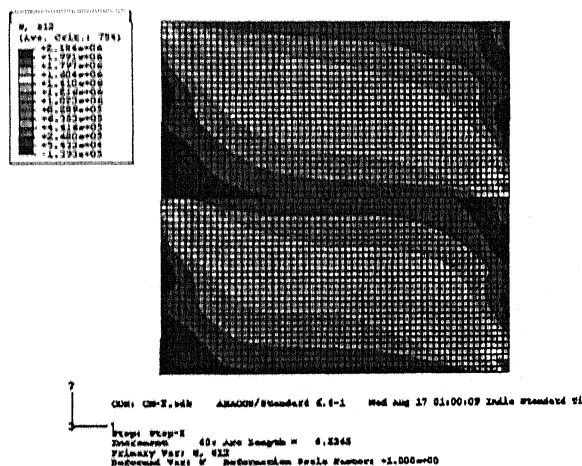
Figure 3.47 Contours of the shear stress in Confinement Scheme 2 (boundary and horizontal at mid height confinement elements) using masonry 1 (weak masonry) at 0.62% story drift right-wards.
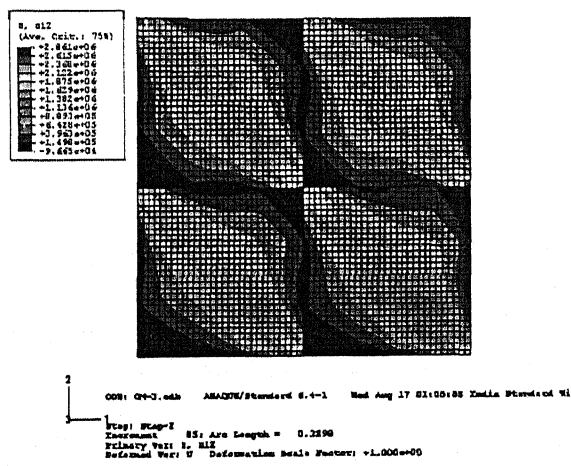
Figure 3.48 Contours of the shear stress in Confinement Scheme 3 (boundary and cross confinement elements) using masonry 1 (weak masonry) at 0.74% story drift right-wards.
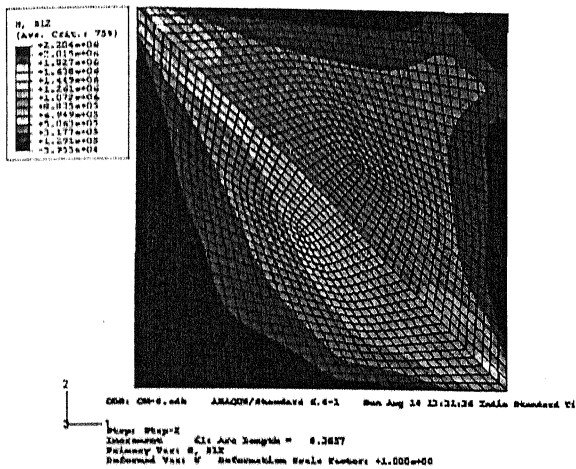
Figure 3.49 Contours of the shear stress in Confinement Scheme 4 (boundary and single diagonal confinement elements) using masonry 1 (weak masonry) at 0.16% story drift right-wards.
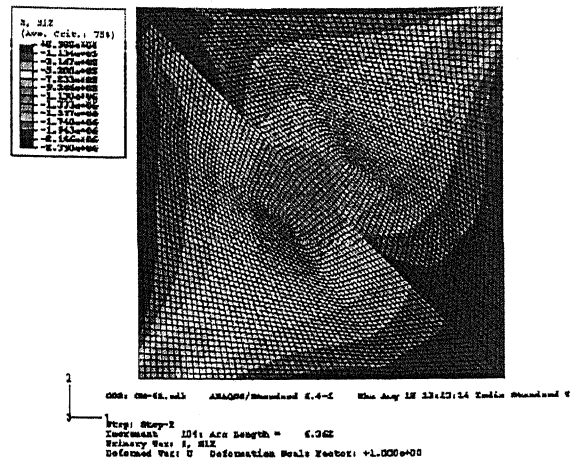
Figure 3.50 Contours of the shear stress in Confinement Scheme 4 (boundary and single diagonal confinement elements) using masonry 1 (weak masonry) at 0.41% story drift left-wards.
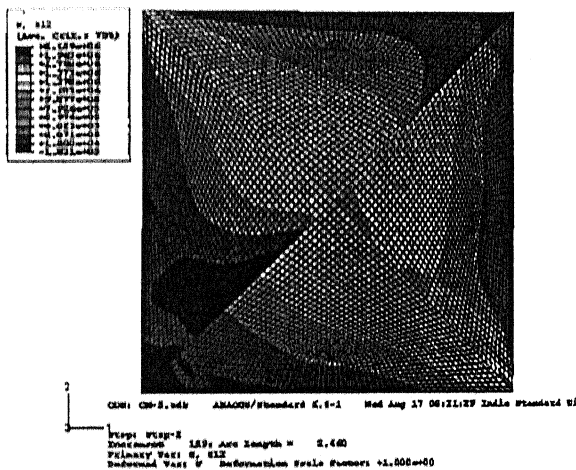
Figure 3.51 Contours of the shear stress in Confinement Scheme 5 (boundary and cross diagonal confinement elements) using masonry 1 (weak masonry) at 0.40% story drift right-wards.
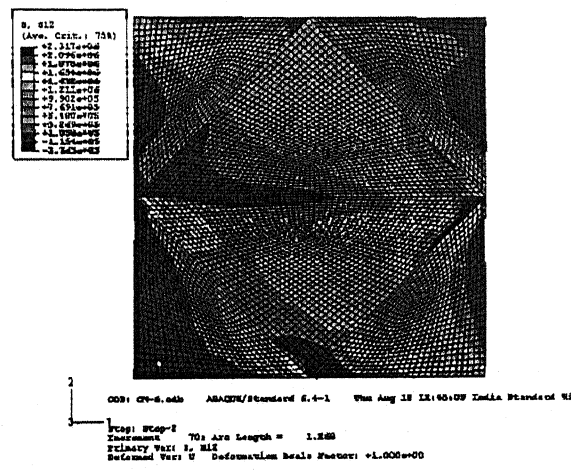
Figure 3.52 Contours of the shear stress in Confinement Scheme 6 (boundary and star confinement elements) using masonry 1 (weak masonry) at 0.59% story drift right-wards.

85
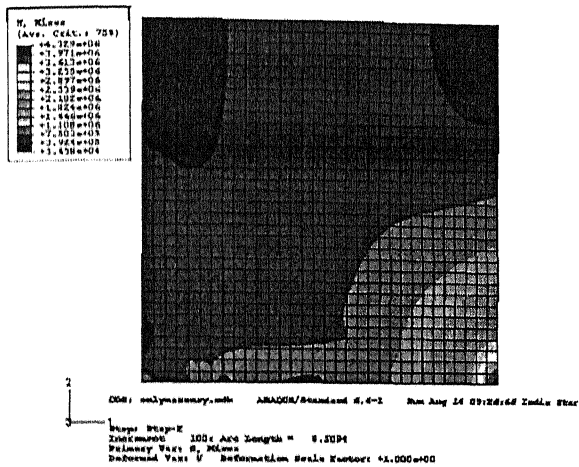
Figure 3.53 Contours of the Von-Mises stress in Unconfined Masonry model using masonry 1 (weak masonry) at 0.56% story drift right-wards.
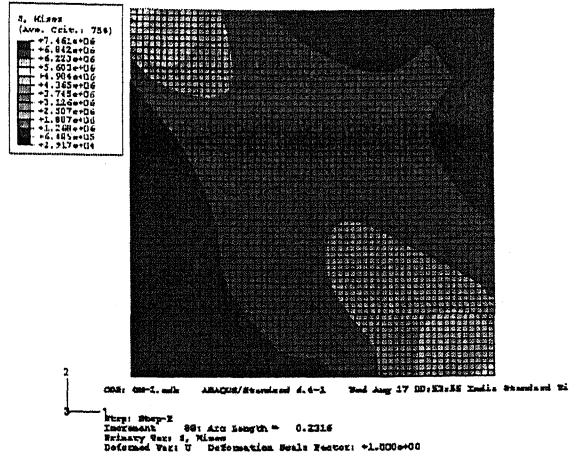
Figure 3.54 Contours of the Von-Mises stress in Confinement Scheme 1 (only boundary confinement elements) using masonry 1 (weak masonry) at 0.46% story drift right-wards.

Figure 3.55 Contours of the Von-Mises stress in Confinement Scheme 2 (boundary and horizontal at mid height confinement elements) using masonry 1 (weak masonry) at 0.62% story drift right-wards.

Figure 3.56 Contours of the Von-Mises stress in Confinement Scheme 3 (boundary and cross confinement elements) using masonry 1 (weak masonry) at 0.74% story drift right-wards.

Figure 3.57 Contours of the Von-Mises stress in Confinement Scheme 4 (boundary and single diagonal confinement elements) using masonry 1 (weak masonry) at 0.16% story drift right-wards.

Figure 3.58 Contours of the Von-Mises stress in Confinement Scheme 4 (boundary and single diagonal confinement elements) using masonry 1 (weak masonry) at 0.41% story drift left-wards.

Figure 3.59 Contours of the Von-Mises stress in Confinement Scheme 5 (boundary and cross diagonal confinement elements) using masonry 1 (weak masonry) at 0.40% story drift right-wards.

Figure 3.60 Contours of the Von-Mises stress in Confinement Scheme 6 (boundary and star confinement elements) using masonry 1 (weak masonry) at 0.59% story drift right-wards.

87

Figure 3.61 Contours of the shear stress in Unconfined Masonry model using masonry 2 (stiff masonry) at 0.18% story drift right-wards.

Figure 3.62 Contours of the shear stress in Confinement Scheme 1 (only boundary confinement elements) using masonry 1 2 (stiff masonry) at 0.16% story drift right-wards.

Figure 3.63 Contours of the shear stress in Confinement Scheme 2 (boundary and horizontal at mid height confinement elements) using masonry 2 (stiff masonry) at 0.42% story drift right-wards.

Figure 3.64 Contours of the shear stress in Confinement Scheme 3 (boundary and cross confinement elements) using masonry 2 (stiff masonry) at 0.47% story drift right-wards.
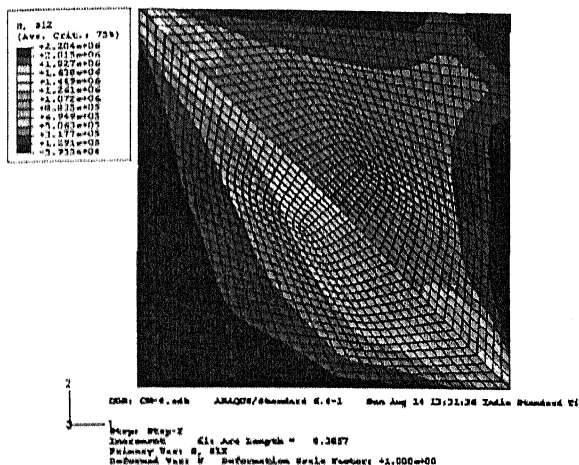
Figure 3.65 Contours of the shear stress in Confinement Scheme 4 (boundary and single diagonal confinement elements) using masonry 2 (stiff masonry) at 0.07% story drift right-wards.

Figure 3.66 Contours of the shear stress in Confinement Scheme 4 (boundary and single diagonal confinement elements) using masonry 2 (stiff masonry) at 0.11% story drift left-wards.
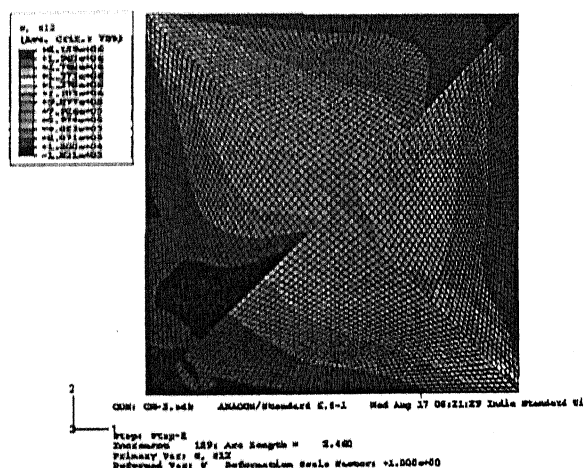
Figure 3.67 Contours of the shear stress in Confinement Scheme 5 (boundary and cross diagonal confinement elements) using masonry 2 (stiff masonry) at 0.13% story drift right-wards.
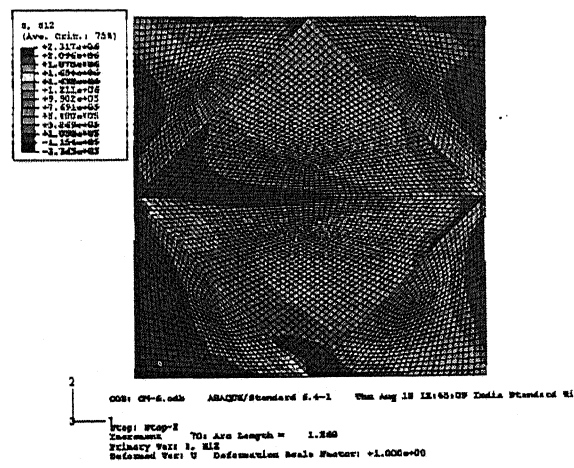
Figure 3.68 Contours of the shear stress in Confinement Scheme 6 (boundary and star confinement elements) using masonry 2 (stiff masonry) at 0.13% story drift right-wards.

89
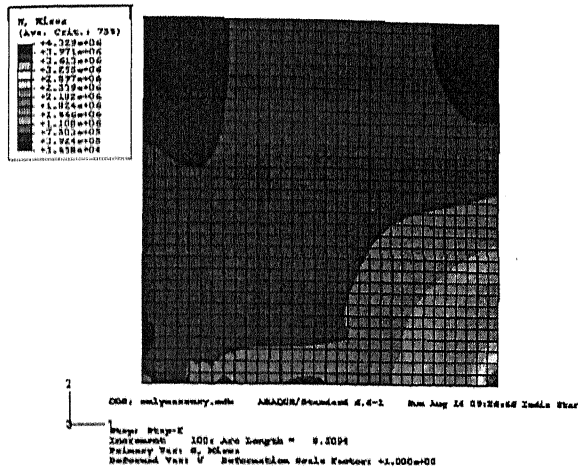
Figure 3.69 Contours of the Von-Mises stress in Unconfined Masonry model using masonry 2 (stiff masonry) at 0.18% story drift right-wards.

Figure 3.70 Contours of the Von-Mises stress in Confinement Scheme 1 (only boundary confinement elements) using masonry 1 2 (stiff masonry) at 0.16% story drift right-wards.

Figure 3.71 Contours of the Von-Mises stress in Confinement Scheme 2 (boundary and horizontal at mid height confinement elements) using masonry 2 (stiff masonry) at 0.42% story drift right-wards.

Figure 3.72 Contours of the Von-Mises stress in Confinement Scheme 3 (boundary and cross confinement elements) using masonry 2 (stiff masonry) at 0.47% story drift right-wards.

Figure 3.73 Contours of the Von-Mises stress in Confinement Scheme 4 (boundary and single diagonal confinement elements) using masonry 2 (stiff masonry) at 0.07% story drift right-wards.

Figure 3.74 Contours of the Von-Mises stress in Confinement Scheme 4 (boundary and single diagonal confinement elements) using masonry 2 (stiff masonry) at 0.11% story drift left-wards.

Figure 3.75 Contours of the Von-Mises stress in Confinement Scheme 5 (boundary and cross diagonal confinement elements) using masonry 2 (stiff masonry) at 0.13% story drift right-wards.

Figure 3.76 Contours of the Von-Mises stress in Confinement Scheme 6 (boundary and star confinement elements) using masonry 2 (stiff masonry) at 0.13% story drift right-wards.

91
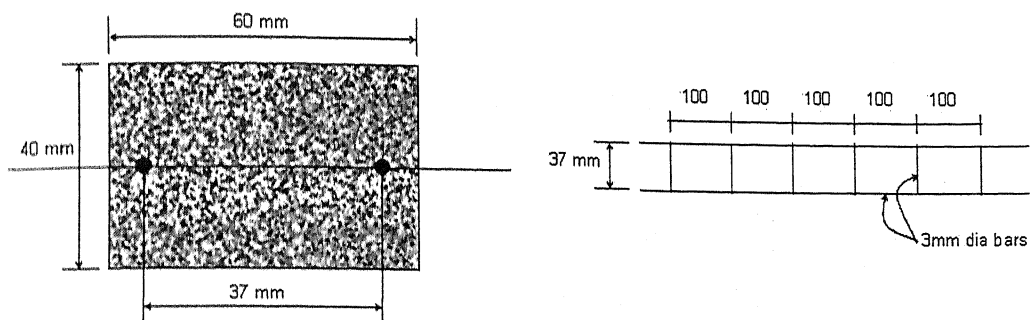
Figure 4.1 Cross section and reinforcement of confinement grid members used in specimen 1.
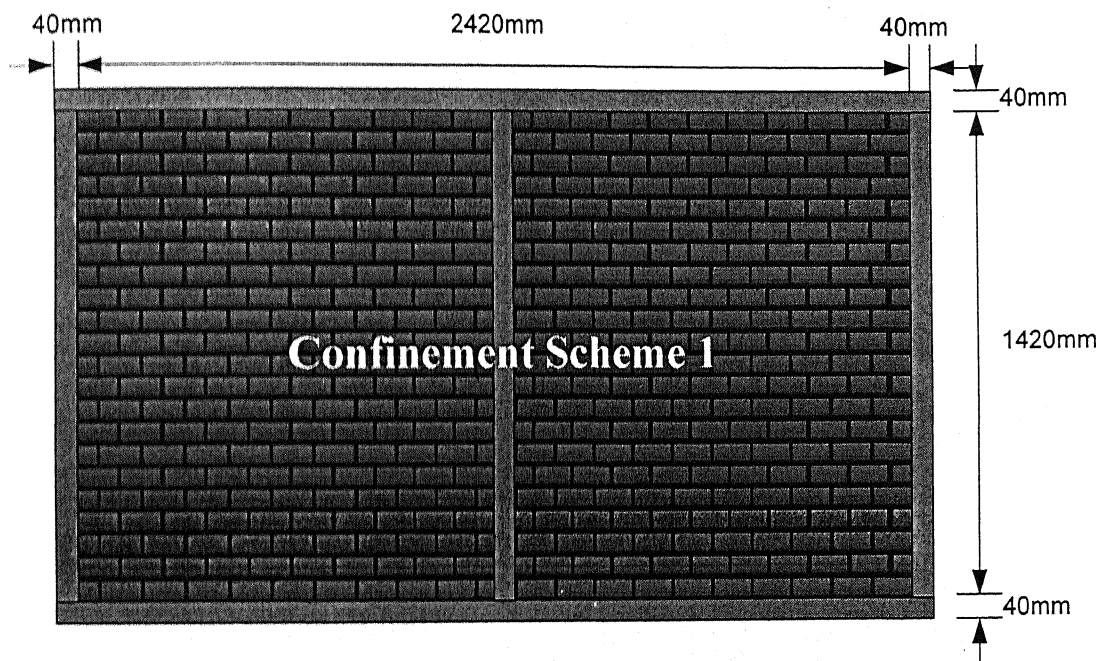
Figure 4.2 Confinement scheme 1 used in experimental studies.
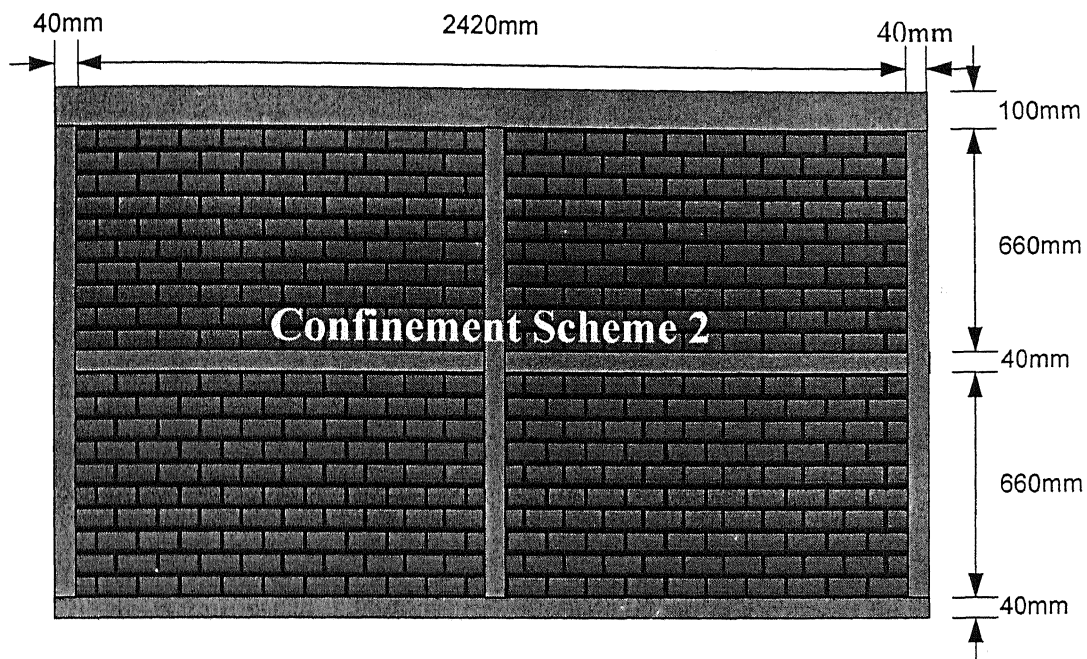
Figure 4.3 Confinement scheme 2 used in experimental studies.
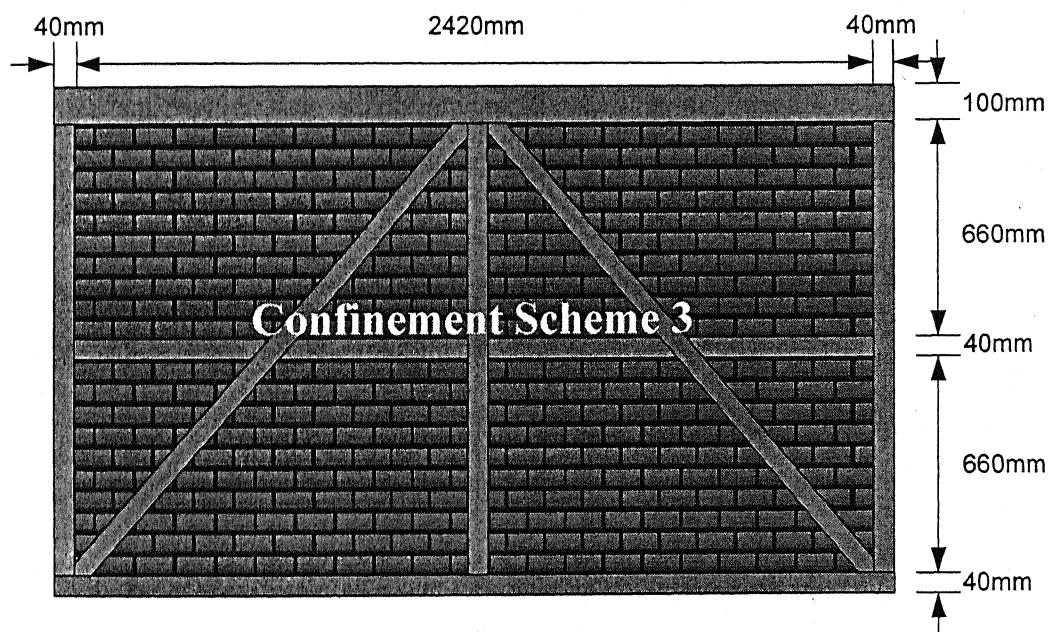
Figure 4.4 Confinement scheme 3 used in experimental studies.
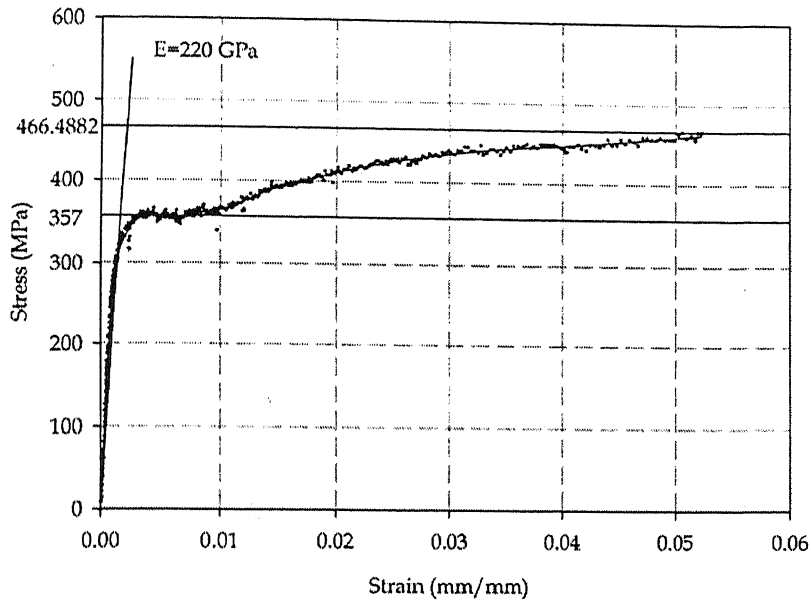
Figure 4.5   Tensile behaviour of Steel used in confinement grid members of first Specimen and also in FE analysis.
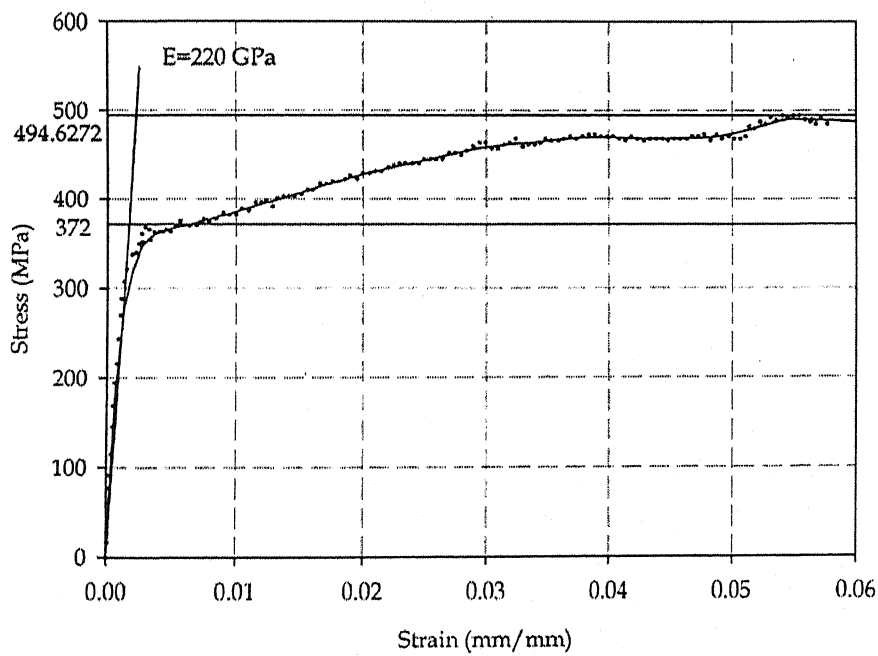
Figure 4.6   Tensile behaviour of Steel used in confinement grid members of second and third Specimens.
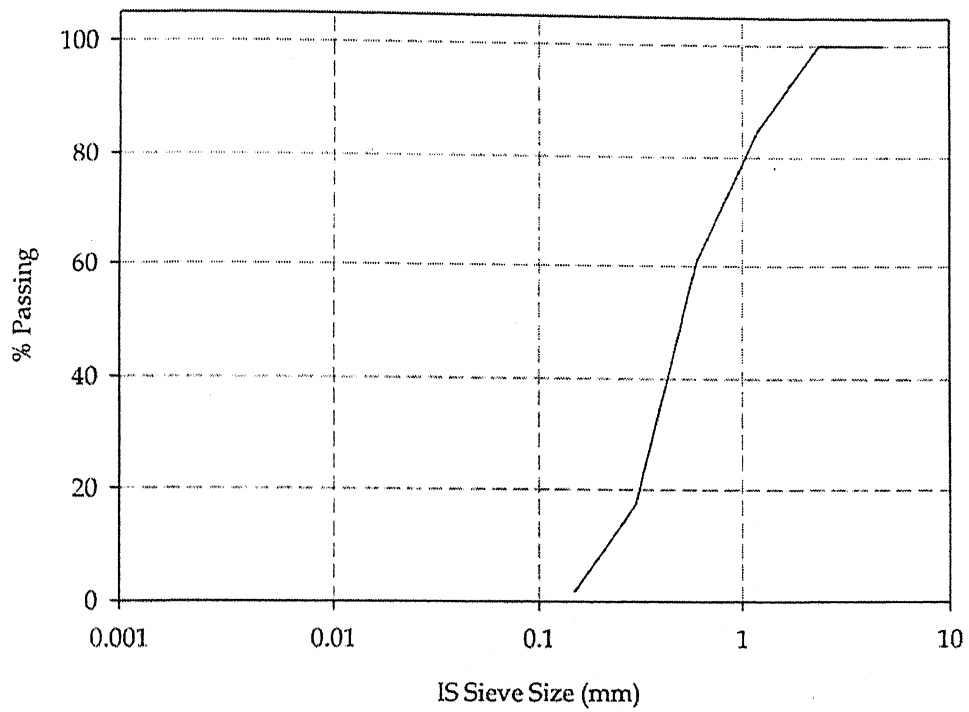
Figure 4.7 Grading curve of sand used in the masonry.
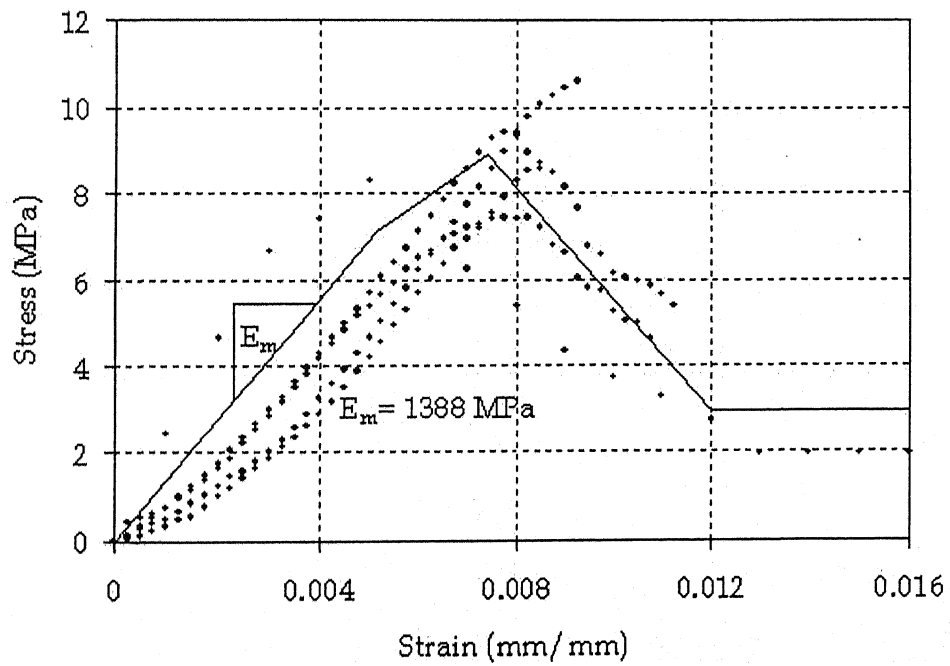
Figure 4.8 Compressive behaviour of masonry.

95
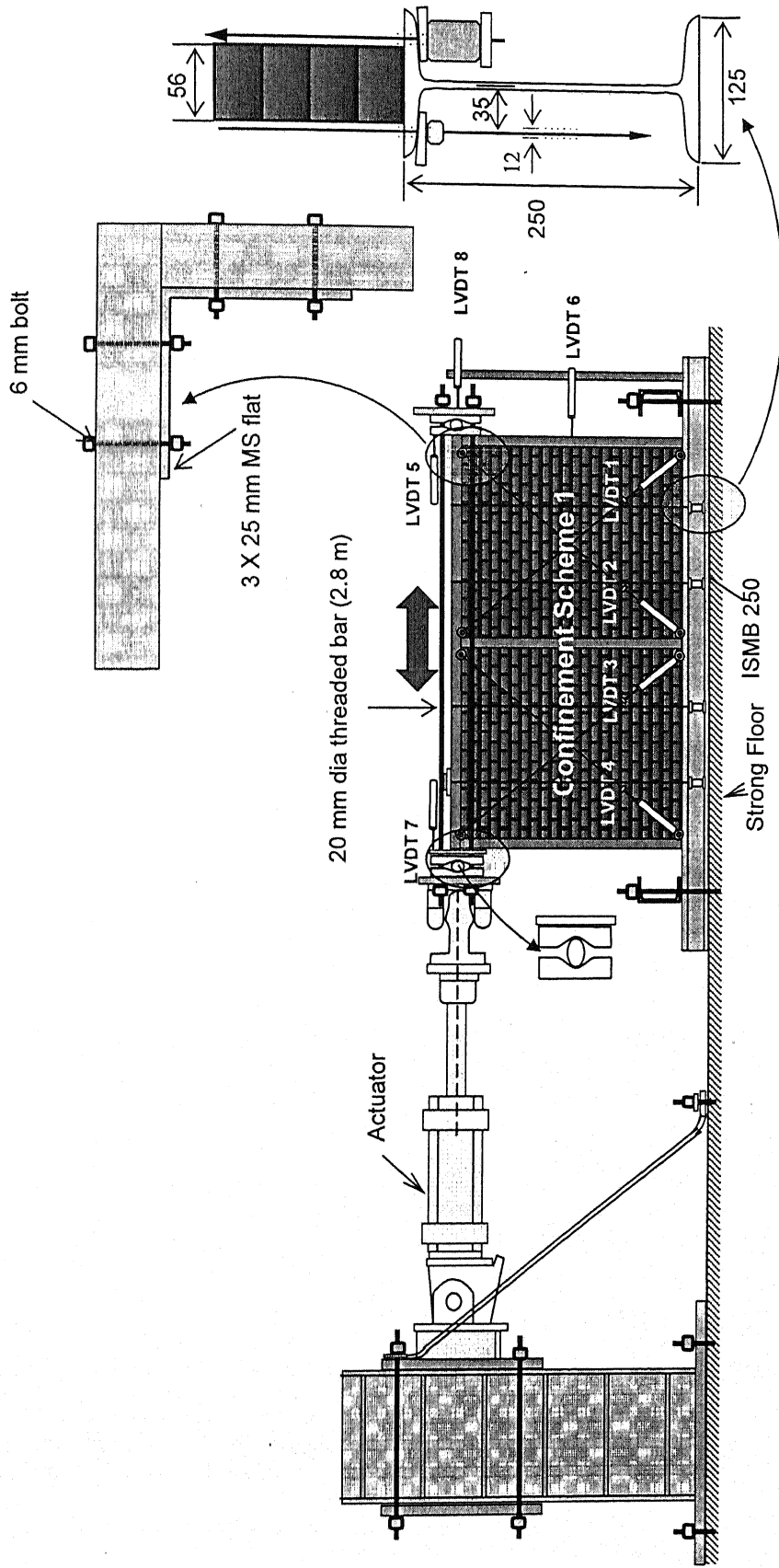
Figure 4.9   Schematic of the test setup and the first test specimen.
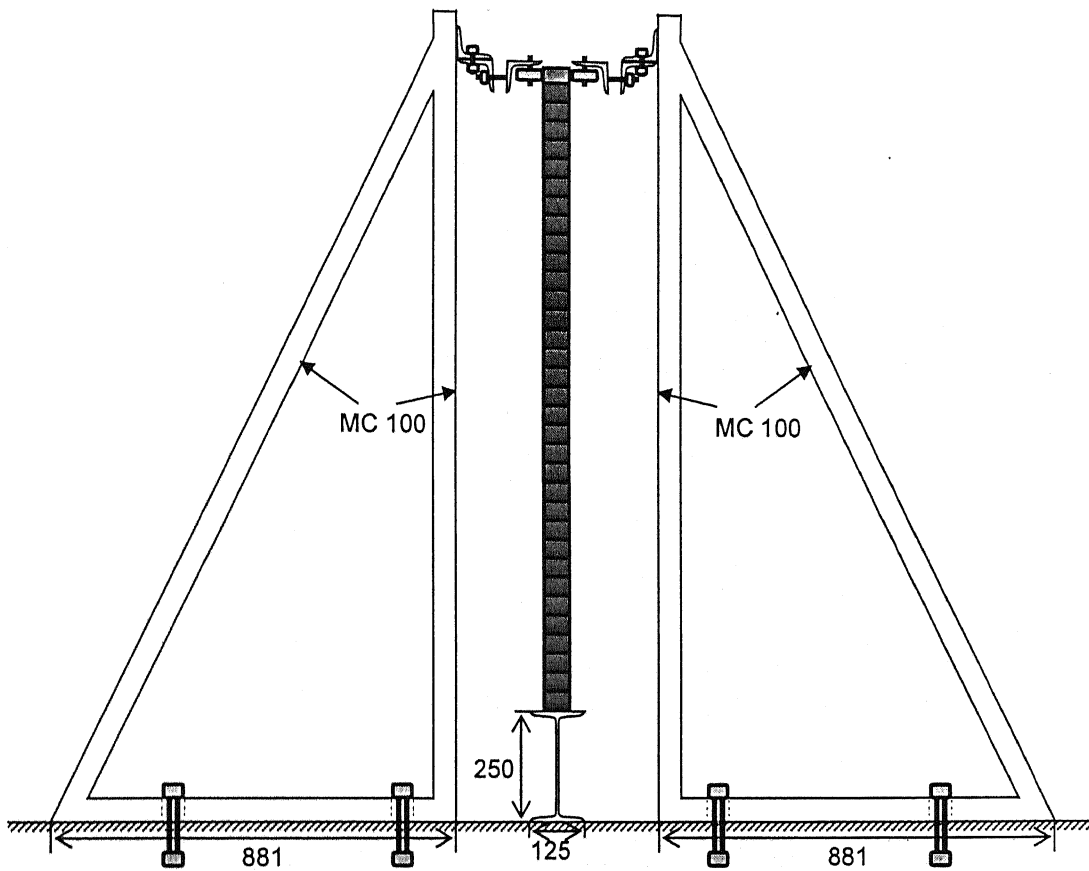
Figure 4.10   Schematic of the lateral load resisting mechanism.
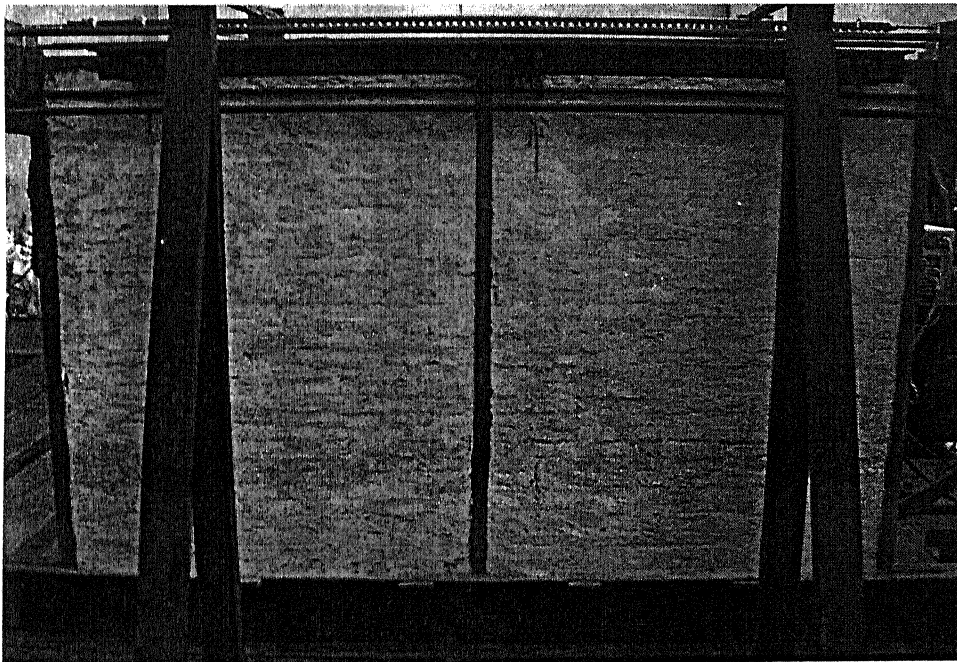
Figure 4.11   First Specimen at the beginning of the test
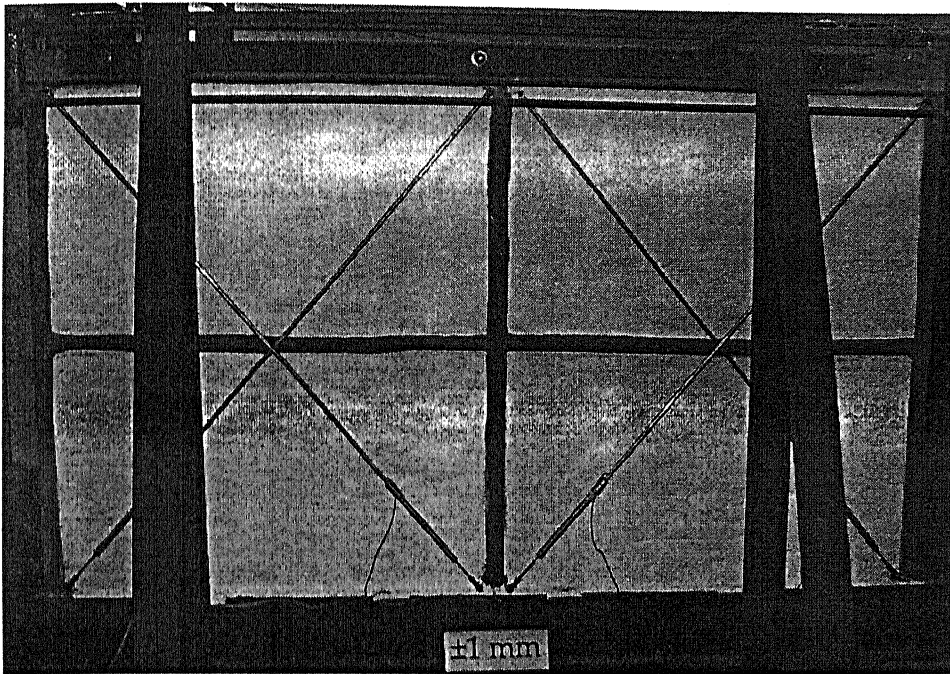
Figure 4.12   Second Specimen at the beginning of the test.
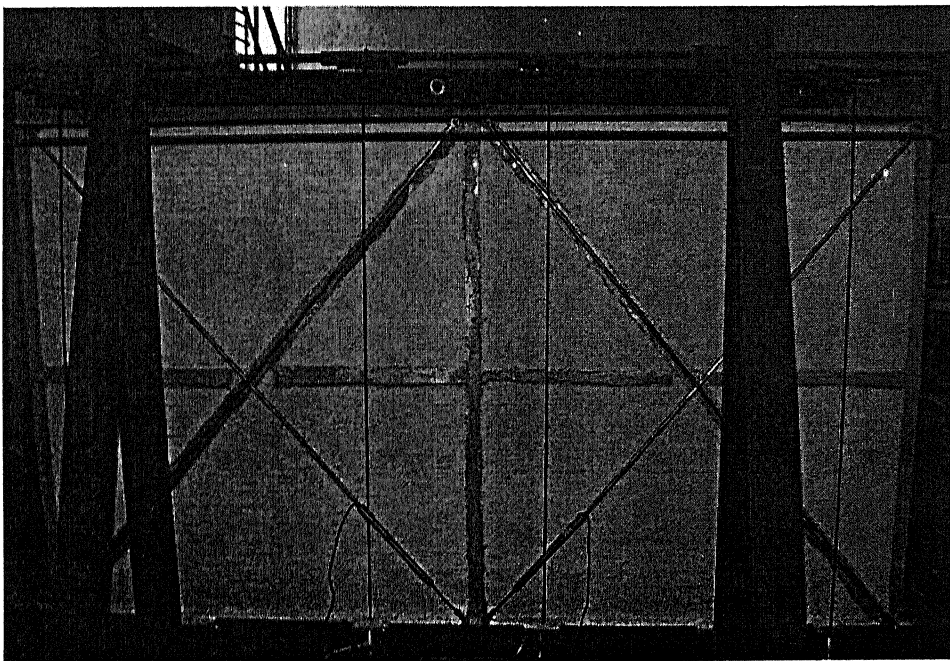
Figure 4.13   Third Specimen at the beginning of the test.
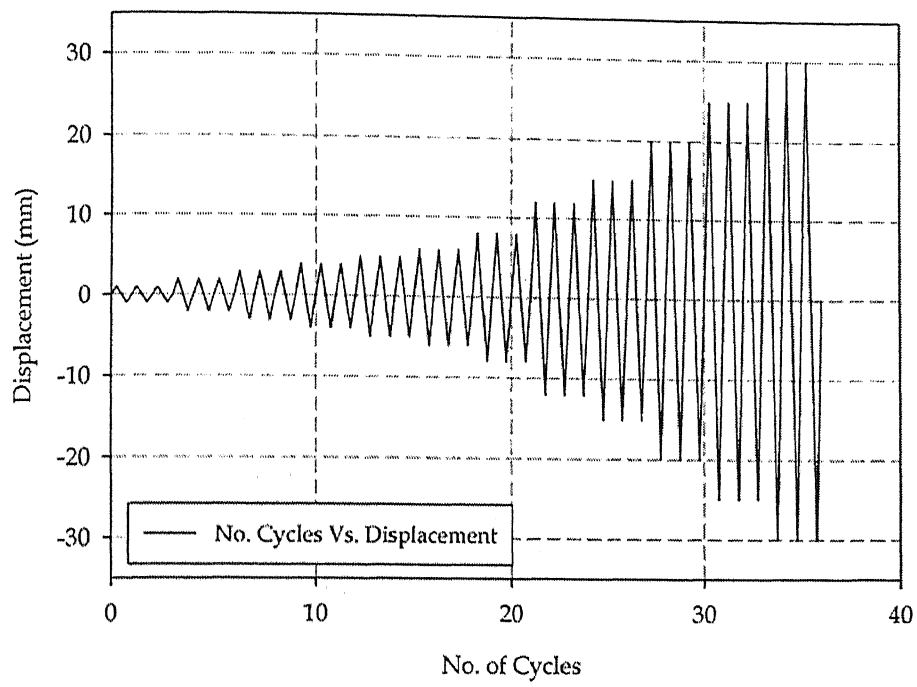
Figure 4.14   Loading history used in the study.
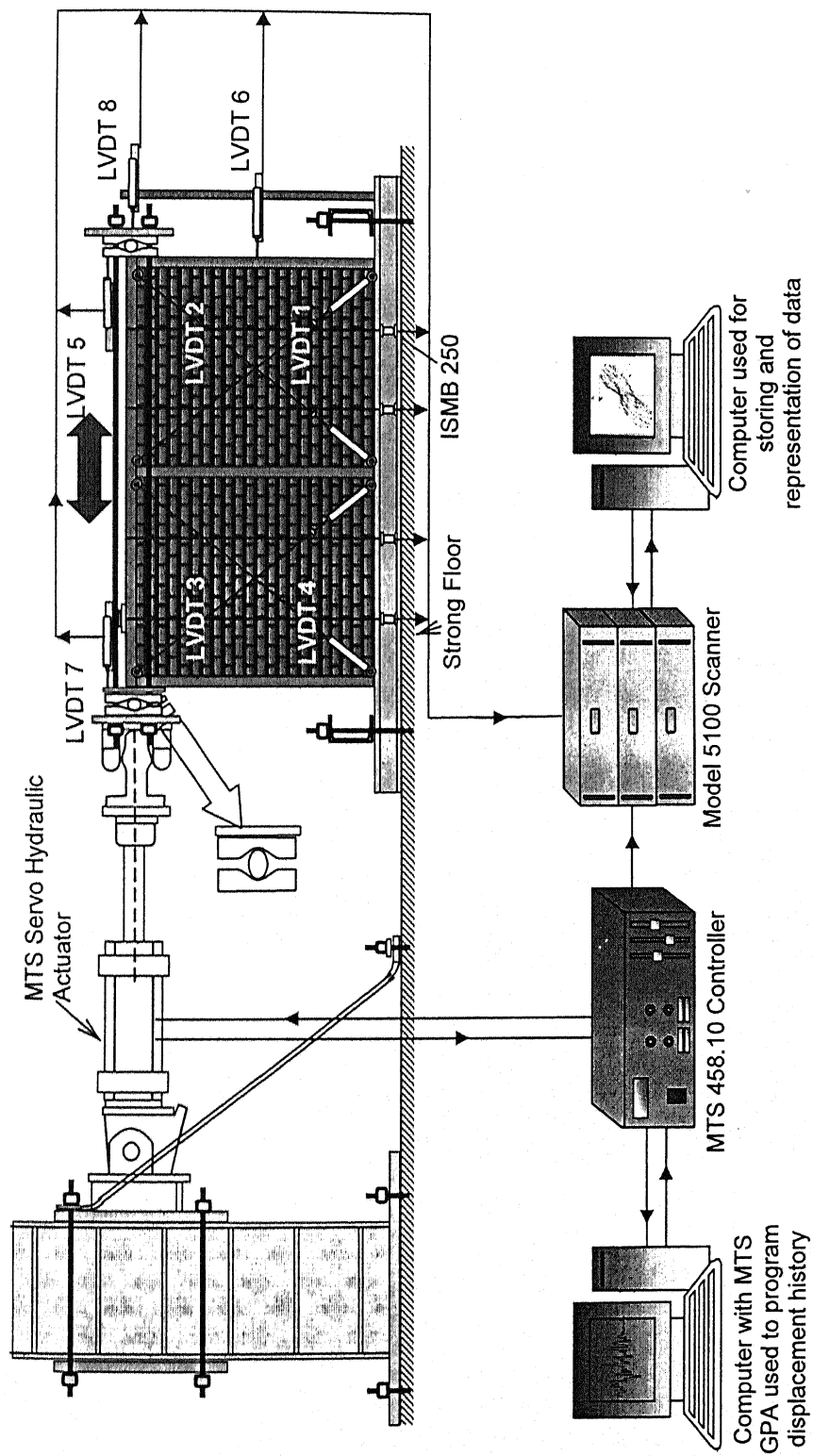
Figure 4.15   Block diagram of the testing system used in the present experimental study

Labels within the figure:

- LVDT 8
- LVDT 6
- LVDT 5
- LVDT 7
- LVDT 2
- LVDT 1
- LVDT 3
- LVDT 4
- ISMB 250
- Strong Floor
- MTS Servo Hydraulic Actuator
- Computer used for storing and representation of data
- Model 5100 Scanner
- MTS 458.10 Controller
- Computer with MTS GPA used to program displacement history
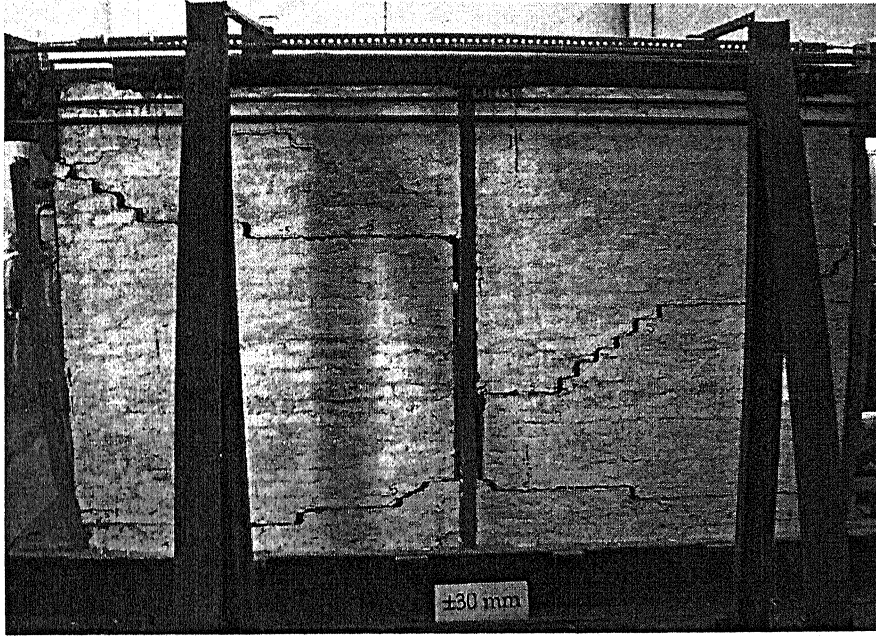
Figure 4.16   First Specimen at the conclusion of the test
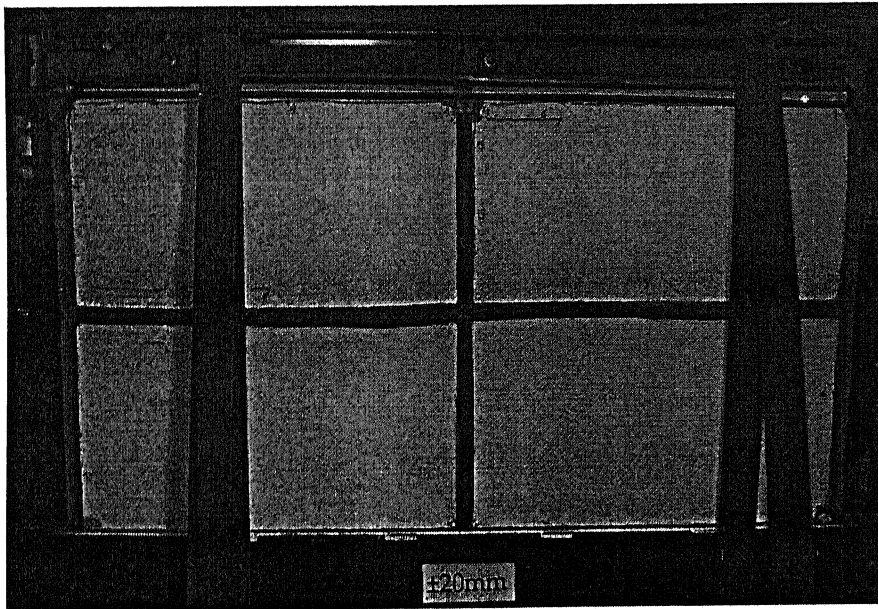
Figure 4.17   Second Specimen at the conclusion of the test
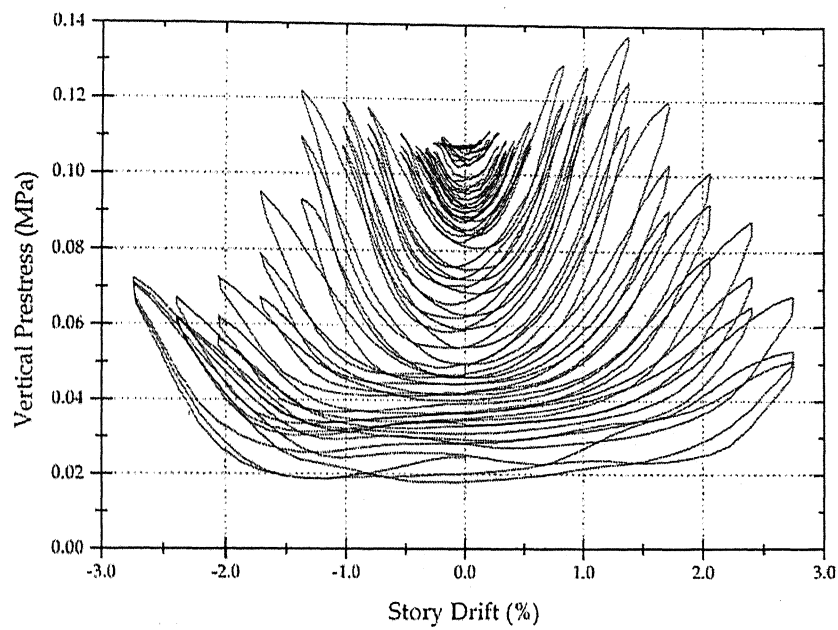
Figure 4.18 Variation vertical prestress on specimen 3 with story drift.
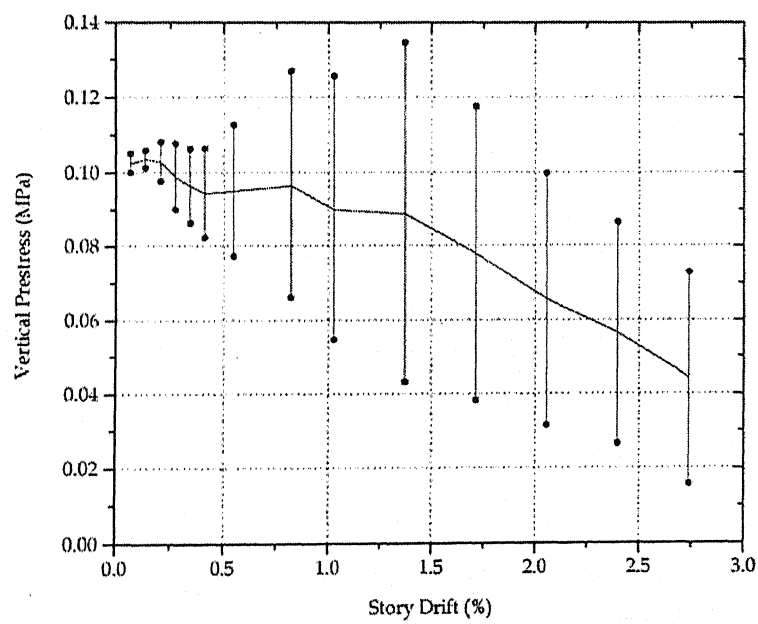
Figure 4.19 Envelope of variation vertical prestress on specimen 3 with story drift.

102
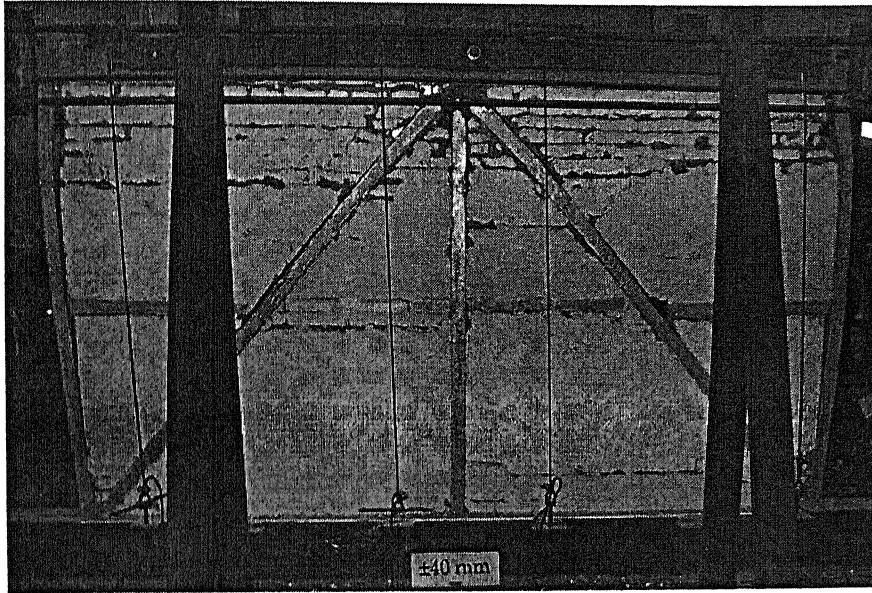
Figure 4.20   Third Specimen at the conclusion of the test
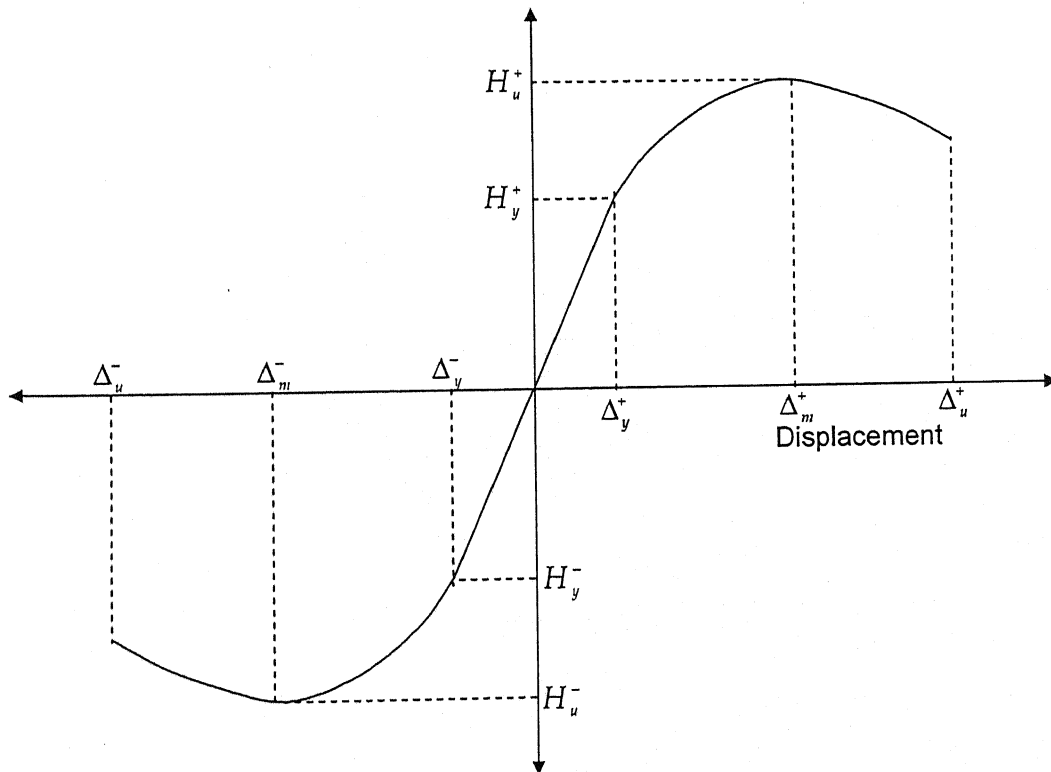
Figure 4.21   Schematic representations showing various behavioural quantities on the envelope backbone load-displacement curve.

103
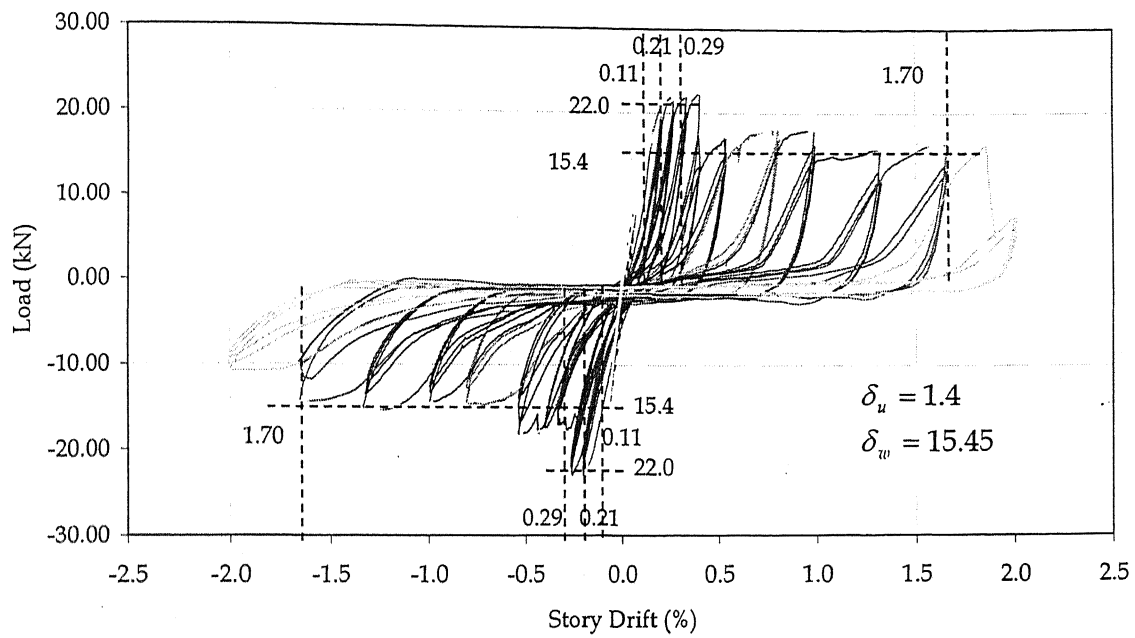
Figure 4.22 Hysteretic behaviour of Specimen 1.
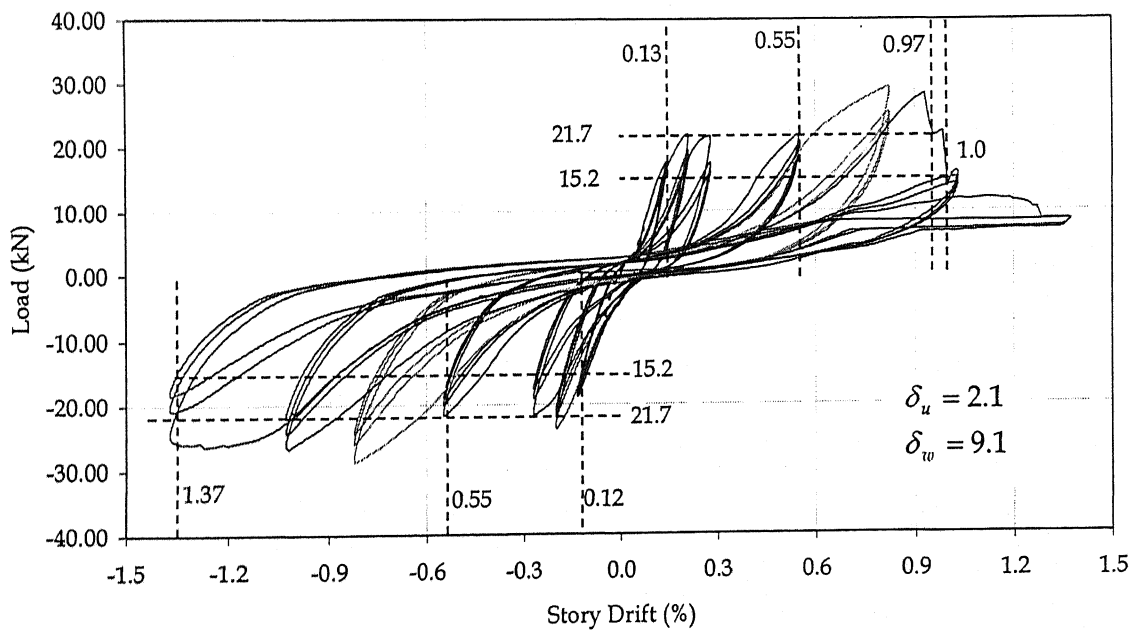
Figure 4.23 Hysteretic behaviour of Specimen 2.

104
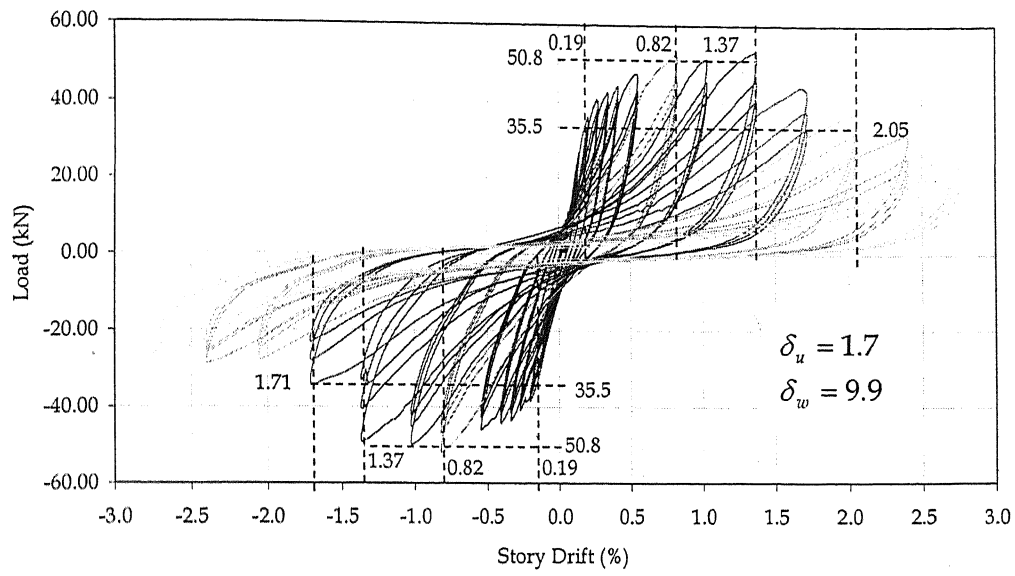
Figure 4.24 Hysteretic behaviour of Specimen 3.
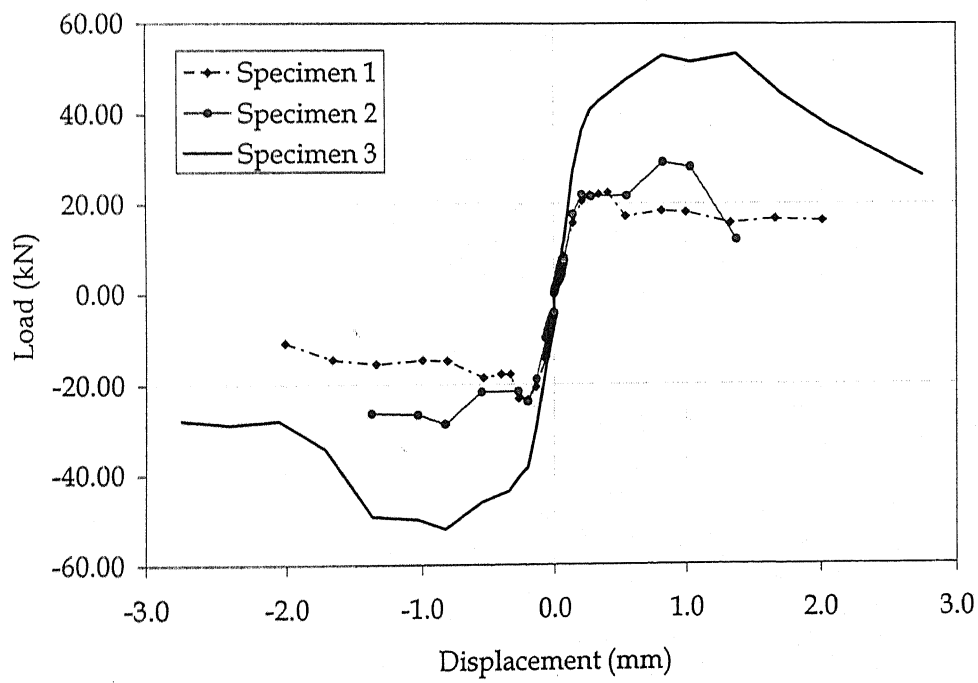
Figure 4.25 Envelope values of shear resistance of all the specimens.

$$\delta_u = \frac{V_u}{\Delta_u}$$

$$\delta_w = \frac{V_w}{\Delta_w}$$
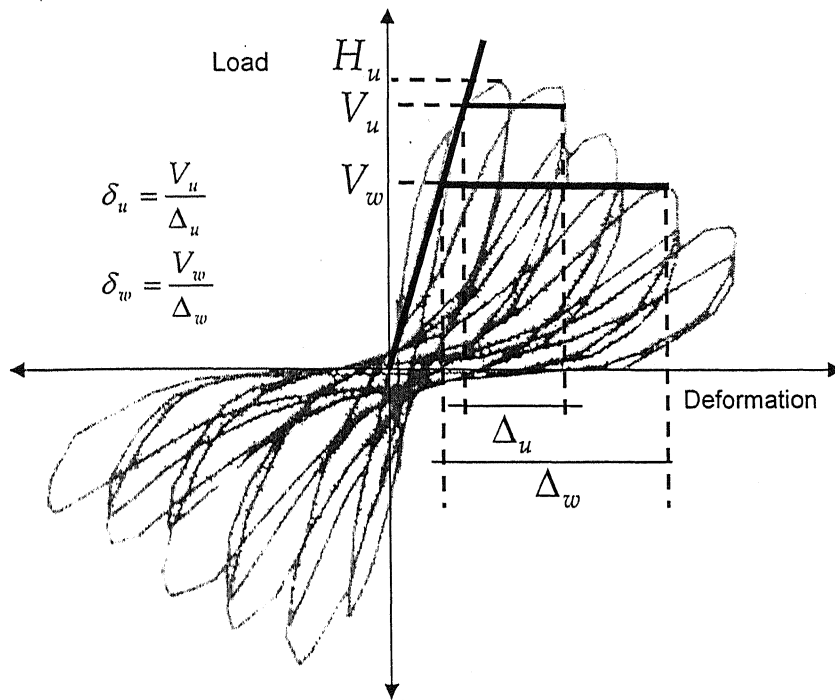
Figure 4.26   Schematic diagram showing definition of ductility indicators.
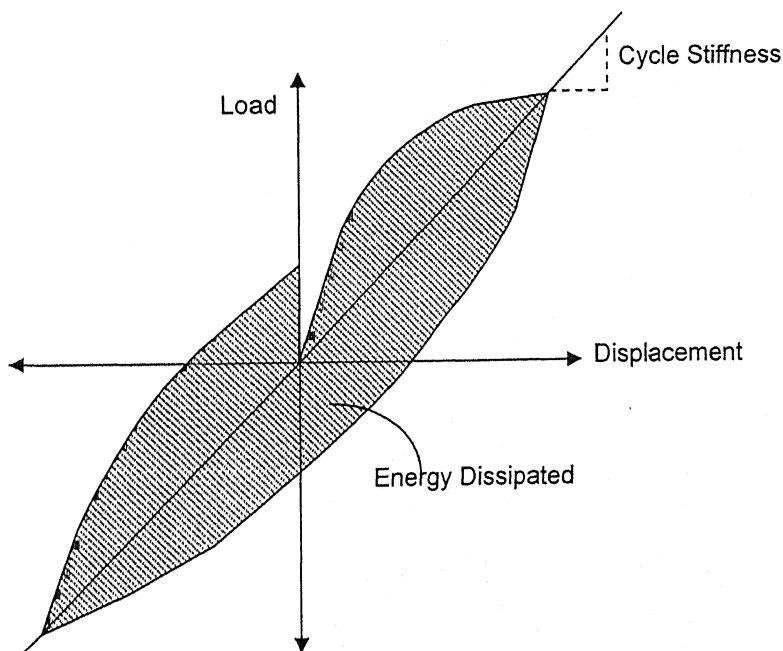
Figure 4.27   Schematic representation showing energy dissipation and cycle stiffness on the hysteresis loop.
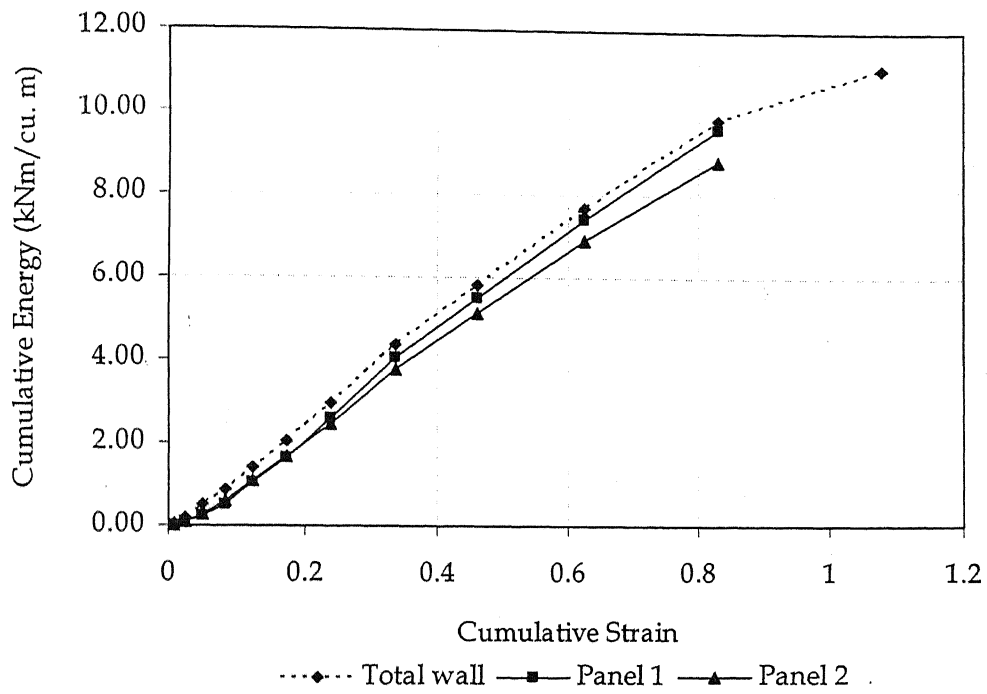
Figure 4.28 Cumulative energy dissipated per unit volume vs. cumulative strain in specimen 1.
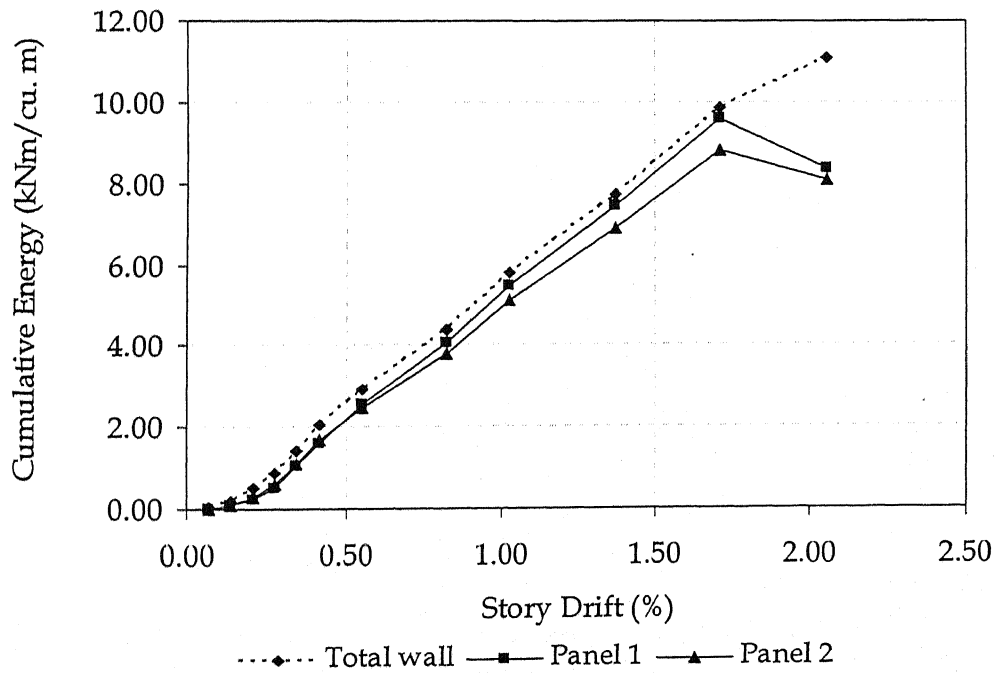
Figure 4.29 Cumulative energy dissipated per unit volume vs. story drift in specimen 1.

107
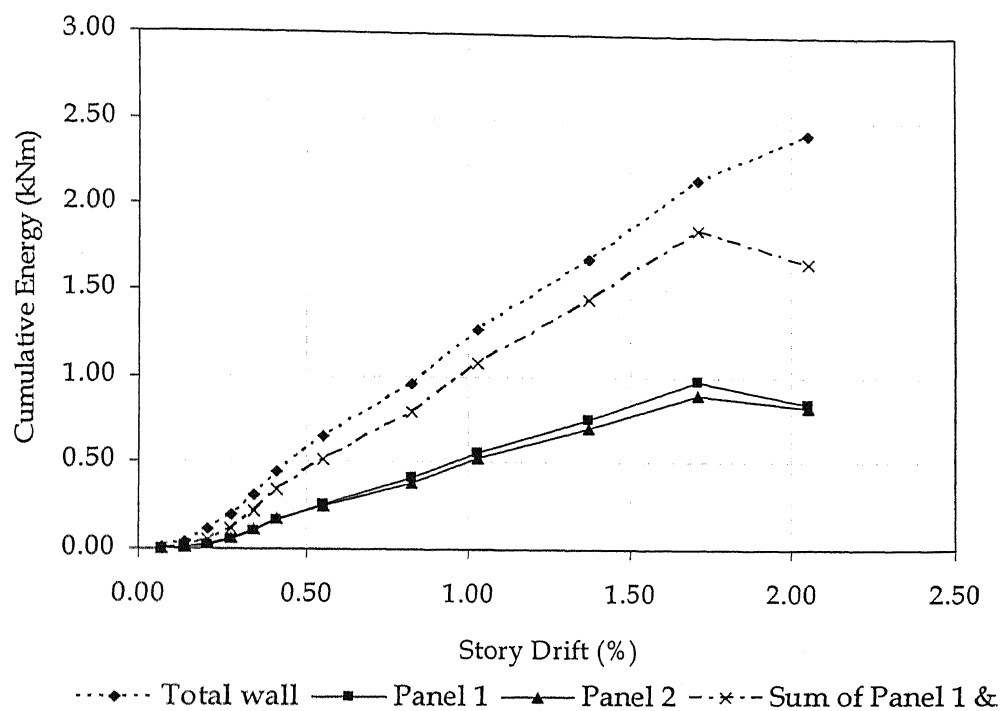
Figure 4.30 Total cumulative energy dissipated vs. story drift in specimen 1.
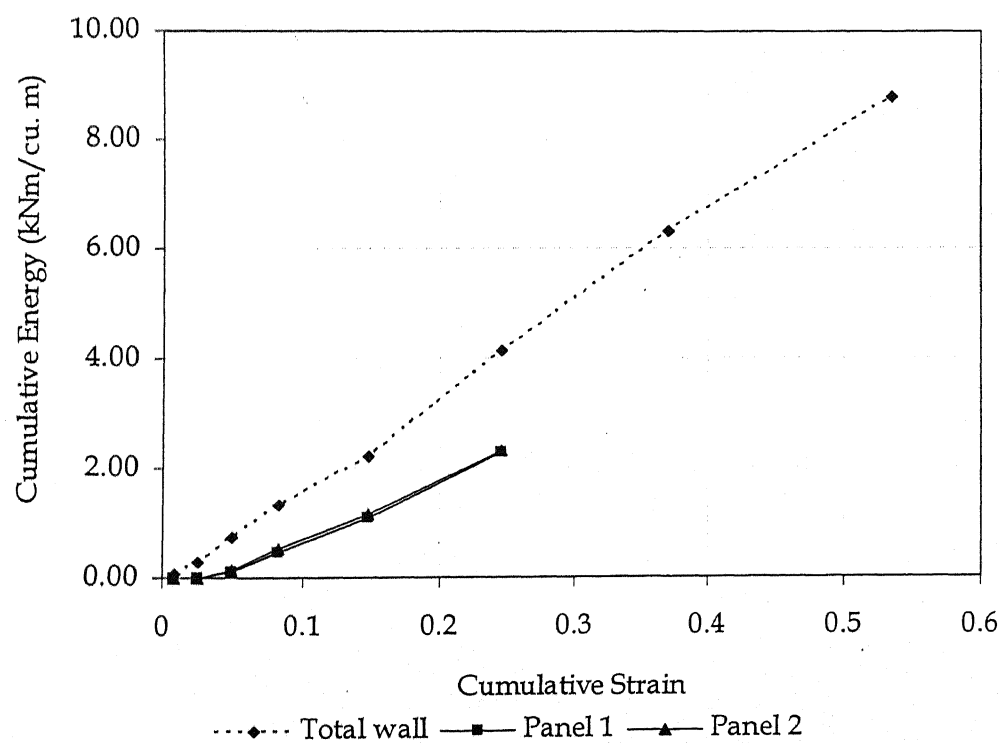
Figure 4.31 Cumulative energy dissipated per unit volume vs. cumulative strain in specimen 2.
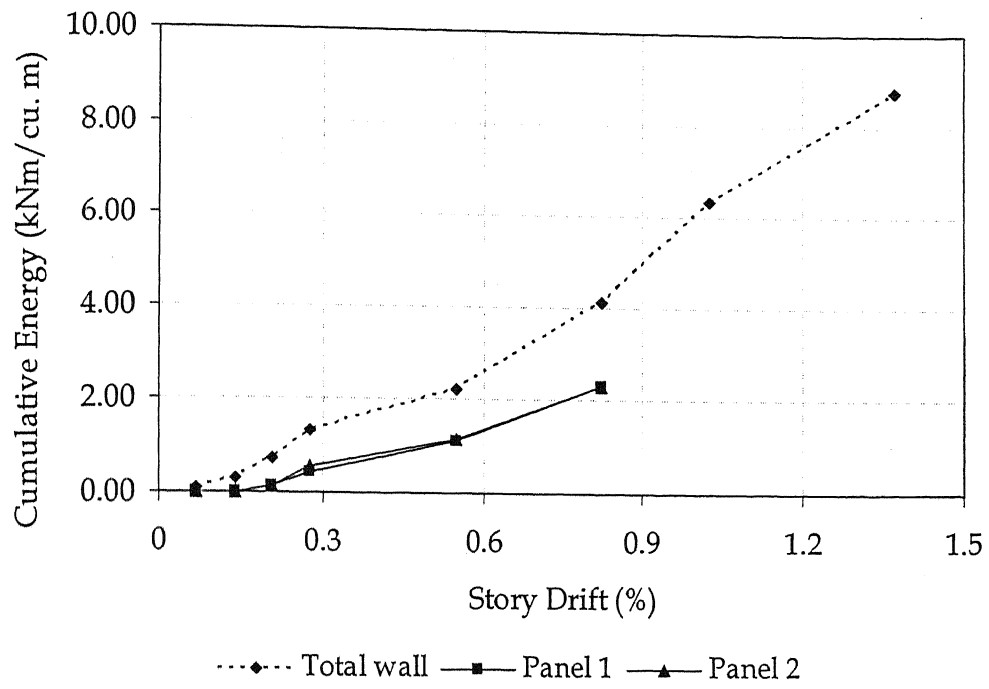
Figure 4.32   Cumulative energy dissipated per unit volume vs. story drift in specimen 2.
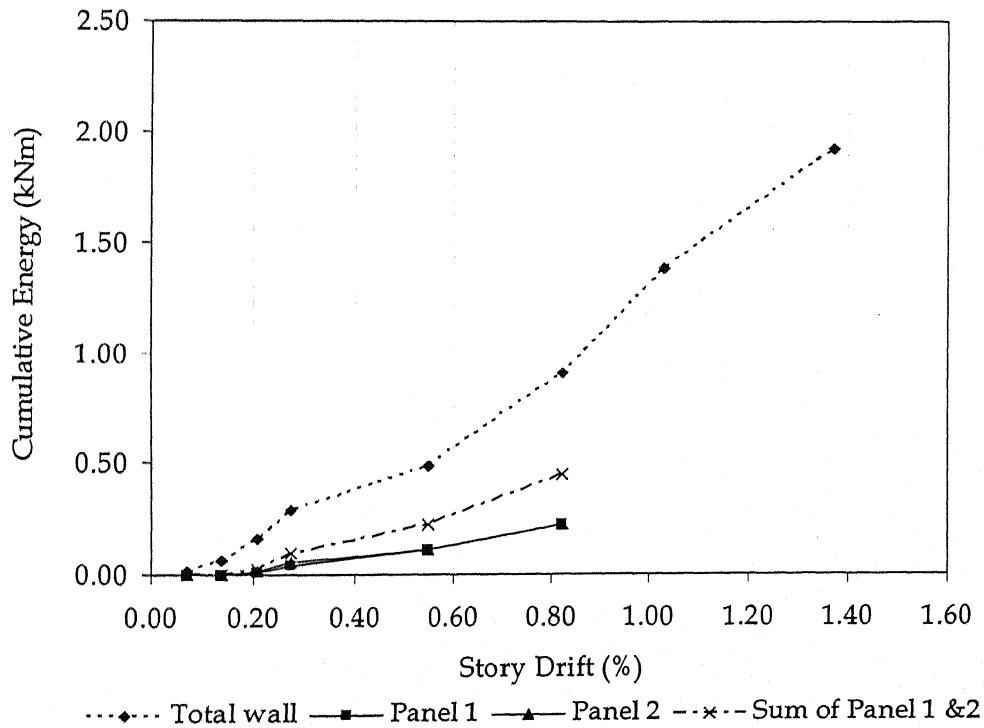
Figure 4.33   Total cumulative energy dissipated vs. story drift in specimen 2.
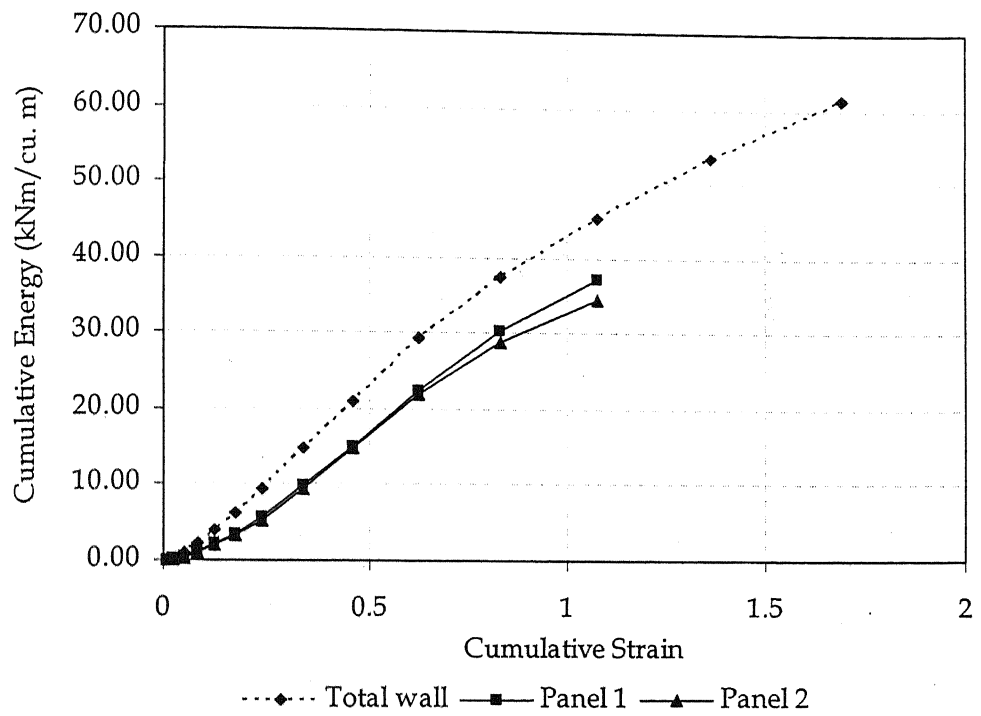
Figure 4.34 Cumulative energy dissipated per unit volume vs. cumulative strain in specimen 3.
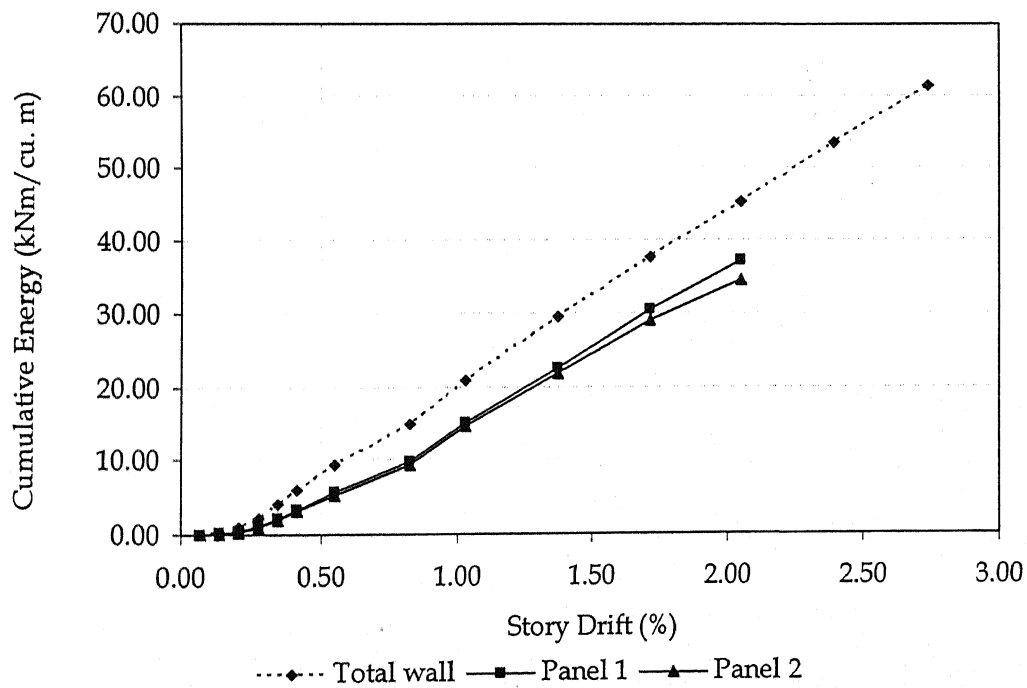
Figure 4.35 Cumulative energy dissipated per unit volume vs. story drift in specimen 3.

110
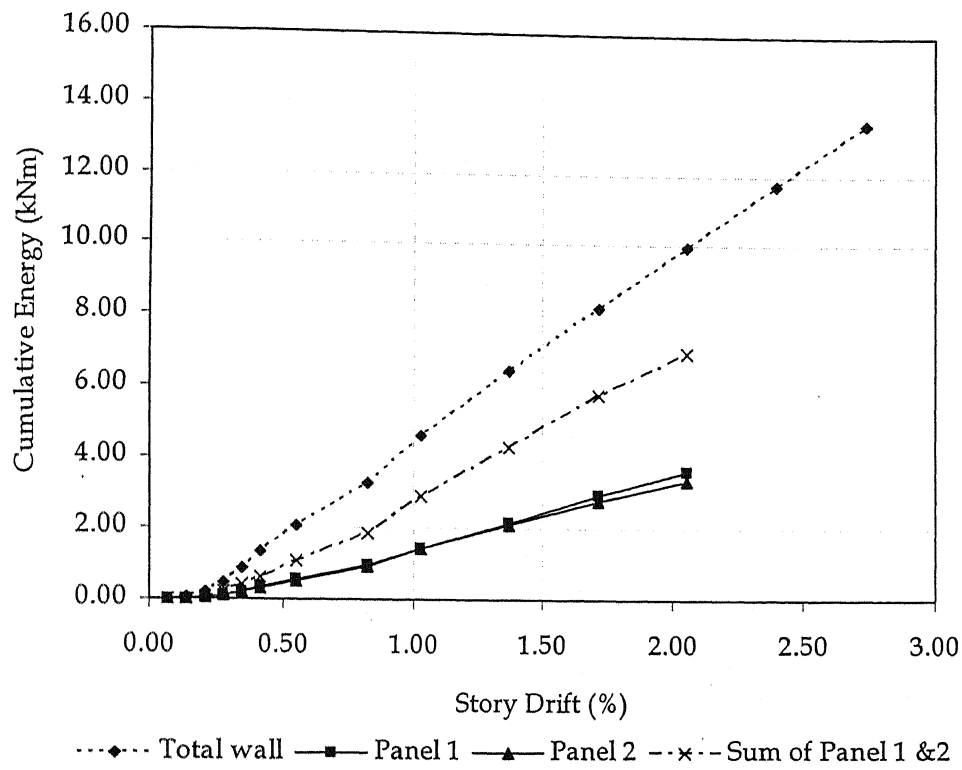
Figure 4.36   Total cumulative energy dissipated vs. story drift in specimen 3.
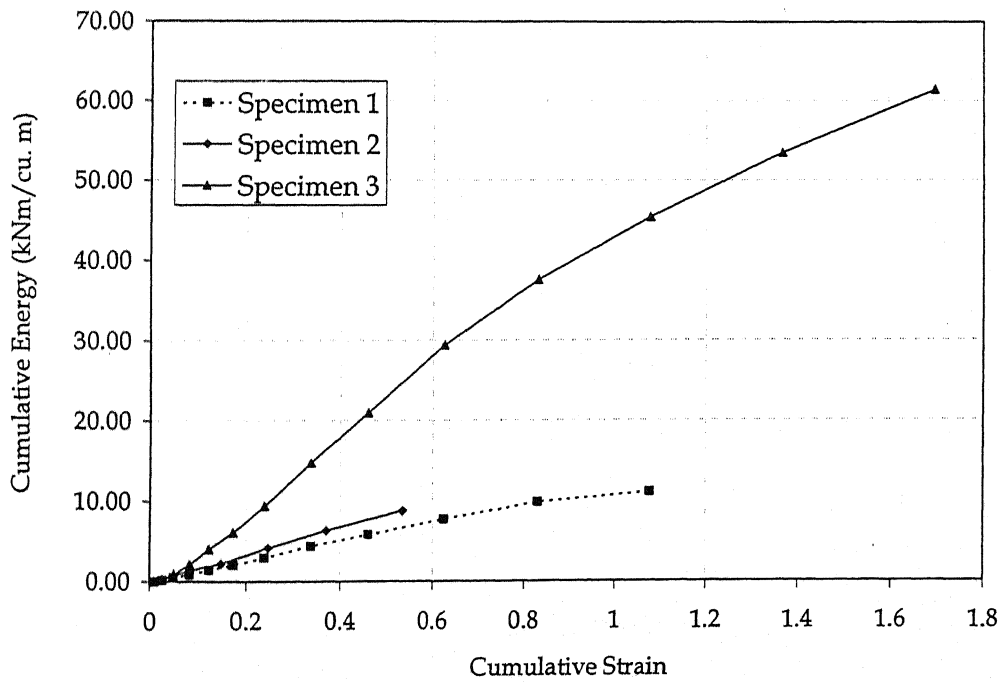
Figure 4.37   Comparison of cumulative energy dissipated per unit volume vs. cumulative strain in all specimens.

111
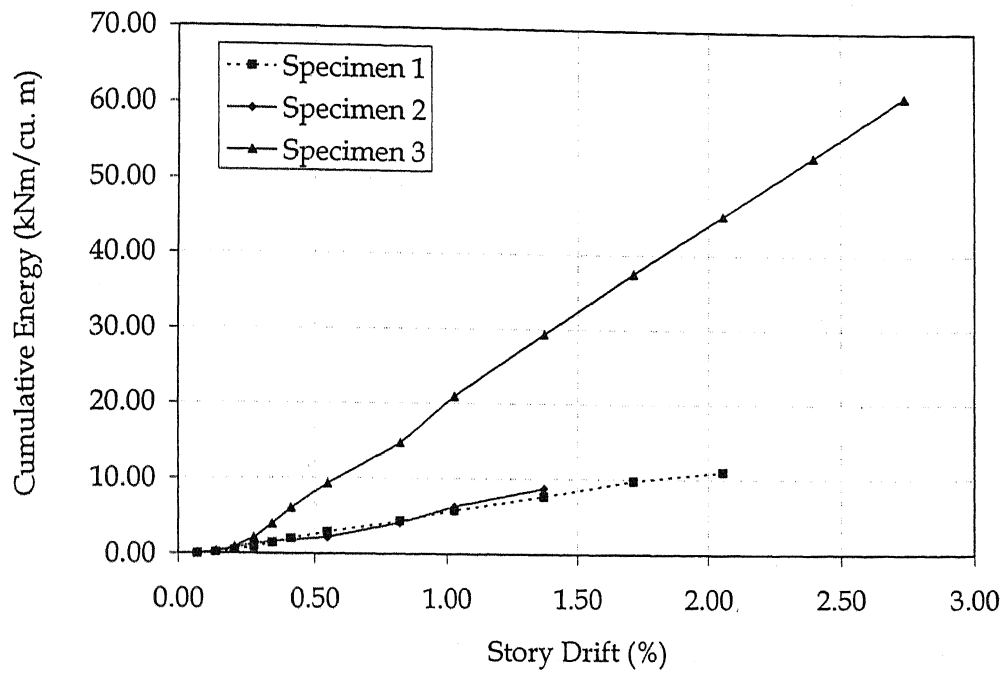
Figure 4.38 Comparison of cumulative energy dissipated per unit volume vs. story drift in all specimens.
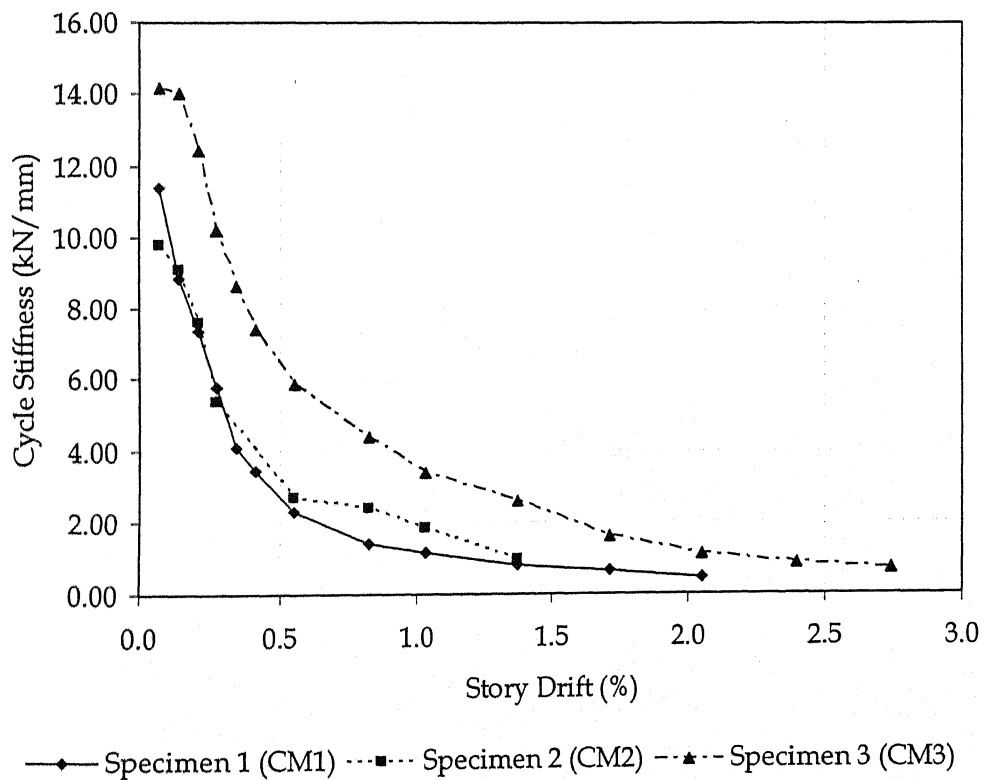
Figure 4.39 Variation of the cycle stiffness of specimens with story drift.
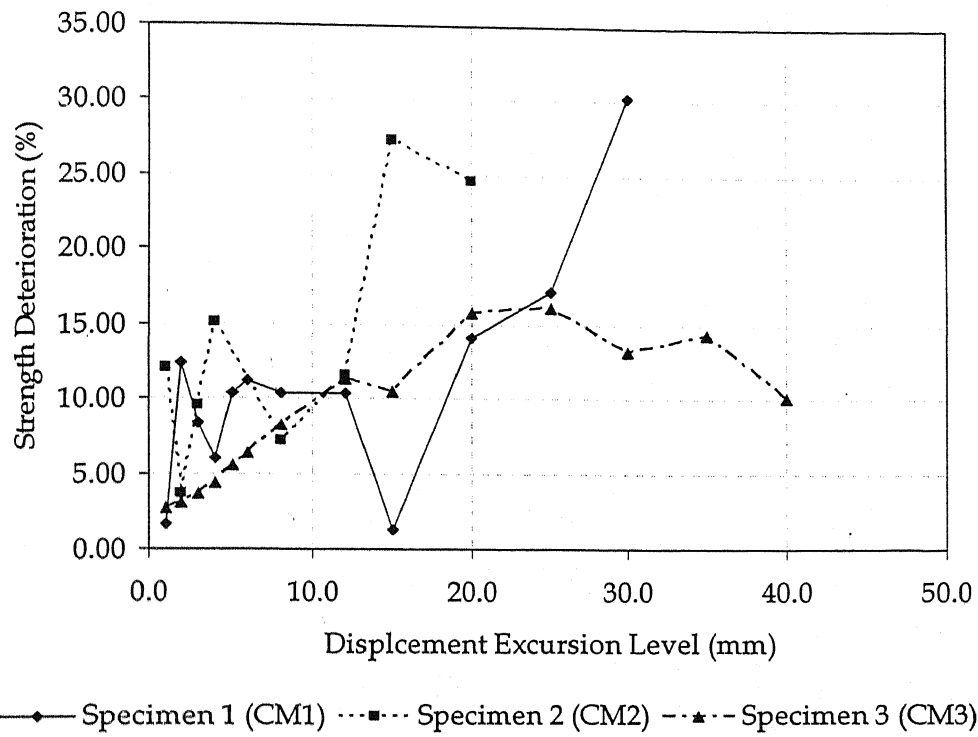
Figure 4.40 Variation of strength deterioration of specimens with story drift.
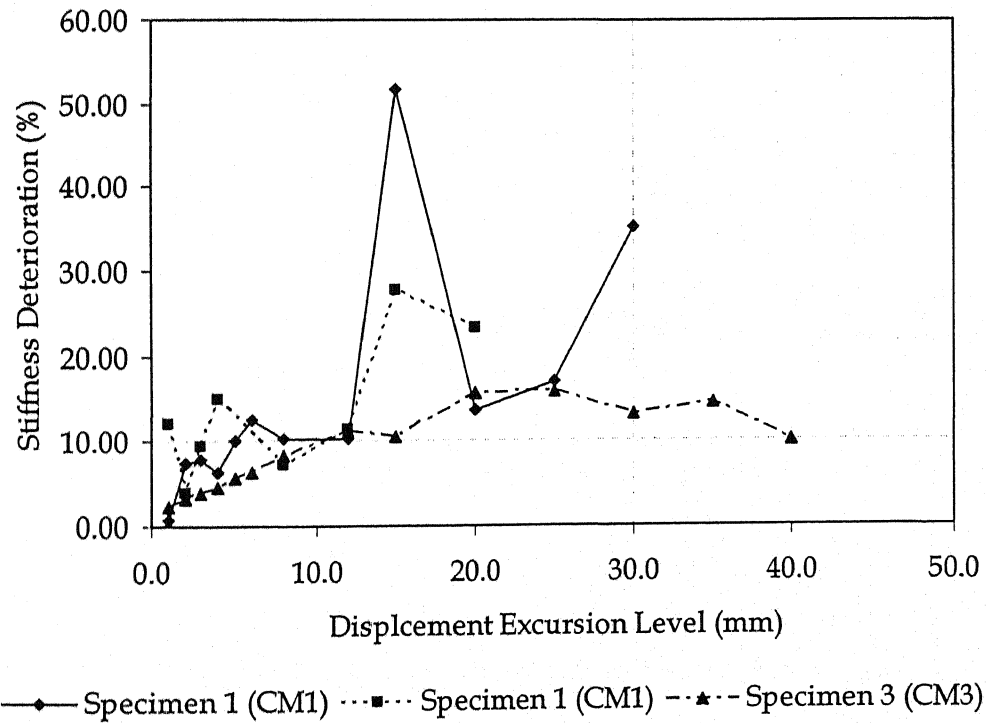
Figure 4.41 Variation of stiffness deterioration of specimens with story drift.
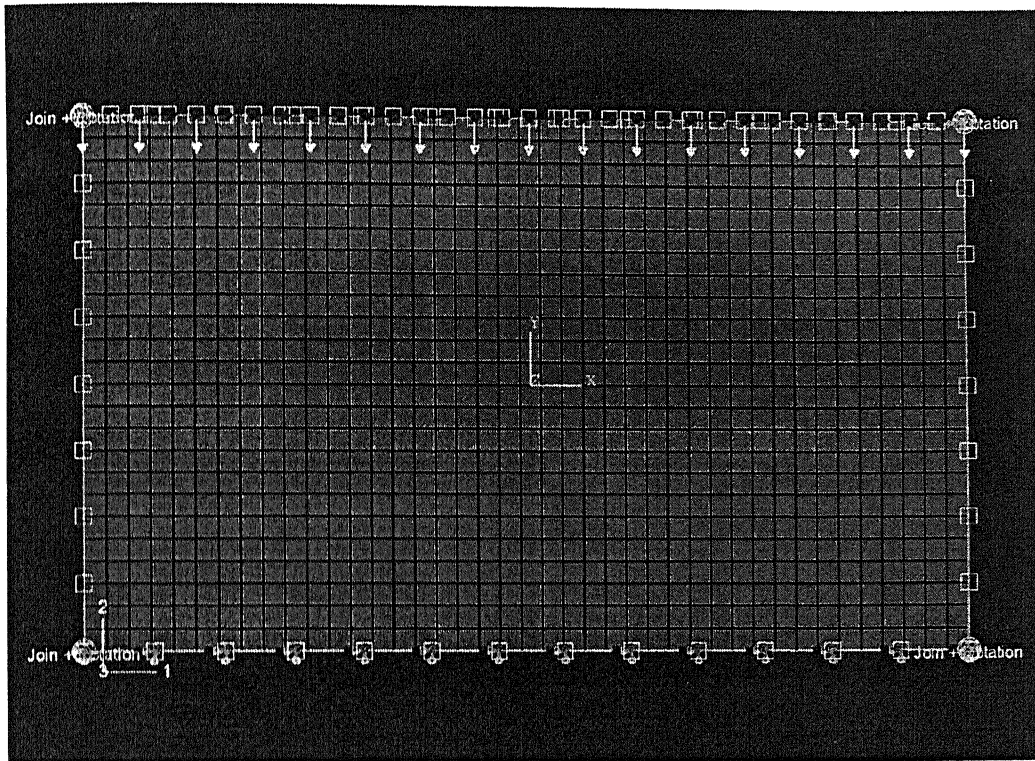
Figure 5.1   FE representation of specimen 1.
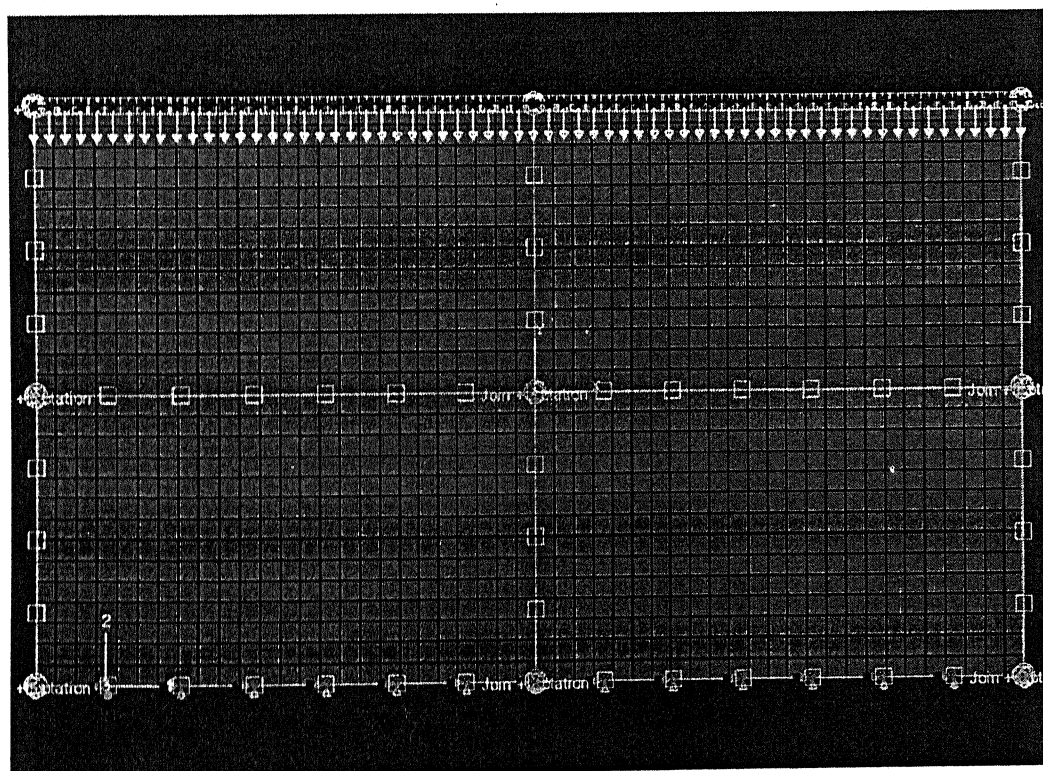
Figure 5.2   FE representation of specimen 2.

114
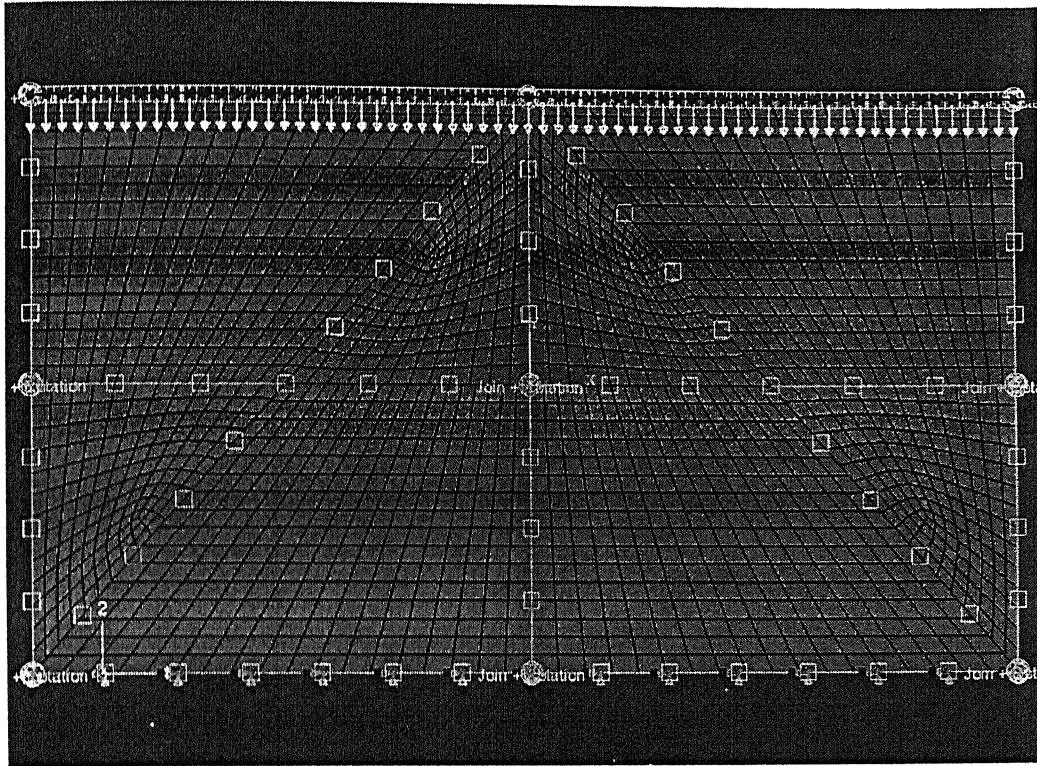
Figure 5.3   FE representation of specimen 3.
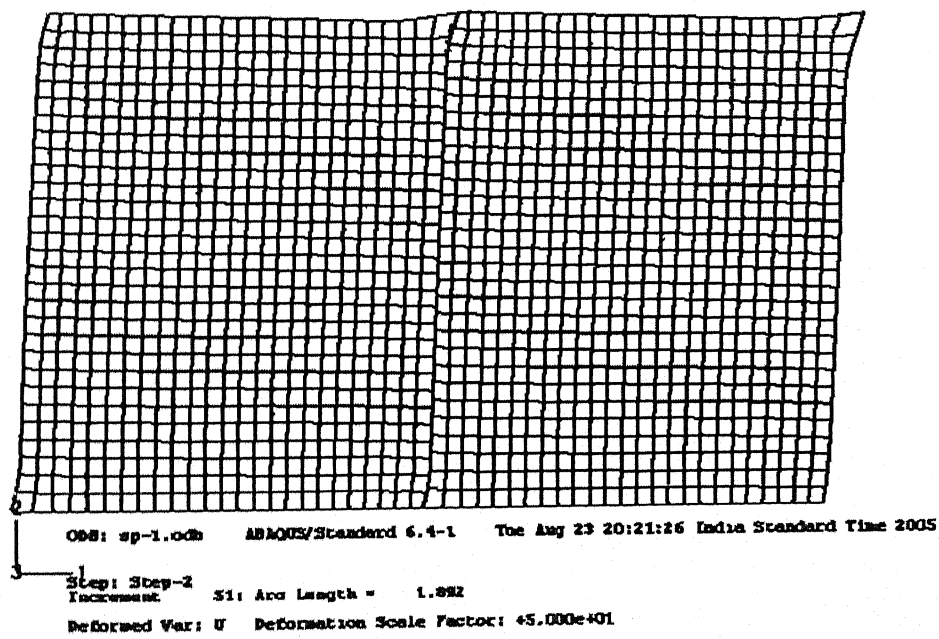
Figure 5.4   Deformed geometry of specimen 1 at 0.17% story drift right-
wards.

115

ODB: sp-2.odb   ABAQUS/Standard 6.4-1   Tue Aug 23 19:38:37 India Standard Time 2005

Step: Step-2
Increment   73: Arc Length =   4.856
Deformed Var: U   Deformation Scale Factor: +5.000e+01
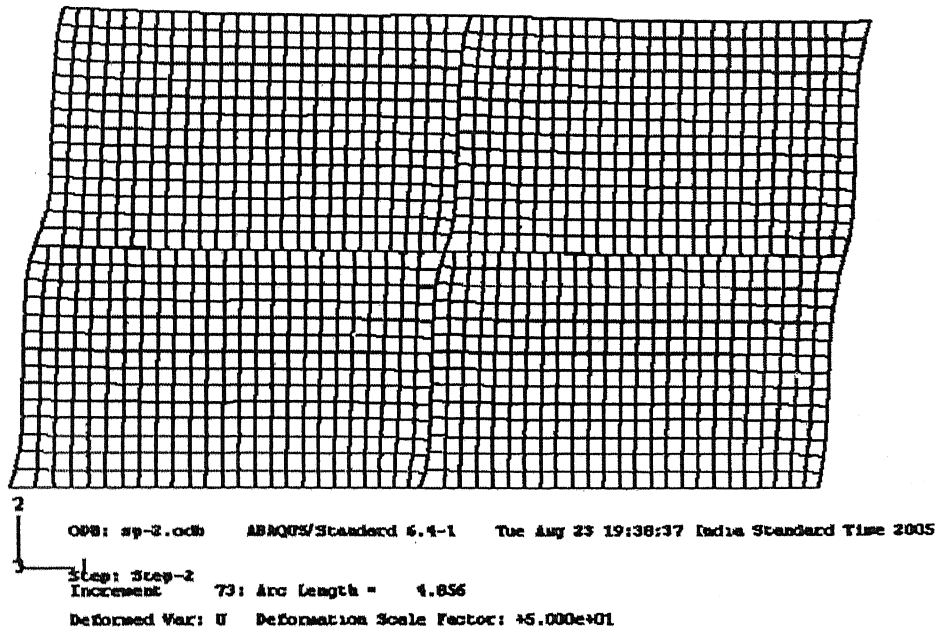
Figure 5.5 Deformed geometry of specimen 2 at 0.23% story drift rightwards.

ODB: Spec13.odb   ABAQUS/Standard 6.4-1   Mon Aug 15 16:44:12 India Standard Time 2005

Step: Step-2
Increment   82: Arc Length =   4.302
Deformed Var: U   Deformation Scale Factor: +5.000e+01
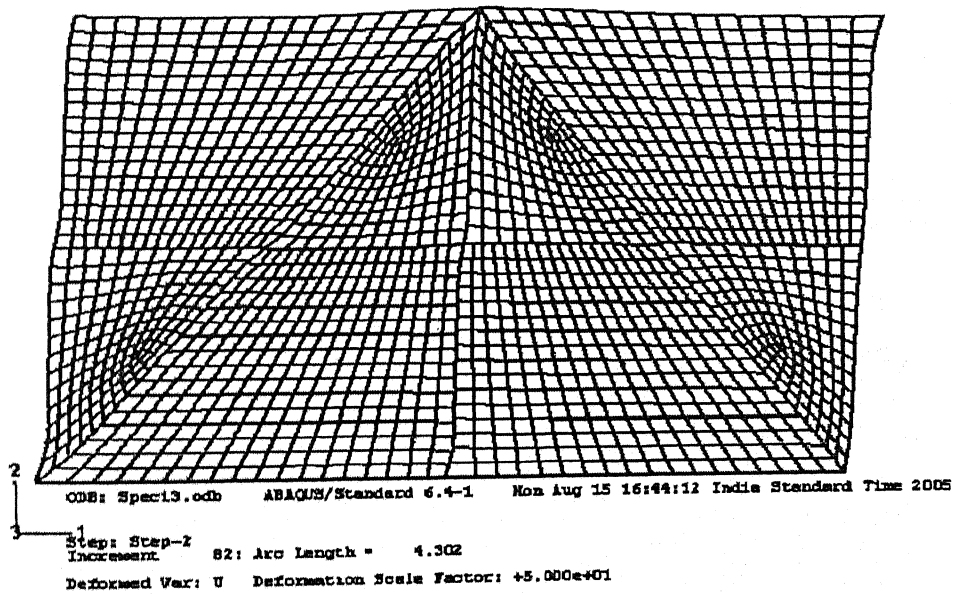
Figure 5.6 Deformed geometry of specimen 3 at 0.17% story drift rightwards.

116
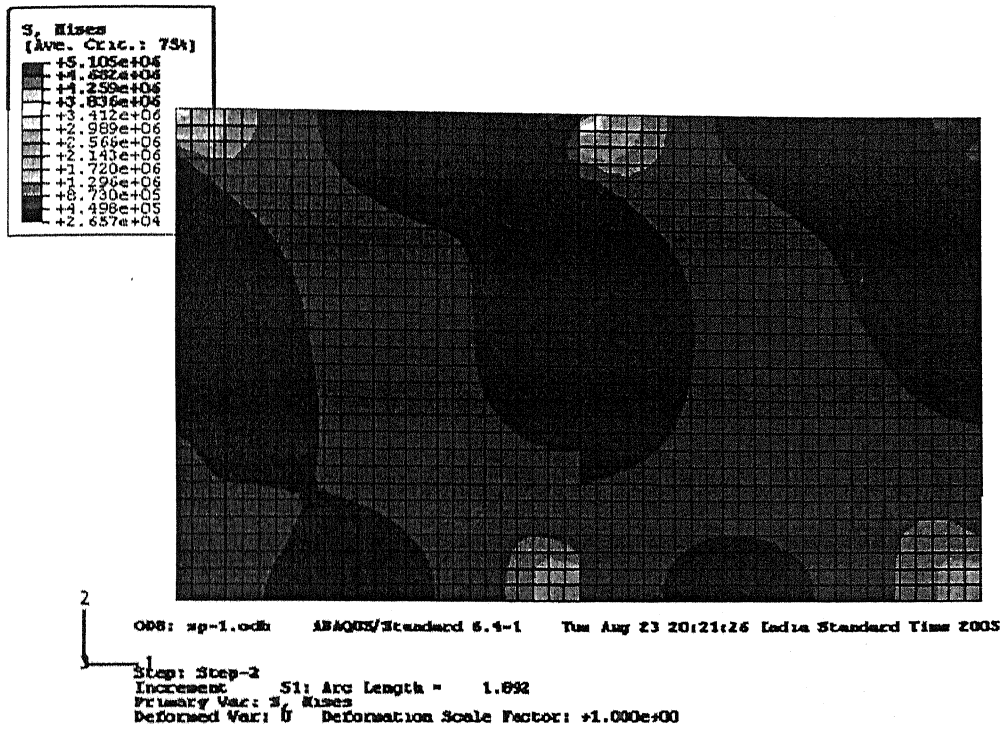
Figure 5.7   Contours of the Von-Mises stress in specimen 1 at 0.17% story drift right-wards.
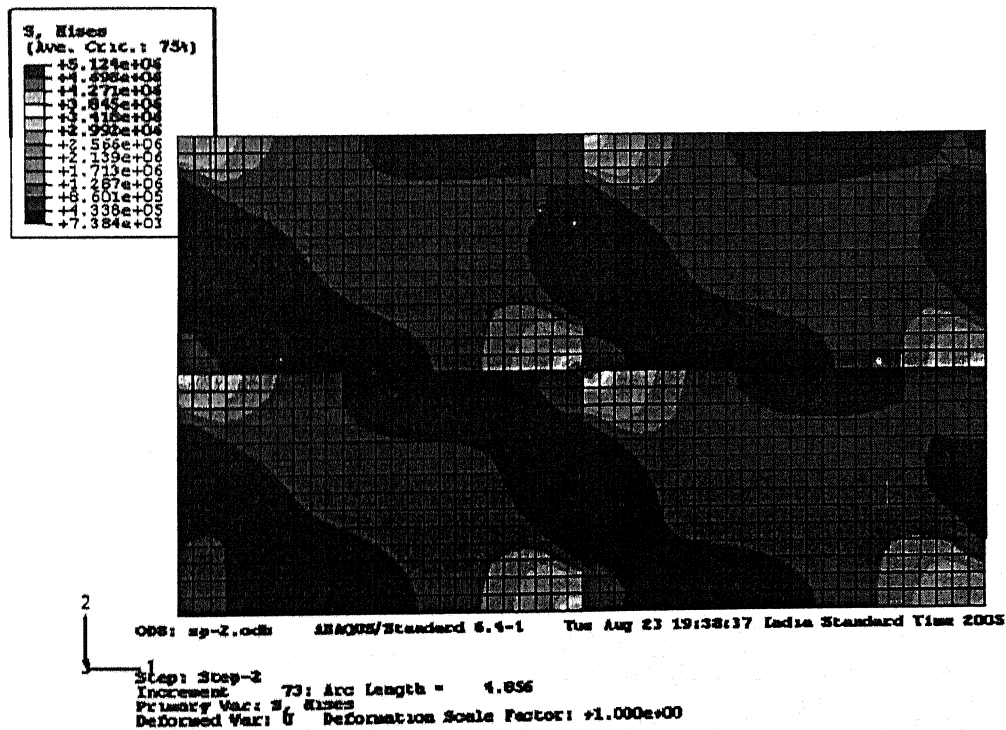
Figure 5.8   Contours of the Von-Mises stress in specimen 2 at 0.13% story drift right-wards.
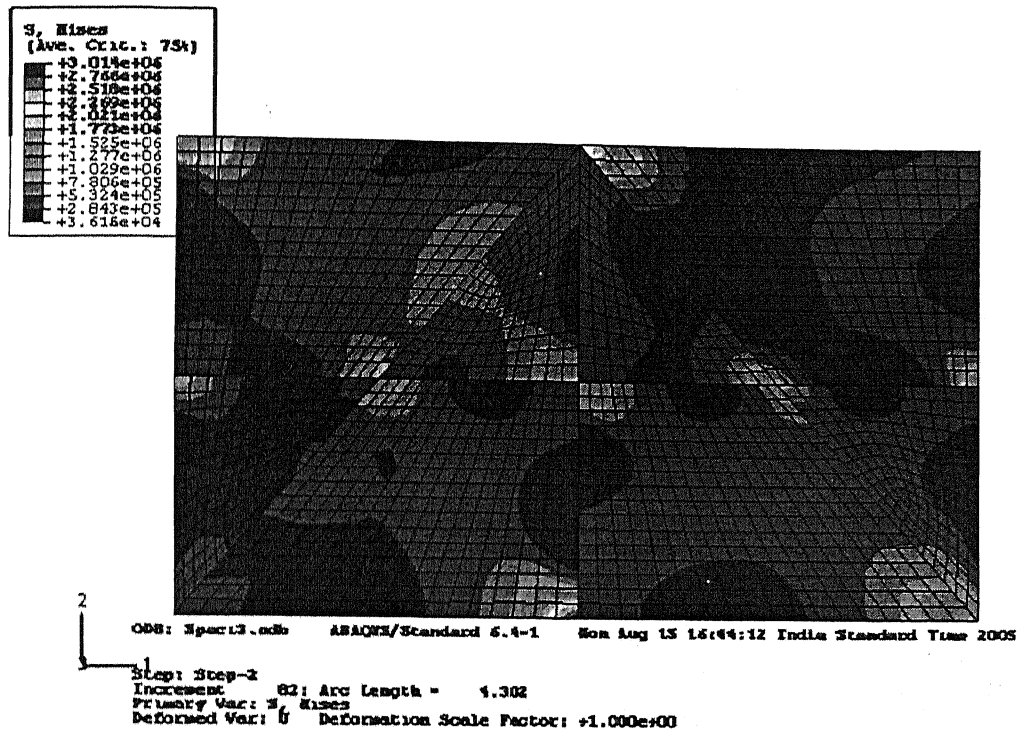
Figure 5.9   Contours of the Von-Mises stress in specimen 3 at 0.17% story drift right-wards.
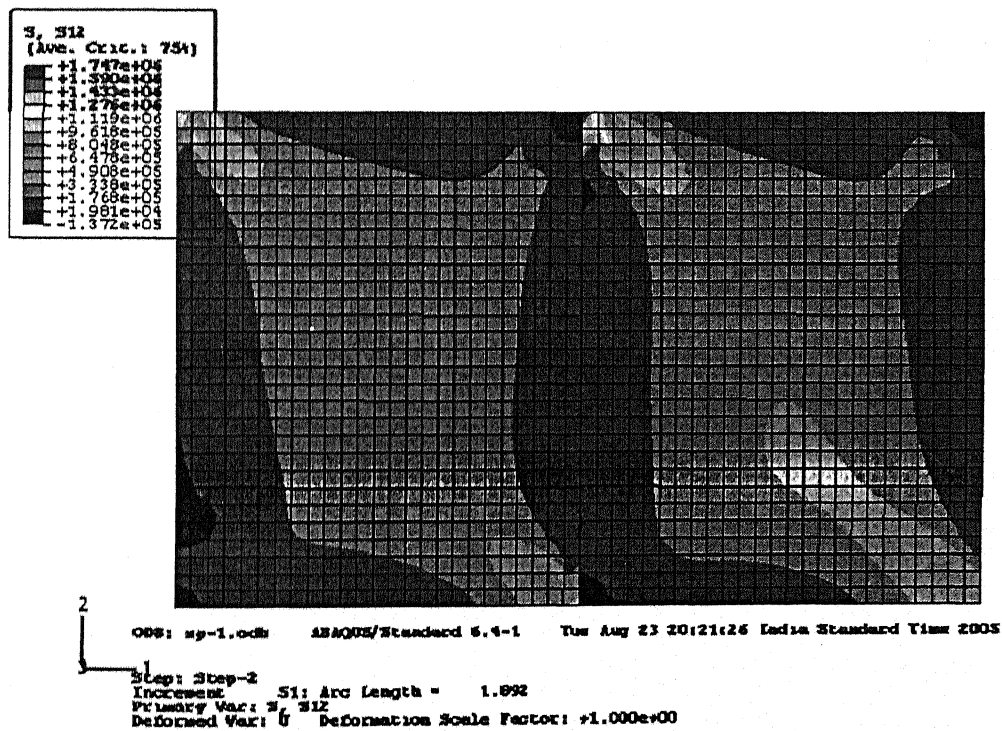
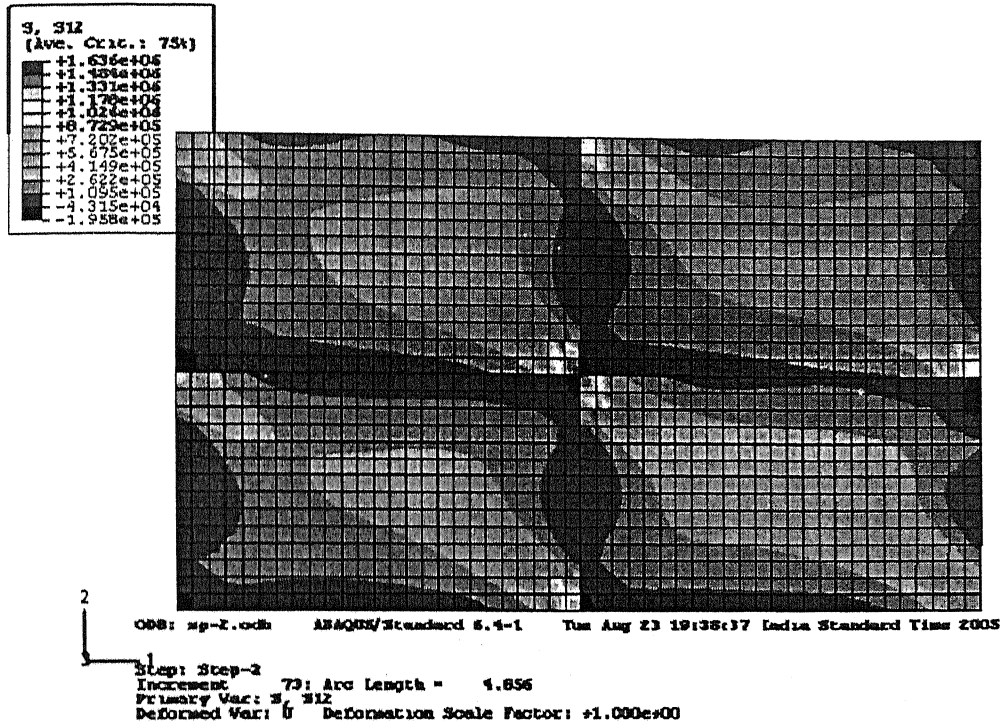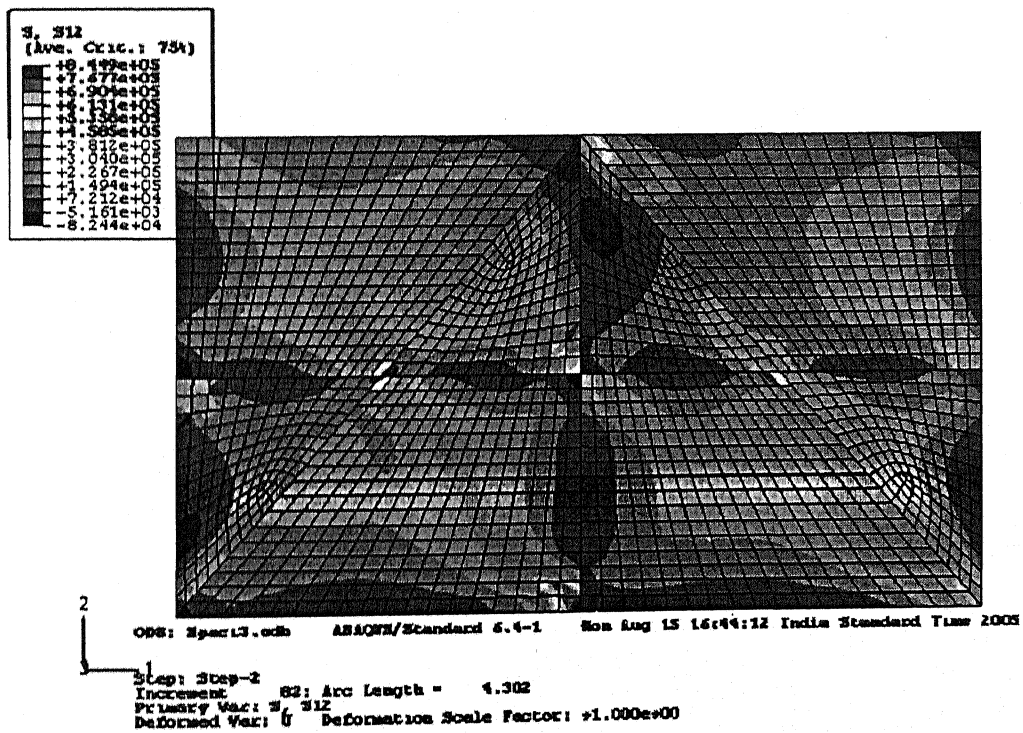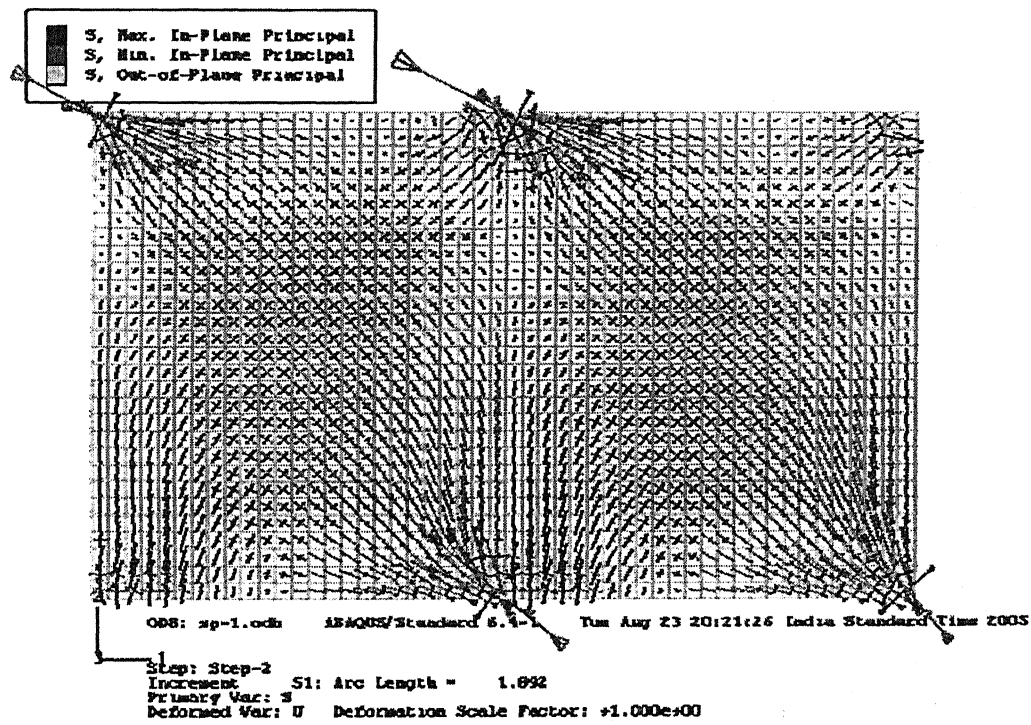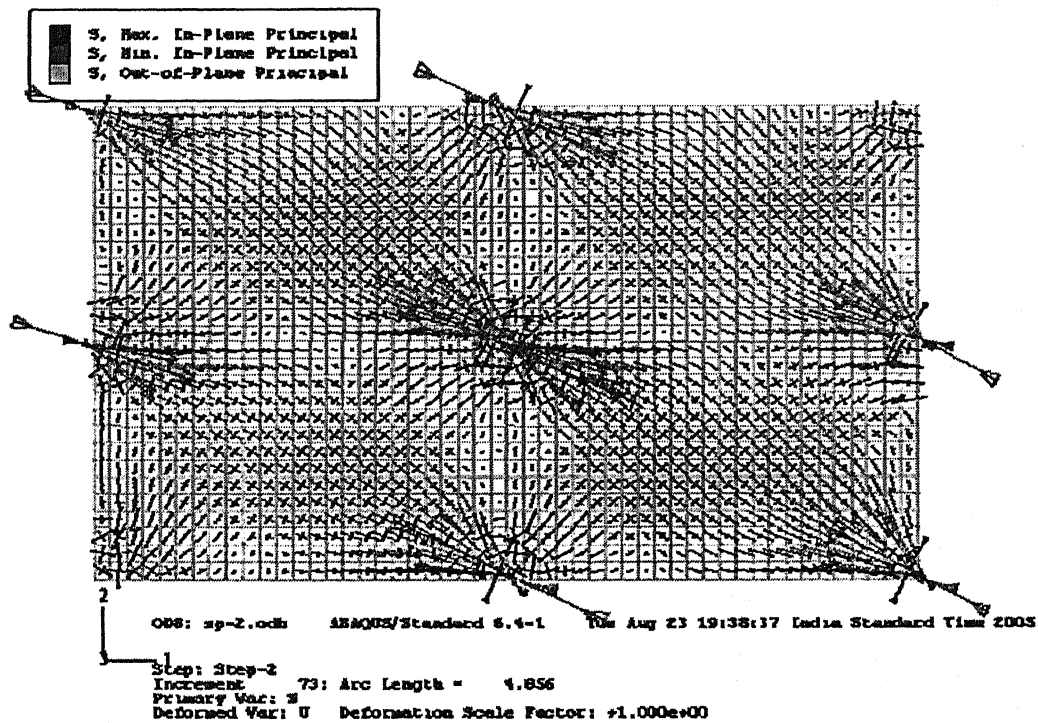Figure 5.10   Contours of the shear stress in specimen 1 at 0.17% story drift right-wards.

Figure 5.11   Contours of the shear stress in specimen 2 at 0.23% story drift right-wards.

Figure 5.12   Contours of the shear stress in specimen 3 at 0.17% story drift right-wards.

Figure 5.13 Vector plot of major principal stress in specimen 1 at 0.17% story drift right-wards.

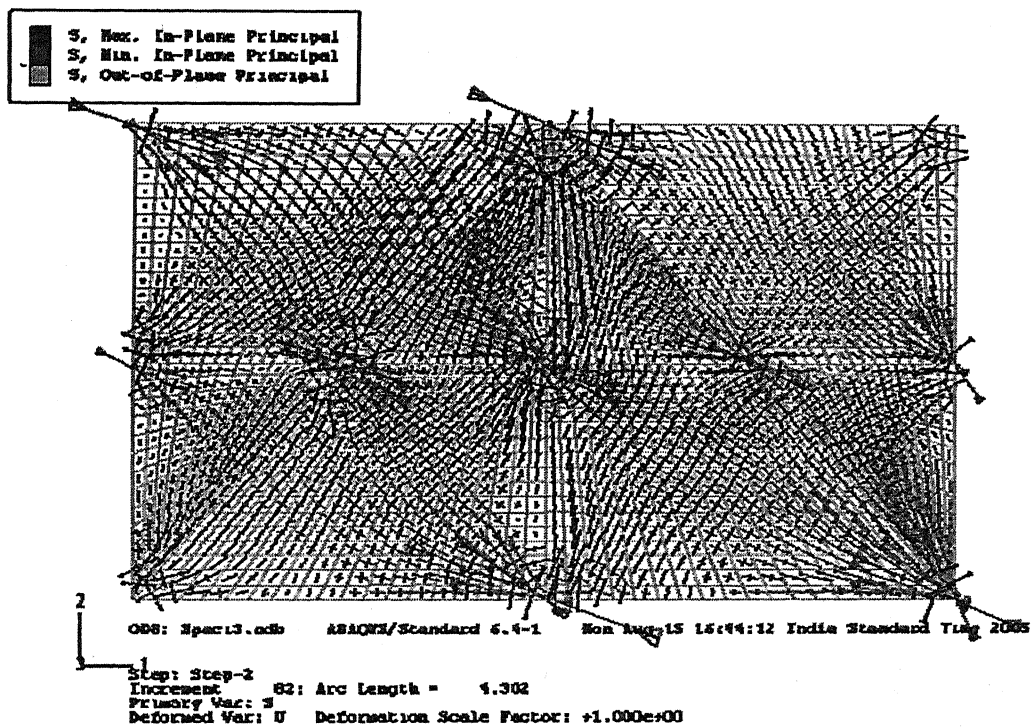**Figure 5.14** Vector plot of major principal stress in specimen 2 at 0.23% story drift right-wards.

Figure 5.15 Vector plot of major principal stress in specimen 3 at 0.17% story drift right-wards.

Figure 5.16 Comparison between Experimental and FE values of lateral shear for specimen 1.
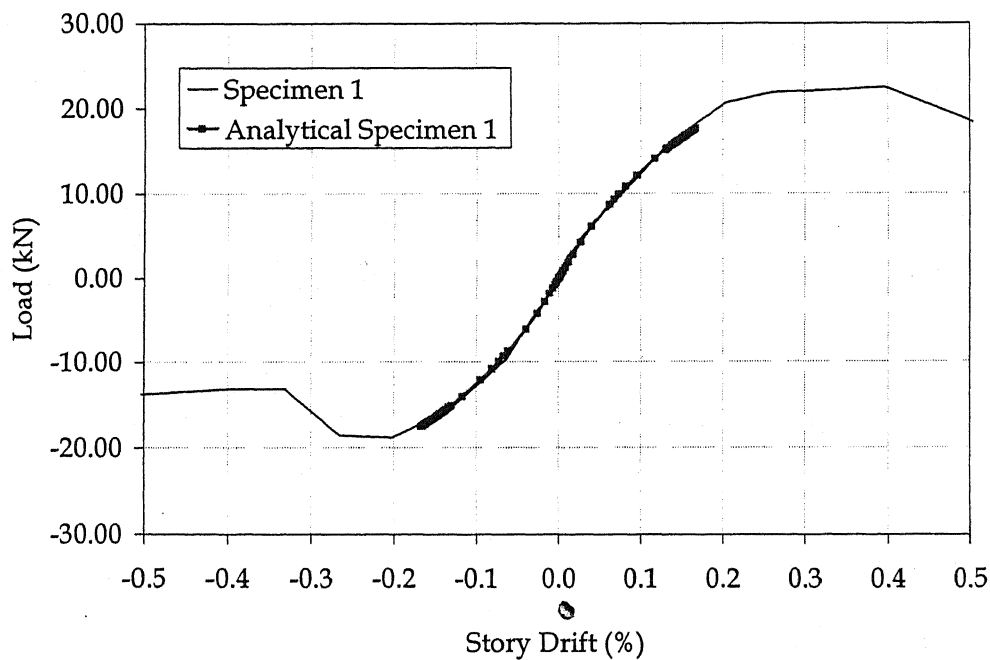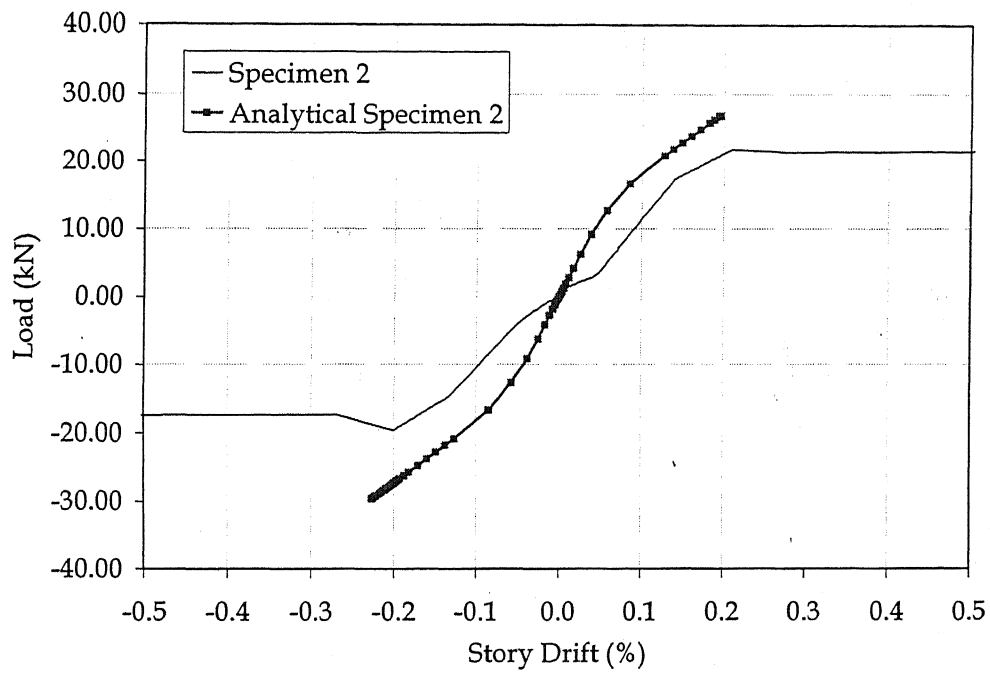
121

Figure 5.17 Comparison between Experimental and FE values of lateral shear for specimen 2.
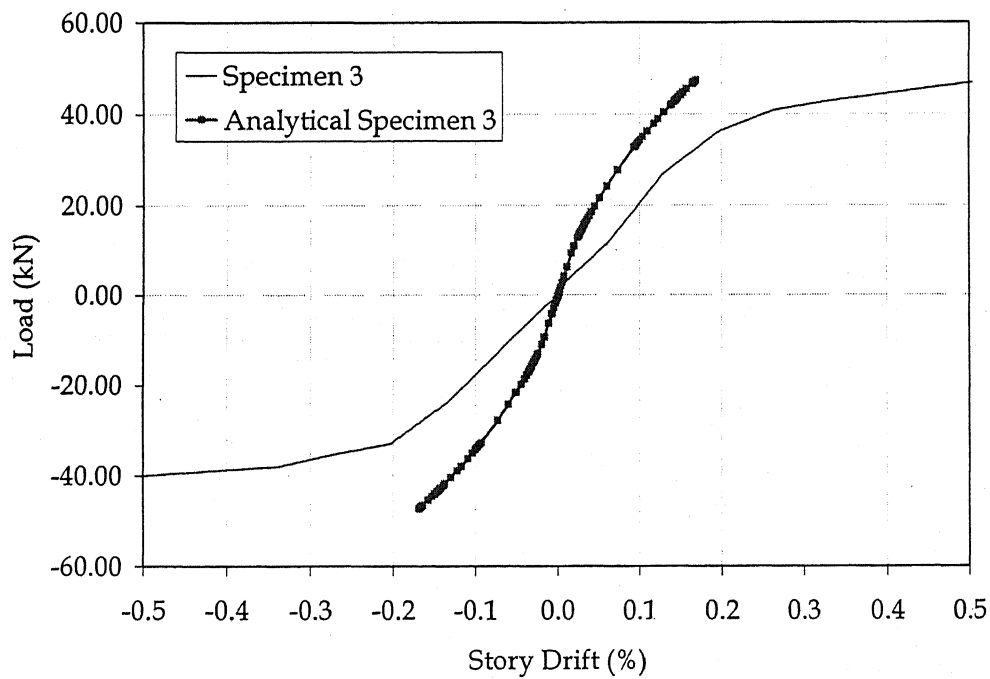

Figure 5.18 Comparison between Experimental and FE values of lateral shear for specimen 3.